REPORT DOCUMENTATION PAGE

Form Approved
OMB No. 0704-0188

1. AGENCY USE ONLY (Leave blank)	2. REPORT DATE	3. REPORT TYPE AND DATES COVERED
		FINAL 01 Aug 96 To 30 Apr 97

4. TITLE AND SUBTITLE

DOMAN-INVERTED ELECTROOPTIC POLYMERS FOR HIGH-SPEED POLARIZATION-INSENSITIVE 2X2 CROSS BAR SWITCHES

5. FUNDING NUMBERS

F49620-96-C-0039

62173C

1660/01

6. AUTHOR(S)

DR SUNING TANG

7. PERFORMING ORGANIZATION NAME(S) AND ADDRESS(ES)

RADIATION RESEARCH SOCIETY
3925 W. BRAKERLAND, SUITE 420
AUSTIN TX 78759

8. PERFORMING ORGANIZATION REPORT NUMBER

AFOSR-TR-97

0296

9. SPONSORING MONITORING AGENCY NAME(S) AND ADDRESS(ES)

AFOSR/NL
110 DUNCAN AVE ROOM B115
BOLLING AFB DC 20332-8050

DR CHARLES Y-C. LEE

19971002 022

11. SUPPLEMENTARY NOTES

12a. DISTRIBUTION AVAILABILITY STATEMENT

Approved for public release;
distribution unlimited.

12b. DISTRIBUTION CODE

13. ABSTRACT (Maximum 200 words)

The primary objectives of the Phase I work were to explore the feasibility and advantages of using domain inverted polyemrs, to improve the performance of electro-optic modulators, and to establish the technical foundation for the design and fabrication of a new class of electro-optical modulators with improved performance, simplified structure, and relaxed fabrication tolerance. The improved performance includes high modulation efficiency, a highly linearized modulation transfer curve, high-speed operation, low driving voltage, and polarization-insensitive operation. By accomplishing the tasks of the Phase I effort, we have established the theoretical and technical foundation for the realization of high performance Y-branch waveguide modulators based on domain-inverted polymers and a uniform traveling-wave electrode. At present, all the building blocks essential for the fabricaiton and modeling of the proposed innovative devices are available. The achievements strongly encourage us to pursue further R&D efforts in PhaseII, aimed at the fabricaiton of high performance EO modulators as required by BMDO and Air Froce for their advanced RF photonic system [1,15]. High-speed optical analog modulators also play an important role in a wide variety of practical applications, including CATV fiber-optic links [16,17], optoelectronic interconnects [11,12], and microwave instruments [2].

14. SUBJECT TERMS

DTIC QUALITY INSPECTED 4

15. NUMBER OF PAGES

16. PRICE CODE

17. SECURITY CLASSIFICATION OF REPORT	18. SECURITY CLASSIFICATION OF THIS PAGE	19. SECURITY CLASSIFICATION OF ABSTRACT	20. LIMITATION OF ABSTRACT
(U)	(U)	(U)	(UL)

RADIANT RESEARCH, INC.

Highly Efficient Linear Waveguide Modulators based on Novel Domain-Inverted Electro-optic Polymers

Phase I Final Report

BMDO Topic No.: BMDO96-014

Contract No.: F49620-96-C-0039

Contractual Point of Contact:

Mrs. Clara W. Chen
President
phone: 512-305-0295
fax: 512-305-0298

Technical Points of Contact:

Dr. Suning Tang
Principal Investigator
phone: 512-305-0297
fax: 512-305-0298
email: suning@mail.utexas.edu

Dr. Ray T. Chen
Technical Consultant
phone: 512-471-7035
fax: 512-471-8575
email: raychen@uts.cc.utexas.edu

1997

TABLE OF CONTENTS

1.0 IDENTIFICATION AND SIGNIFICANCE OF THE PROBLEM OR OPPORTUNITY

1.1 The Problem

Lightwave transmission via low-loss, low-dispersion single-mode fiber has become the choice for high capacity commercial communication systems[1]. Presently, optical communication systems have been employed in local and wide area networks including both military and civilian premises. From the viewpoint of transmission, a lightwave offers the potential of enormous information bandwidth. However, the rapid growth in the transmission capacity of fiberoptic waveguides would be of little value if there was not an equal growth in modulation rates.

Electro-optic modulators in the integrated-optic embodiment are the most promising candidates for wideband lightwave applications[1-5]. These devices, if properly designed using advanced electro-optic (EO) materials, should exhibit wider bandwidth, linearized conversion with a higher modulation efficiency (depth), lower drive power, and polarization-independent operation. Such a device has important applications not only to the military systems but also to the commercial market. The major important applications are in (**a**) satellite receiver systems for distributed RF signals over large distances with high signal quality; (**b**) remote connection of cellular radio systems by high-quality, low-loss RF photonics without the need for complicated and expensive digital processing equipment; and (**c**) LANs for low distortion distribution of RF signals in large building complexes, aircraft, and television network systems.

The most mature technology to date for fabrication of EO modulators is based on ferroelectric crystals[1-5], such as $LiNbO_3$ and $LiTaO_3$, etc. In this technology, relatively low-loss channel waveguides with good spot size matching to single-mode fibers can be conveniently fabricated. The electro-optic modulation is obtained by using the electro-optic effect. Although several commercial (expensive) EO modulators are currently available, their performance is severely limited by these existing ferroelectric crystals and conventional device structures[3-7].

On one hand, these limitations are due to the intrinsic properties of the existing electro-optic materials[6,7]. For example, the bandwidth of these modulators is known to be mainly limited by the velocity-mismatch between the guided optical wave and the modulating microwave signal, arising from the intrinsic high dielectric constants of these ferroelectric crystals such as $LiNbO_3$. Another severe problem using these materials is that inorganic-material-based EO devices made out of $LiNbO_3$ and III-V compound semiconductors are inherently polarization-dependent. As a result, these modulators require launching of a specific linearly polarized light (TE or TM depending on crystal orientation), which simultaneously requires an expensive rotational alignment. The problem of polarization-dependence also imposes a serious limitation on optical modulation

depth[8]. If the interaction length is not exactly equal for the TE and TM modes, then 100% modulation cannot be obtained.

On the other hand, the performance of existing modulators is severely limited by their conventional designs based on conventional fabrication technologies[3]. High performance modulators can only be fabricated if high precision and complicated device schemes are attained, which causes a very high fabrication cost. For example, the modulation performance of a conventional modulator is severely degraded by distortions caused by the nonlinearity of the modulation curve which typically exhibits sine-squared behavior[3]. Complicated device structures have to be employed in order to improve the modulation linearity and modulation depth[9]. In view of the rapidly increasing demand for highly efficient and highly linearized external modulators, it is therefore of paramount importance to develop practical viable schemes for improving modulator performance.

Organic electro-optical polymers exhibit a low and nondispersive dielectric constant. Very high frequency broadband traveling wave modulators can be made of these materials with simple planar circuit structures because of the close velocity match between the light wave and the microwave[10-14]. More importantly, the intrinsic property of EO polymers provides us with an exclusive opportunity for creating multiple electro-optical domains in any direction of interest in a single polymer thin film. As a result, a new class of EO modulators can be generated with improved performance, simplified structure and relaxed fabrication tolerance.

In order to provide a wider bandwidth, higher modulation efficiency (depth), lower drive power, linearized conversion, and polarization-independent operation, conventional inorganic-material-based electro-optic (EO) modulating devices using such materials as $LiNbO_3$, $LiTaO_3$, GaAs, InP, and liquid crystals are deficient in meeting the following crucial requirements:

(1) The material dispersion and the large dielectric constant of inorganic EO materials make the modulation bandwidth small and limited. A traveling-wave EO modulator has a baseband frequency response that is bandwidth limited because of the mismatch between the phase velocities of the guided optical mode and the modulating microwave signal[13]:

$$\Delta f L = \frac{c}{4 \left| n_{eff} - \sqrt{\varepsilon}_{reff} \right|}$$

where Δf is the 3 dB bandwidth, L denotes the electrode length, c is the speed of light, n_{eff} is the effective index of refraction, and ε_{eff} is the effective dielectric constant.

Straightforward evaluation of this limit for $LiNbO_3$ and III-V modulators yields products less than 20 GHz cm with improvements obtainable at the cost of circuit and fabrication complexity. Broadening the bandwidth requires shortening the electrode length which leads to an increased drive power requirement for maintaining the same optical modulation depth[3].

(2) Inorganic-material-based devices, such as Ti:$LiNbO_3$ EO modulators, are inherently polarization-dependent. There are two main reasons for the polarization-dependency of devices based on ferroelectric crystals such as $LiNbO_3$. First, the index perturbations due to in-diffusion of titanium are different for the extraordinary and ordinary indices. This means that different waveguides are formed for the TE and TM polarization, respectively[3]. The second reason for the polarization-dependency is the different electro-optic coefficients seen by the two states of polarization; the extraordinary mode sees r_{33} and the ordinary mode sees r_{13} (or r_{23}, which is equal to r_{13}); r_{13} is approximately a factor of 3 less than r_{33}. As a result, different drive voltages are required for the two states of polarization.

(3) Fabrication and integration of inorganic-material-based guided-wave EO devices are restricted by their non-thin-film features. As a result, the fabricated modulator is not transferable to other substrates in order to be integrated with light sources and microwave driving circuits. This significantly restricts the implementation of an integrated optoelectronic device.

(4) The orientation of the ferroelectric domain of inorganic materials is fixed by their crystal structures. Although domain inversion has been demonstrated in some ferroelectric crystals such as $LiNbO_3$, it is impossible to engineer the domain in a ferroelectric crystal with any orientation of interest. Therefore, innovative device structures employing multiple ferroelectric domains are restricted and limited when inorganic materials are employed. For example, domain inversion in X-cut $LiNbO_3$ has not yet been demonstrated, which is preferred for practical applications. The reverse poling technique suitable for Z-cut substrates is not likely to be applicable for domain inversion on X-cut substrates because the poling field is not antiparallel to the direction of the optical axis.

(5) Finally, the fabrication costs associated with inorganic material systems are high. Fabrication of nonlinear waveguides is a complicated process in ferroelectric crystals such as $LiNbO_3$. To facilitate the processes involved in making these EO modulators, such very sophisticated equipment as MBE and MOCVD are required to carry out the tasks. The

cost-ineffectiveness of these systems makes such an endeavor incompatible with the small business environment. To date, most of these devices are possible for large corporations such as NTT, HP, and Lucent, and by advanced research labs such as the Naval Research Labs. It is tactically not wise for a small business to compete with these large companies, where hundreds of millions of dollars have already been spent in upgrading inorganic-material-based device research. In the SBIR arena, further technology developments are needed to solve these problems in a technically and financially viable way.

1.2 The Opportunity

In this Phase II research program, Radiant Research, Inc. (RRI) proposes reliability-tested domain-inverted polymers for fabricating a new class of high performance analog modulators. Recognizing the real need for efficient external analog modulators in a wide variety of commercial and military applications, the proposed high performance domain-inverted modulators are targeted at wideband RF photonic systems in order to provide a near-lossless and distortionless conversion of analog electronic signals to the optical domain. Such an innovative device is highly desired for advanced BMDO and Air Force defense systems including antenna systems, RF receivers, satellite communications, electronic warfare (EW) systems, and electronic signals intelligence (ELINT) systems. It eliminates all the aforementioned bottlenecks associated with inorganic materials. A fiber-pigtailed module will be delivered to the BMDO and Air Force by the end of the phase II program.

In contrast to any existing electro-optic devices, the proposed highly-efficient EO analog modulators are based on innovative EO polymer waveguides with domain-inverted (DI) sections as shown in Fig. 1(a). The application of domain-inverted sections in electro-optical waveguides has the potential to substantially improve the modulator performance with considerable simplification of device configuration. Fig. 1(b) shows the modulation transfer curve of the proposed modulator. It is shown that highly linearized modulation can be achieved with ~100 modulation depth using very low driving voltage. As shown in Fig. 1(a), the $\Delta\beta$ reversal modulator in the Y-branch coupler is realized by using a domain-inverted polymer in conjunction with a single uniform traveling-wave electrode. As a result, uniform electrodes (not micro-structured phase-reversal electrodes and not multi-section electrodes) can be employed, which makes electrode fabrication, packaging, and matching to a microwave source much easier for high-speed operation. Because of the application of domain inversion, high performance EO modulators can be realized with the following unique properties:

1. High modulation efficiency (~100%),
2. Highly linearized modulation transfer curve,
3. High speed operation (>100 GHz),
4. Polarization-insensitive operation,
5. Very low driving voltage (< 5 V),
6. Simplified electrode structure (single uniform electrode),
7. Relaxed fabrication tolerance, and
8. No DC bias voltage.

This proposed domain-inverted modulator structure is fully compatible with an efficient push-pull traveling-wave electrode structure utilizing the largest γ_{33} electro-optic interaction possible for polarization-insensitive operation. It should be noted that the optical power is automatically set at the 3 dB half-power modulating point without any applied DC bias voltage for the proposed high performance analog modulators. Additionally, the device can be used as a 1x2 optical switch, requiring no DC bias.

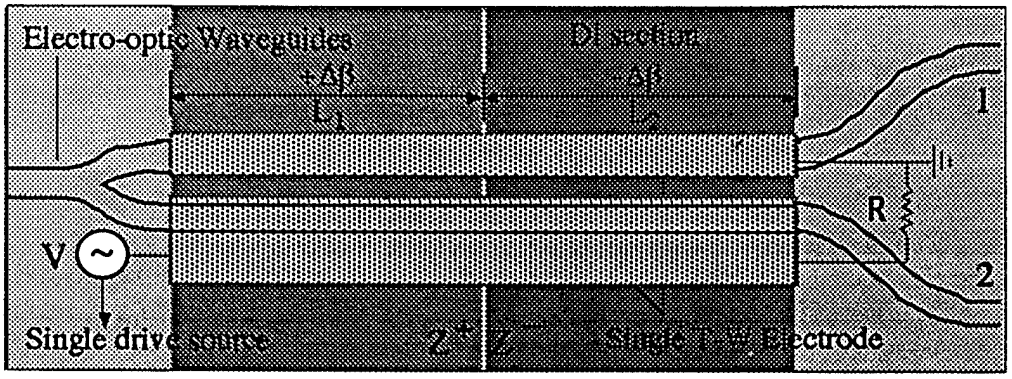

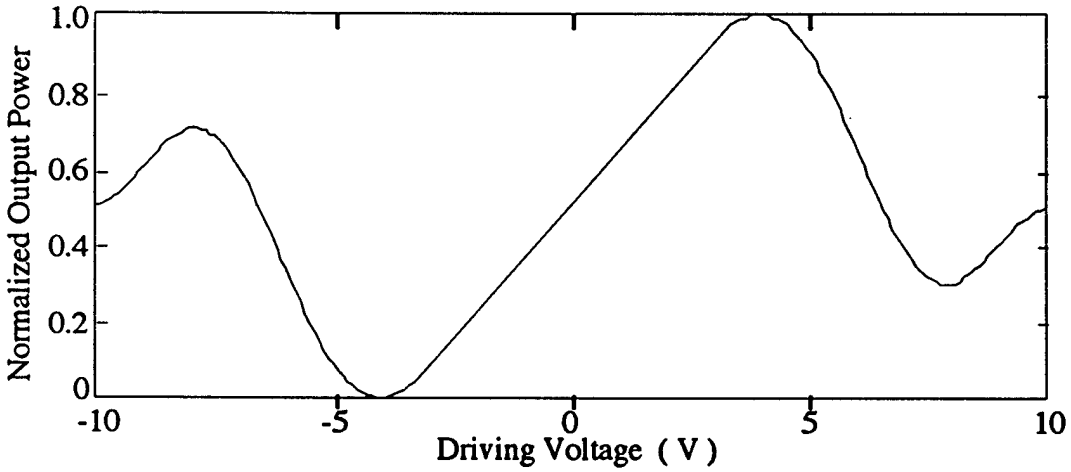

Fig. 1. (a) Schematic of the proposed modulator using a uniform T-W electrode and domain-inverted sections. (b) Calculated modulation transfer curve of the proposed device.

The proposed polymer-based domain-inverted device outperforms existing inorganic-material-based modulators with the following exclusive characteristics:

1. Wide modulation bandwidth due to much less material dispersion

Polymeric electro-optic polymers exhibit a relatively low and nondispersive dielectric constant. Very high-speed traveling-wave modulators can be made from these materials with simple planar-circuit structures because of the close velocity match between the light wave and the microwave. A high modulation speed over 120 GHz is expected. Note that both $LiNbO_3$ and III-V compound semiconductors have a dielectric constant ($\varepsilon = 28$) much larger than that of EO polymers ($\varepsilon = 4$).

2. Flexible device substrate due to the thin film nature of EO polymers

The thin film nature of EO polymers allows us to fabricate the proposed device using standard thin film technologies originally developed for microelectronics industries. Unlike inorganic crystal-based systems where each fabrication process is substrate-dependent, an EO polymer-based modulator is transferable to any substrate of interest. From the system implementation point of view, such a flexibility greatly enhances the ability and feasibility of fabricating an optoelectronic modulating module that has a monolithic integration with silicon based CMOS circuits, and with III-V laser diodes and photodetectors.

3. Flexible electro-optic poling and flexible domain inversion

The intrinsic property of EO polymers provides us with an opportunity for creating multiple domains in many orientations in a single EO polymer film, which is not achievable for any existing inorganic based EO crystals such as $LiNbO_3$. For EO polymers, the ferroelectric domain is a result of a noncentrosymmetric polymeric structure, which is easily created by aligning chromophores into a noncentrosymmetric order by the application of an external electric field. In other words, a ferroelectric domain can be created in any direction of interest according to the orientation of an external field. Because of the thin-film nature of EO polymer, the required poling (and reverse-poling) voltage is much lower for EO polymer (<500 V) than for $LiNbO_3$ (>5,000 V).

4. Polarization independent modulators

Polarization independent operation is due to the exclusive characteristics of the thin film multiple domain-inverted polymers. Polymer-based single-mode symmetric-channel waveguides can be easily fabricated, which have an equalized waveguide index perturbation as well as

waveguide modal dispersion for both TE (transverse electric) and TM (transverse magnetic) states of polarization. With a properly electric-poled (domain-rotated) EO polymer, a randomly polarized signal, constituted of an arbitrary combination of TE and TM guided waves, can be equally modulated. As a result, a polarization-independent modulation can be achieved. Fig. 2 shows a possible schematic diagram for realizing a polarization-insensitive EO modulator. Note that conventional $LiNbO_3$-based EO modulators are polarization-sensitive for the following two reasons. First, the index perturbations due to in-diffusion of titanium are different for the extraordinary and ordinary indices. The second reason is that the two states of polarization see different electro-optic coefficients; the extraordinary mode sees r_{33} and the ordinary mode sees r_{13}; r_{13} is approximately a factor of 3 less than r_{33}.

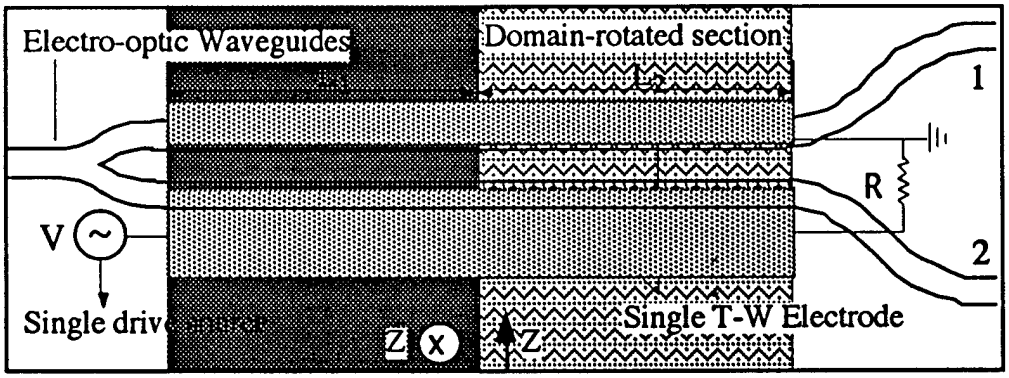

Fig. 2. Top view of a polarization-insensitive 1x2 electro-optic modulator using electric-poled 90° domain-rotated polymers. On the left side, the polymer is surface-normally poled. On the right side, the polymer is in-plane poled.

5. Large modulating efficiency over a highly linearized modulation transfer curve

Unlike conventional modulators that have a poor optical modulation depth and nonlinear modulation transfer curve (sine-squared behavior), the proposed domain-inverted Y-branch waveguide modulators can provide a highly linearized modulation transfer curve while ensuring a near-lossless conversion (100% modulation depth) of analog electronic signals to the optical signals. Such a high performance (linearized modulation with -30 dB nonlinear distortion and ~100% modulation depth) is based on the innovative approach of domain inversion (See Fig. 3). Conventional modulators can only provide -20 dB nonlinear distortion with modulation depth less than 70% for linearized operation. Note that modulating efficiency is defined by modulation depth: 10% optical modulation depth equals 10% efficiency, 100% modulation depth equals 100% efficiency. Highly efficient and linearized conversion of RF-carrier-based signals to optical-carrier-based signals is of paramount importance for BMDO and Air Force applications.

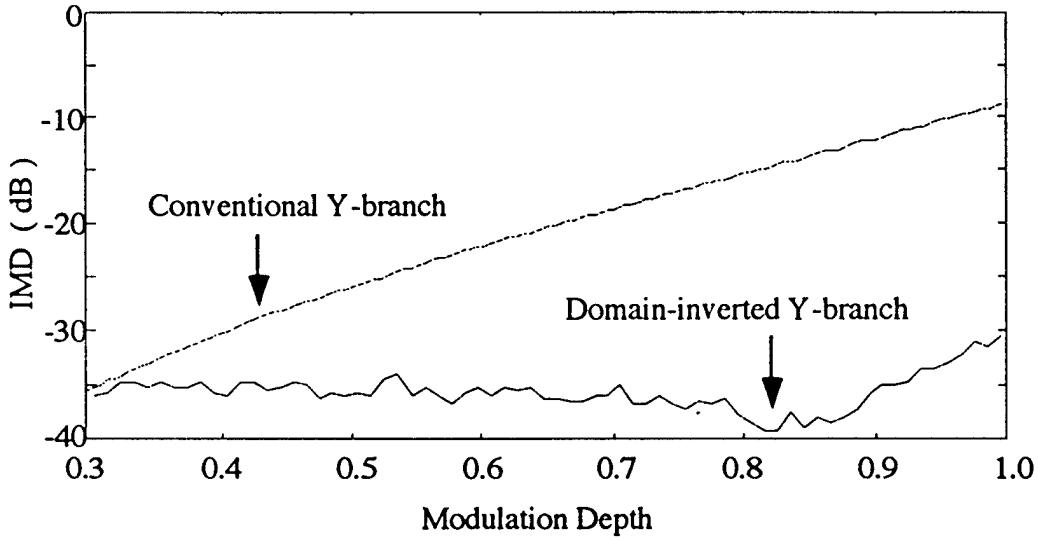

Fig. 3. Comparison of the intermodulation distortion (IMD) as a function of optical modulation for the proposed domain-inverted Y-branch and conventional Y-branch.

6. Low-driving-voltage and a relaxed fabrication tolerance

In order to automatically set at the 3 dB half-power modulator operating point without any applied DC bias voltage, the Y-branch structure shown in Fig. 1(a) is selected. This device structure has one input and two output waveguides. The input single-mode waveguide branches into a pair of symmetric single-mode waveguides of length $L = L_1 + L_2$ which are optically coupled. For conventional devices without domain-inverted sections, the length L must be exactly equal to sin 45° = 0.707 times the coupling length ℓ of the coupled waveguide pair in order to obtain 100% modulation depth, which imposes a strict limitation on device interaction length. Other choices such as $L = \frac{3\sqrt{2}}{2}\ell$, $\frac{5\sqrt{2}}{2}\ell$, and $\frac{7\sqrt{2}}{2}\ell$ cannot be employed due to their complicated nonlinear modulation transfer curves, shown in Fig. 4(a). It should be noted that lower driving voltage can not be obtained by simply selecting longer device length because the ratio of $(L/\ell)/(\Delta\beta L/\pi)$ for 100% modulation falls on a 45° line through the origin in the switching diagram (see Sec. 3.3 for details).

However, for the proposed domain-inverted modulators, a linearized modulation transfer curve with 100% modulation depth can be obtained with the freedom of selecting longer device lengths, exclusively provided by the domain inversion. Fig. 4(b) shows the calculated modulation transfer curve for the proposed domain-inverted modulators using the same material parameters of Fig. 4(a). Linearity of the modulation transfer curve is improved together with the driving voltage

by employing domain inversion. Lower driving voltage is obtained because the ratio of $(L/\ell)/(\Delta\beta L/\pi)$ for 100% modulation falls in a 67.5° (>45°) line through the origin in the switching diagram (see Sec. 3.3 for details). Note that symmetric domain inversion ($L_1 = L_2$) is employed in the calculation. We expect that asymmetric domain-inverted sections will further improve the modulation linearity and reduce the driving voltage, which will be fully investigated in Phase II.

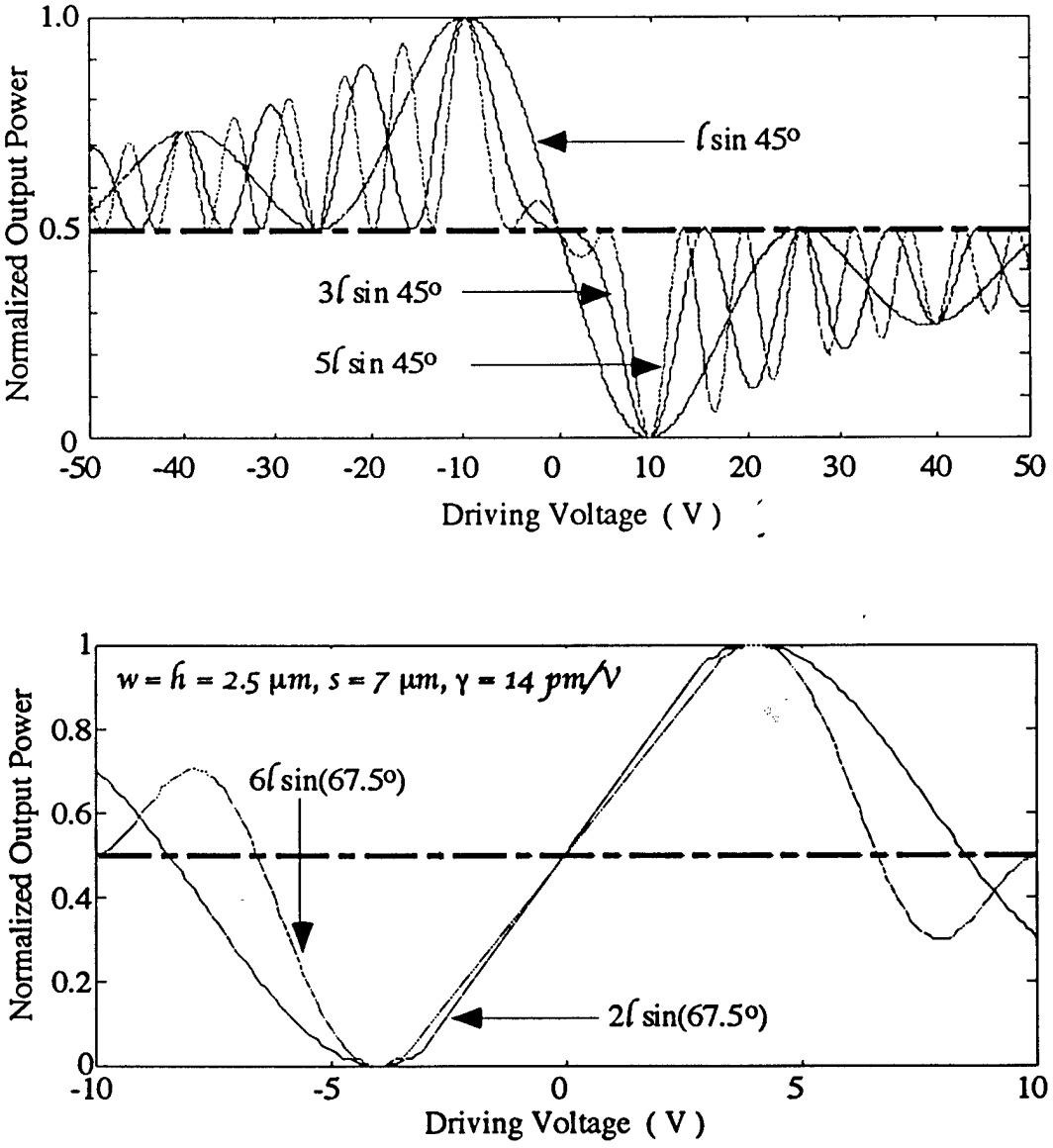

Fig. 4. (a) Calculated modulation transfer curve for conventional Y-branch waveguide coupler.
(b) Calculated modulation transfer curve for domain-inverted Y-branch.

7. Simplified electrode structure using domain-inverted polymers

The application of domain-inverted sections in electro-optic waveguides substantially simplified the electrode configuration for a linearized modulation. For conventional modulators, a linearized modulation is obtained using multiple electrode sections[3,9] in order to provide the required $\Delta\beta$ reversals, which makes high-speed operation impossible. Due to the employment of domain-inverted polymers, the required $\Delta\beta$ reversal can be realized by using a uniform traveling wave electrode (not the micro-structured phase-reversal electrodes), which makes electrode fabrication, device packaging, and matching to a microwave source much easier. It should be noted that the proposed domain inversion approach is exclusively suitable for EO polymer-based modulators due to their nondispersive dielectric constant. Because of the large walk-off between the optical wave and microwave signal, the required $\Delta\beta$ reversals is a complicated approach and very difficult to achieve.

8. Cost-effective and reliable in manufacturing

The synthesis and fabrication of EO polymer thin films are straightforward. Cost effectiveness is expected. Such an advantage will outpace their counterparts made out of inorganic materials such as $LiNbO_3$, $LiTaO_3$, GaAs, InP, and liquid crystals. Furthermore, both polymeric thin films and glass fibers have an index of refraction of about 1.5. Consequently, there is no need to implement an anti-reflection coating at the fiber/waveguide interface in silicon V-groove-based butt couplings. The packaging cost is thus also reduced. Table 1 compares the differences in material preparation between $LiNbO_3$ and EO polymer. Fig. 5 shows the reliability test result of an LD-3 EO polymer film, which is the polymer to be used in the phase II program. The reliability of the electro-optic coefficient of the LD-3 EO polymer at high temperatures makes the proposed EO polymer-based modulators highly reliable.

The successful funded Phase I research demonstrated the advantage and feasibility of a novel domain-inverted concept for high performance electro-optical modulators. We have selected the waveguide Y-branch as the basic element for our Phase II work since it possesses some intrinsic advantages over other EO modulators, such as no DC bias voltage. In designing a high performance Y-branch modulator, we have simultaneously considered many important device parameters such as modulation depth, driving voltage, fabrication tolerance, polarization-sensitivity, the nonlinearity of its transfer curve, and distortions caused by it. Based on the results of the theoretical modeling of device performance, we concluded that the two-section domain-

inverted waveguide Y-branch is the preferred choice for practical implementation. In this device, a high optical modulation efficiency, linearized modulation transfer curve, very low driving voltage, and relaxed sensitivity to fabrication tolerances can be achieved if domain-inverted polymer is employed. Yet another advantage is that the designed structure can be fully compatible with a single-drive microwave source to ensure high speed operation.

Table 1. Comparison of EO Polymer and $LiNbO_3$ Integrated Optics Technologies

Physical and Device Properties	Lithium Niobate	Organic Polymers
Electro-optic Coefficient (pm/V)	32	20-150
Walk-Off Between N_o and N_m	Large	~0
Dielectric Constant	28	3-4
Crystal Growth Temperature, °C	1000	~100-350
Waveguide Processing Temperature, °C	1000[d]	150-200
Waveguide Processing Time	10 hr.	< 10 min.
Multiple Layers Possible	No	Yes
Fabrication and Processing	Difficult	Simple
Implementability on Different Substrates	No	Yes
$\Delta\beta$ reversal	Complicated	Easy
Domain Rotation	No	Yes
Domain Inversion	Difficult	Simple

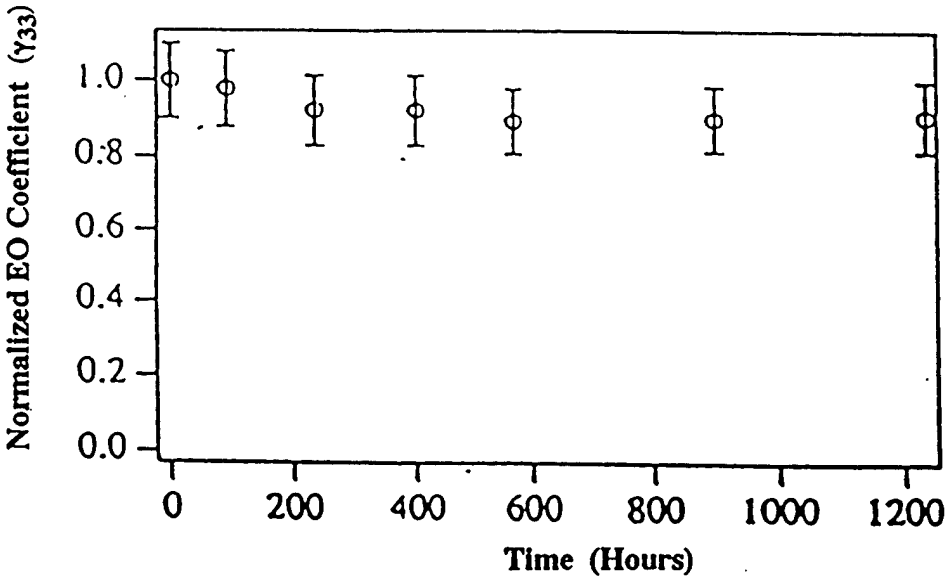

Fig. 5. Reliability test of the second order nonlinearity of the LD-3 EO polymer.

Further R&D effort, which is proposed to be performed under the SBIR Phase II Program, is a logical continuation of the Phase I effort and should extend it to include the fabrication of a fully-packaged working module of a high-performance EO modulator using domain-inverted polymers, and the incorporation of the working module into an optical RF link for evaluation. The success of the proposed Phase II research will prove a new concept of domain-inverted polymers for design and fabrication of electro-optic devices. Based on this concept, a new class of EO devices can be generated together with a new technology called domain-inverted polymers.

2.0 PHASE I ACHIEVEMENTS

The primary objectives of the Phase I work were to explore the feasibility and advantages of using domain inverted polymers, to improve the performance of electro-optic modulators, and to establish the technical foundation for the design and fabrication of a new class of electro-optical modulators with improved performance, simplified structure, and relaxed fabrication tolerance. The improved performance includes high modulation efficiency, a highly linearized modulation transfer curve, high-speed operation, low driving voltage, and polarization-insensitive operation.

By accomplishing the tasks of the Phase I effort, we have established the theoretical and technical foundation for the realization of high performance Y-branch waveguide modulators based on domain-inverted polymers and a uniform traveling-wave electrode. At present, all the building blocks essential for the fabrication and modeling of the proposed innovative devices are available. The achievements strongly encourage us to pursue further R&D efforts in Phase II, aimed at the fabrication of high performance EO modulators as required by BMDO and Air Force for their advanced RF photonic systems[1,15]. High-speed optical analog modulators also play an important role in a wide variety of practical applications, including CATV fiber-optic links[16,17], optoelectronic interconnects[11,12], and microwave instruments[2]. In the following, the major accomplishments of the Phase I efforts are presented. After that, the objectives of the proposed Phase II effort are described, which is a logical continuation and extension of the Phase I work.

2.1 Novel Concept of Domain-Inverted Electro-optic Modulators

We have proposed a novel concept to apply domain-inverted polymers for realizing $\Delta\beta$-type waveguide Y-branch modulators[9,18,19]. As a result, a new class of electro-optic modulators can be developed with improved performance, simplified structure, and relaxed fabrication tolerance. Such a new waveguide Y-branch using domain-inverted polymers is capable of providing the required reversed $\Delta\beta$ modulation using a single uniform electrode, which is fully compatible with a single microwave source for high-speed operation. More importantly, the domain-inverted modulator is capable of providing a near lossless conversion of RF-carrier-based analog signals to optical-carrier-based analog signals with much reduced nonlinear distortion at a very low driving voltage. Rather than the conventional Mach-Zehnder modulator, the proposed Y-branch structure offers two optical outputs instead of one. Optical power normally dissipated in a Mach-Zehnder device is available at the second output, resulting in a doubling of optical power available to the user. Note that the power doubling of optical signals cannot be realized by any other means because the maximum optical power is limited by the onset of stimulated Brillouin scattering (SBS) in the fiber.

In the past, Δß-type operation has been realized by using multiple electrode sections with applied voltages of reversed polarities[9,20]. This straightforward approach has, however, a major drawback owing to the inherent incompatibility with a single drive source. As a result, high-speed operation is impossible for these demonstrated devices. To solve this problem, a substantial amount of effort has been devoted to the development of traveling-wave electrode structures with phase reversals[21,22]. Both periodic[23] and aperiodic[24] phase-reversed electrode structures have been proposed to compensate for the mismatch between the velocities of the guided mode and the modulating microwave[25]. However, the presence of phase reversals in the electrode structure complicates the fabrication of thick electrodes, and more importantly, prevents the use of the efficient push-pull configuration on x-cut $LiNbO_3$, which is preferred for practical applications[6,7] owing to its improved thermal stability over z-cut devices. Electrode phase reversals also unavoidably involve the use of buffer layers which tend to have microwave leakage and cause excess optical loss[25], let alone the additional processing steps required. Due to the above-mentioned problems, high-speed 1x2 electro-optical modulators have not become commercially available so far.

The domain-inversion technique has been developed independently over the past few years, and has primarily been stimulated by the possibility of realizing efficient second-harmonic generation (SHG) in nonlinear crystal waveguides superimposed on a periodic grating-like structure in which adjacent sections are polarized in opposite directions, i.e., their ferroelectric axes are reversed[26-28]. However, this technique has not been applied to electro-optic modulators. **Furthermore, the concept of using domain inverted polymers was first proposed by RRI in our Phase I proposal and first demonstrated through the Phase I effort. The proposed domain-inverted polymers represents a new technology for creating a new class of EO modulators with superior performance over conventional modulators.**

In response to the BMDO and Air Force effort in advancing RF photonics, where modulation efficiency, linearity of conversion, and polarization-independent operation are of paramount importance, RRI proposes a novel Y-branch modulator using a domain-inverted polymer. Only a single uniform traveling-wave electrode is required for obtaining high-speed operation, ensuring a near-lossless conversion of analog electronic signals to the optical domain for RF photonic systems. Compared to conventional Y-branch waveguide modulators, the proposed EO modulator based on domain-inverted polymers has significant advantages including:

1. High modulation efficiency (~100%),
2. Highly linearized modulation transfer curve (IMD <-30 dB),
3. High speed operation (>100 GHz),
4. Polarization-insensitive operation,

5. Very low driving voltage (< 5 V),
6. Simplified electrode structure with relaxed fabrication tolerance, and
7. No DC bias voltage.

Such high performance modulators will find a vast area of commercial and military applications.

We have established the theoretical and technical foundation for the realization of a polymer-based high performance EO modulator based on a waveguide Y-branch and a uniform traveling-wave electrode. At present, all the building blocks essential for the fabrication and modeling of these novel devices are available. The achieved results strongly encourage us to pursue further R&D effort in Phase II, aimed at the fabrication of high performance electro-optic modulators required by BMDO and Air Force.

3.0 Technical Discussion

In this section, the technical details of the proposed Phase II research are described. For a better understanding, the results achieved in the scope of the Phase I effort are also provided.

3.1 Technical approach

There is a trade-off between device complexity and modulating performance for conventional electro-optic modulators. One severe problem associated with conventional electro-optic modulators is the limited modulation efficiency for electro-optical conversion[1-5]. Another problem of conventional modulators based on ferroelectric crystals is the limited bandwidth because of the mismatch between the phase velocities of the guided optical mode and the modulating microwave signal. The polarization dependency may also be a severe problem, i.e., the two states of polarization can not be equally modulated simultaneously by a single driving source at a single voltage. Although the multiple-section-electrode method has been investigated in order to improve the modulation linearity[9,29,30], relax the fabrication tolerance, and reduce the polarization dependence[20], this method complicates the device configuration by using multiple electrodes and multiple driving voltages. As a result, it is impossible to operate at high speed as required by the BMDO and the Air Force. Other design schemes developed thus far have attempted to improve the modulating performance by cascading several modulators, thus trading device compactness for enhanced modulating performance and severely limiting the maximum attainable bandwidth[38]. In this connection, a question of paramount importance is whether it is possible to achieve a high modulating performance while keeping the device compact.

In order to overcome the problems of conventional modulators, we propose a new EO modulator structure based on a Y-branch waveguide coupler using domain-inverted EO polymers and a uniform traveling-wave electrode, as shown in Fig. 6(a). Fig. 6(b) shows a conventional linearized modulator[9]. In the course of the Phase I effort, we have demonstrated that polymer-based domain-inverted Y-branch waveguide couplers with properly chosen structural parameters can possess the optimum combination of the above qualities. The feasibility of achieving a high-speed, high modulation efficiency, highly linearized modulation transfer curve in a simplified fabrication scheme has been proven. Therefore, the technical approach under Phase II research is to fabricate high performance electro-optic modulators using polymer-based Y-branch waveguide couplers with domain-inverted sections. Incorporation of domain-inverted sections in the device scheme allows compact design with a single electrode structure compatible with the coupling to a microwave source. The required domain-inverted sections can be created by a liquid-contact high-temperature electric poling technique, developed in Phase I.

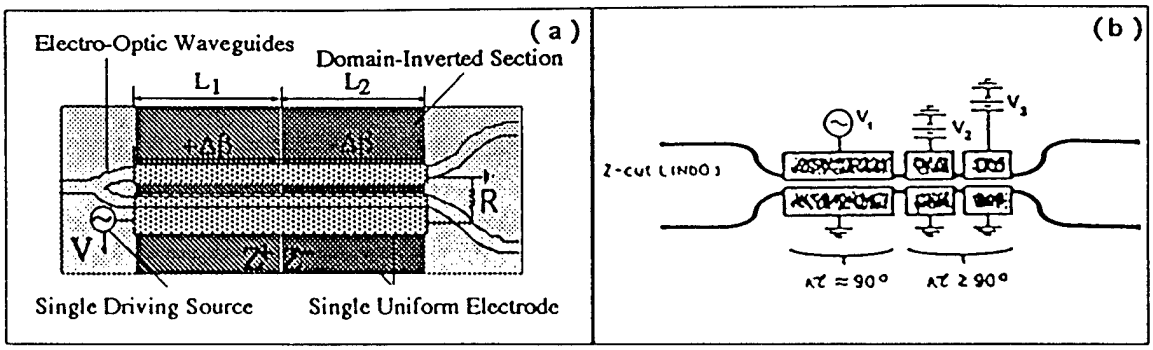

Fig. 6. (a) Proposed Y-branch linearized modulator using domain-inverted EO polymers and a T-W uniform electrode. (b) Conventional linearized modulator using multiple electrodes.

In the following, it can be shown that modulation efficiency, linearity of modulation, and driving voltage are improved by using the domain-inversion technique as proposed. A high-speed polarization-independent modulator can be realized by using a domain-inverted Y-branch waveguide coupler and a single uniform electrode.

3.2. Analog Model of Electro-Optic Modulators

The linearity of EO modulators is often presented in conjunction with modulation depth. In most direct-detection intensity-modulated optical communication or signal processing systems, the output optical electric field of the modulator is given by[17]

$$E(t) = E_o\, G(V) \cos(\omega_{op} t + \phi_{op}) \qquad (1)$$

where E_o is the optical field amplitude input to the modulator, ω_{op} is the optical angular frequency, ϕ_{op} is the optical phase, and G(V) is the function relating the output optical electric field to the applied electric voltage V. The time averaged output intensity for the modulator is given by

$$I(t) = \frac{1}{2} E_o^2 G^2(V) = H[V(t)] I_o \qquad (2)$$

where H(V) is the transfer function and I_o is the constant input optical intensity. The electrical current at the output of a detector is proportional to I(t).

An ideal linear intensity modulator will have H(V) directly proportional to V. However, all practical electro-optic intensity modulators are nonlinear. In many, for example, H(V) is proportional to $\cos^2 V$. Although devices of this type have been employed in the nearly linear

region[35,36], the small modulation depth and large nonlinearities severely restrict their use in advanced analog systems. In general, H(V) can be expanded in the form of a Taylor series about a bias voltage V_b:

$$H(V) = \sum_{n=0}^{\infty} \frac{1}{n!} \left(\frac{d^n H}{dV^n}\right)_{V=V_b} (V - V_b)^n = 1 + \sum_{n=1}^{\infty} h_n (V - V_b)^n \ . \qquad (3)$$

It is apparent that H(V) = 1 at V_b, the bias point, and $I_o h_1$ is the slope (dI/dV) at the bias point. An ideal linear optical modulator has $h_n = 0$ for $n > 1$. When the transfer function is linear, only the first few terms of this expansion are important.

There are two common definitions of intermodulation distortions (IMD) applied to analog modulators, which are derived from either harmonics of the input or third intermodulation terms. We first consider the case where the intermodulation distortions are defined as the harmonics of the input signal. Here the input signal is given by

$$V(t) = V_b + \frac{m}{h_1} \sin(\omega_o t) \qquad (4)$$

where m is the modulation depth ($0 < m < 1$), and $\omega_o t$ is the modulation frequency. The factor $1/h_1$ has the units of voltage and is simply a normalization factor so that m = 1 corresponds to full modulation when H(V) is linear. The power of harmonic signals is derived by substituting (4) into (3) and collecting like-frequency terms.

We obtain the following relative amplitudes of each of the harmonics:

Bias term	$1 + \frac{1}{2} h_2 \left(\frac{m}{h_1}\right)^2$	(5a)
Fundamental	$1 + \frac{3}{4} h_3 \left(\frac{m}{h_1}\right)^3$	(5b)
Second harmonic	$-\frac{1}{2} h_2 \left(\frac{m}{h_1}\right)^2$	(5c)
Third harmonic	$-\frac{1}{4} h_3 \left(\frac{m}{h_1}\right)^3$	(5d)

The intermodulation distortions are proportional to the square of the second and third harmonic terms. These are normally measured relative to the power in the fundamental terms.

For the proposed Y-branch waveguide EO modulators, the device automatically operates at the 3 dB inflection point, virtually eliminating h_2. Therefore, the third-order harmonic remains as the dominant IMD. Based on the traditional definition employed for broad-band analog systems, the IMD is defined as the power at $2\omega_2-\omega_1$ or $2\omega_1-\omega_2$ and is measured with respect to the power in one of the two closely spaced, equal amplitude sine waves at ω_1 and ω_2. The input signal in this case is expressed as

$$V(t) = V_b + \frac{m}{h_1} (\sin(\omega_1 t) + \sin(\omega_2 t)) . \qquad (6)$$

Substituting (6) into (3) and ignoring terms with $n > 3$, we obtain for the amplitude of the IMD

$$S = \frac{3}{4} h_3 (\frac{m}{h_1})^3 . \qquad (7)$$

This third-order IMD is potentially more troublesome than harmonics, because many EO modulators are biased such that h_2 can be neglected.

3.3 Comparative analysis of domain-inverted Y-branch waveguide modulators

A Y-branch waveguide coupler is characterized by (a) the interaction length L, (b) the coupling coefficient κ, or the conversion length $l = \pi/2\kappa$, the minimum length required to obtain complete crossover, and (c) the mismatch $\delta\beta = \beta_1-\beta_2$ between the propagation constants β_1 and β_2 of the two waveguides. Complete crossover is achieved when the two waveguides are phase matched with $\delta\beta = 0$ and when the interaction length is an exact odd multiple of $(\sqrt{2}/2)\ell$, where ℓ is the coupling length. In order to calculate the interaction length L, the coupling coefficient κ, and the mismatch $\delta\beta = \beta_1-\beta_2$, we need to first determine the waveguide dimensions (w, t) and the waveguide separation (s).

Fig. 7 shows the cross section of the Y-branch waveguide coupler, formed by two parallel identical channel waveguides. We have developed simulation software to determine the required waveguide dimensions (w, t), interaction length (L), and waveguide separation (s) for the proposed electro-optic modulators employing a domain-inverted polymer waveguide coupler and a uniform traveling-wave electrode. There are a few important practical concerns in device design:

a) two channel waveguides in the directional coupler must be in single-mode operation,

b) the waveguide dimension must be close to the single-mode fiber dimension at a desired wavelength to ensure effective optical coupling,

c) the waveguide separation must be large enough for electrode fabrication, and

d) the interaction length and waveguide separation must be optimized to ensure a low driving voltage.

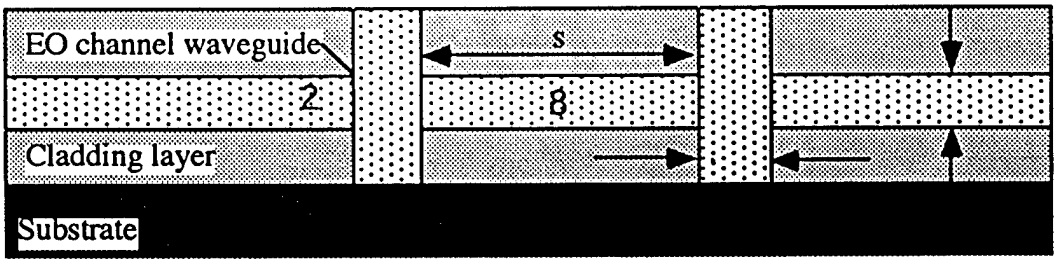

Fig. 7. Schematic diagram of the waveguide directional coupler under consideration.

3.3.1 Waveguide dimensions

The following calculation is to determine the required cutoff dimension for a polymer-based single-mode waveguide, to be used to construct the waveguide directional couplers. Referring to the rectangular channel waveguide shown in Fig. 7, the wave equation involved here can be derived from Maxwell's equations[31-34] as

$$\left(\frac{\partial^2}{\partial x^2}+\frac{\partial^2}{\partial y^2}+\frac{\partial^2}{\partial z^2}\right)E = -k^2n^2E \quad . \tag{8}$$

It has the general solution as a plane wave:

$$E = A\exp j(\omega t + k_x x + k_y y + k_z z) \tag{9}$$

where n is the refractive index of the medium and k is the wave vector. Substituting (9) in (8) corresponding to an individual area in Fig. 7, we have the equations for area 2, 4, 5, 6, and 8 as follows:

$$\begin{cases} +k_{x5}^2 + k_{y5}^2 + k_{z5}^2 = k_5^2 \\ +k_{x4}^2 - k_{y4}^2 + k_{z4}^2 = k_4^2 \\ +k_{x6}^2 - k_{y6}^2 + k_{z6}^2 = k_6^2 \\ -k_{x2}^2 + k_{y2}^2 + k_{z2}^2 = k_2^2 \\ -k_{x8}^2 - k_{y8}^2 + k_{z8}^2 = k_8^2 \end{cases} \tag{10}$$

where $k_i = n_i k_o = 2\pi/\lambda$, and i = 2, 4, 5, 6, 8. The momentum conservation law requires

$$\begin{cases} k_{x5} = k_{x4} = k_{x6} \\ k_{y5} = k_{y2} = k_{y8} \\ k_{z5} = k_{z2} = k_{z4} = k_{z6} = k_{z8} = \beta \end{cases} \quad (11)$$

where β is the effective propagation constant. Combining equations (3) and (4), we obtain

$$\begin{cases} k^2_{x2} = k_5^2 - k_2^2 - k^2_{x5} \\ k^2_{x8} = k_5^2 - k_8^2 - k^2_{x5} \\ k^2_{y4} = k_5^2 - k_4^2 - k^2_{y5} \\ k^2_{y6} = k_5^2 - k_6^2 - k^2_{y5} \end{cases} \quad (12)$$

To satisfy the boundary conditions between these areas, we can get the equations for the waveguide area 5 as[32]

$$\begin{cases} k_{x5}a = p\pi - \tan^{-1}\dfrac{k_{x2}}{k_{x5}} - \tan^{-1}\dfrac{k_{x8}}{k_{x5}} \\ k_{y5}b = q\pi - \tan^{-1}\dfrac{n_5^2 k_{y4}}{n_4^2 k_{y5}} - \tan^{-1}\dfrac{n_5^2 k_{y6}}{n_6^2 k_{y5}} \end{cases} \quad (13)$$

for TM mode, and

$$\begin{cases} k_{x5}a = p\pi - \tan^{-1}\dfrac{n_5^2 k_{x2}}{n_4^2 k_{x5}} - \tan^{-1}\dfrac{n_5^2 k_{x8}}{n_6^2 k_{x5}} \\ k_{y5}b = q\pi - \tan^{-1}\dfrac{k_{y4}}{k_{y5}} - \tan^{-1}\dfrac{k_{y6}}{k_{y5}} \end{cases} \quad (14)$$

for TE mode, where p, q=0,1,2,... are the mode numbers.

For each pair of (p,q), we can get k_{X5} and k_{Y5} by solving equations (12), (13), and (14), to obtain the mode effective propagation constant,

$$\beta = (k_5^2 - k_{x5}^2 - k^2_{y5})^{\frac{1}{2}} \quad (15)$$

and the effective index

$$n_{eff} = \beta / k_0 \quad . \quad (16)$$

According to Eq. (13) and (14), the cutoff widths for TE_{pq} and TM_{pq} modes are

$$a_{cut}^{TM} = \left[p\pi + \tan^{-1}\left(\frac{n_{eff2}^2 - n_{eff8}^2}{n_{eff5}^2 - n_{eff2}^2} \right) \right] / \left[k_0 \left(n_{eff5}^2 - n_{eff2}^2 \right)^{\frac{1}{2}} \right] \qquad (17)$$

and

$$a_{cut}^{TE} = \left[p\pi + \tan^{-1}\left(\frac{(n_{eff2}^2 - n_{eff8}^2) n_{eff5}^2}{(n_{eff5}^2 - n_{eff2}^2) n_{eff8}^2} \right) \right] / \left[k_0 \left(n_{eff5}^2 - n_{eff2}^2 \right)^{\frac{1}{2}} \right] \qquad (18)$$

where $n_{eff5} = 1.55 > n_{eff2} = n_{eff8} = 1.53$ is assumed. The waveguide cutoff width for single-mode operation is calculated as $w = 3.3\ \mu m$ for both TE and TM mode at the wavelength of 1.3 μm. Waveguide thickness $t = 2.5\ \mu m$ is assumed in the calculation. Because the channel is surrounded by the same cladding material, the TE mode and TM mode are degenerate in this symmetric arrangement.

3.3.2. Conventional Y-branch waveguide modulators

For comparison, we start with a conventional Y-branch coupler as shown in Fig. 8. To simplify, we name the switching state, where the light crosses over completely from one guide to the other, the "cross" state ⊗; and the state in which the light passes straight through, appearing at the output of the same guide, the "bar" state ⊖. Application of a voltage V to the uniform traveling-wave waveguide electrode induces a phase mismatch $\Delta\beta(V) = \beta_1 - \beta_2$ between the propagation constants of guides 1 and 2. We describe the light in the two guides by complex amplitudes R(z) and S(z), which vary slowly along the z axis, i.e., the propagation direction.

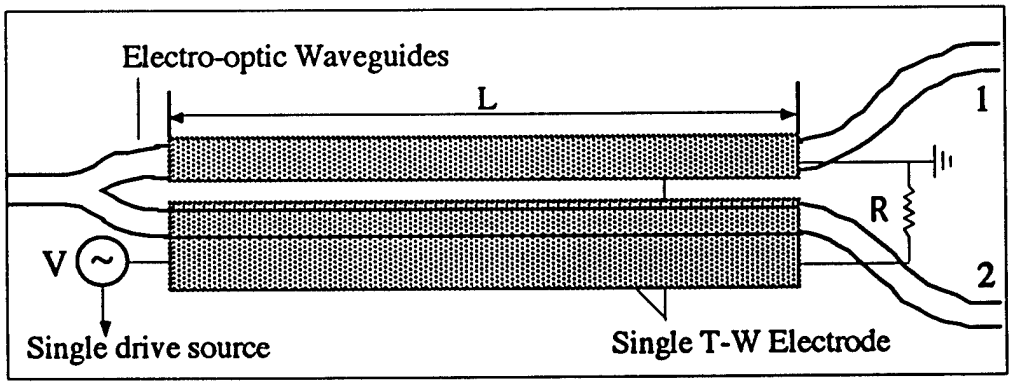

Fig. 8. A 1x2 Y-branch waveguide coupler consisting of two optical channel waveguides with an interaction length L and a uniform traveling-wave electrode.

We assume that the energy exchange between the two guides is governed by the coupled-wave equations[19,31,34]

$$\frac{\partial R}{dz} - j\delta R = -j\kappa S \qquad (19)$$

$$\frac{\partial S}{dz} + j\delta S = -j\kappa R \qquad (20)$$

where $\delta = \Delta\beta/2$ and κ is the coupling coefficient given by,

$$\begin{cases} \kappa = \dfrac{2k_{x2}^2 k_{x1} e^{-qs}}{\beta\omega\left(k_{x1}^2 + k_{x2}^2\right)} \\ \beta = k_0 n_{eff} \\ k_{x2} = \left(n_2^2 k_0^2 - \beta^2\right)^{\frac{1}{2}} \\ k_{x1} = \left(\beta^2 - n_1^2 k_0^2\right)^{\frac{1}{2}} \end{cases} \qquad (21)$$

where $\delta = \Delta\beta/2$. β is calculated by Eq. (15) and $\Delta\beta$ is caused by the driving voltage given by

$$\begin{cases} \Delta\beta^{TM} = \dfrac{1}{2} k_0 n_2^{\,3} \gamma_{33} \dfrac{v}{d} \\ \Delta\beta^{TE} = \dfrac{1}{2} k_0 n_2^{\,3} \gamma_{13} \dfrac{v}{d} \end{cases} \qquad (22)$$

where γ_{13} *and* γ_{33} are electro-optic coefficients, v is the applied voltage, and d is the separation between the two electrodes.

For input amplitudes $R_o = S_o$, in a Y-branch structure, the solution of the coupled-wave equations can be written in the matrix form

$$\begin{bmatrix} R \\ S \end{bmatrix} = \begin{bmatrix} A & -jB \\ -jB^* & A^* \end{bmatrix} \begin{bmatrix} \dfrac{1}{\sqrt{2}} \\ \dfrac{1}{\sqrt{2}} \end{bmatrix} \qquad (23)$$

$$\begin{cases} A = \cos L\sqrt{\kappa^2 + \delta^2} + j\dfrac{\delta}{\sqrt{\kappa^2 + \delta^2}} \sin L\sqrt{\kappa^2 + \delta^2} \\ B = \dfrac{\delta}{\sqrt{\kappa^2 + \delta^2}} \sin L\sqrt{\kappa^2 + \delta^2} \end{cases} \qquad (24)$$

The device is in the cross state when $A - jB = 0$, i.e.,

$$\cos L\sqrt{\kappa^2+\delta^2} + j\frac{\delta-\kappa}{\sqrt{\kappa^2+\delta^2}}\sin L\sqrt{\kappa^2+\delta^2} = 0 \qquad (25)$$

Which implies:

$$\left(\frac{\pi}{l}\right)^2 + \left(\frac{\Delta\beta L}{\pi}\right)^2 = (2n+1)^2 \qquad (n=0, 1, ...) \qquad (26)$$

and

$$\frac{L}{l} = \frac{\Delta\beta L}{\pi} \qquad (27)$$

These conditions lead to some isolated points marked ⊗ in the switching diagram shown in Fig. 9.

The modulator is in the bar states when $A^* - jB^* = 0$, i.e.,

$$\cos L\sqrt{\kappa^2+\delta^2} - j\frac{\delta+\kappa}{\sqrt{\kappa^2+\delta^2}}\sin L\sqrt{\kappa^2+\delta^2} = 0 \qquad (28)$$

which is equivalent to

$$\left(\frac{\pi}{l}\right)^2 + \left(\frac{\Delta\beta L}{\pi}\right)^2 = (2n+1)^2 \qquad (29)$$

and

$$\frac{L}{l} = -\frac{\Delta\beta L}{\pi} \qquad (30)$$

These conditions lead to some isolated points marked ⊖ in the switching diagram shown in Fig. 9.

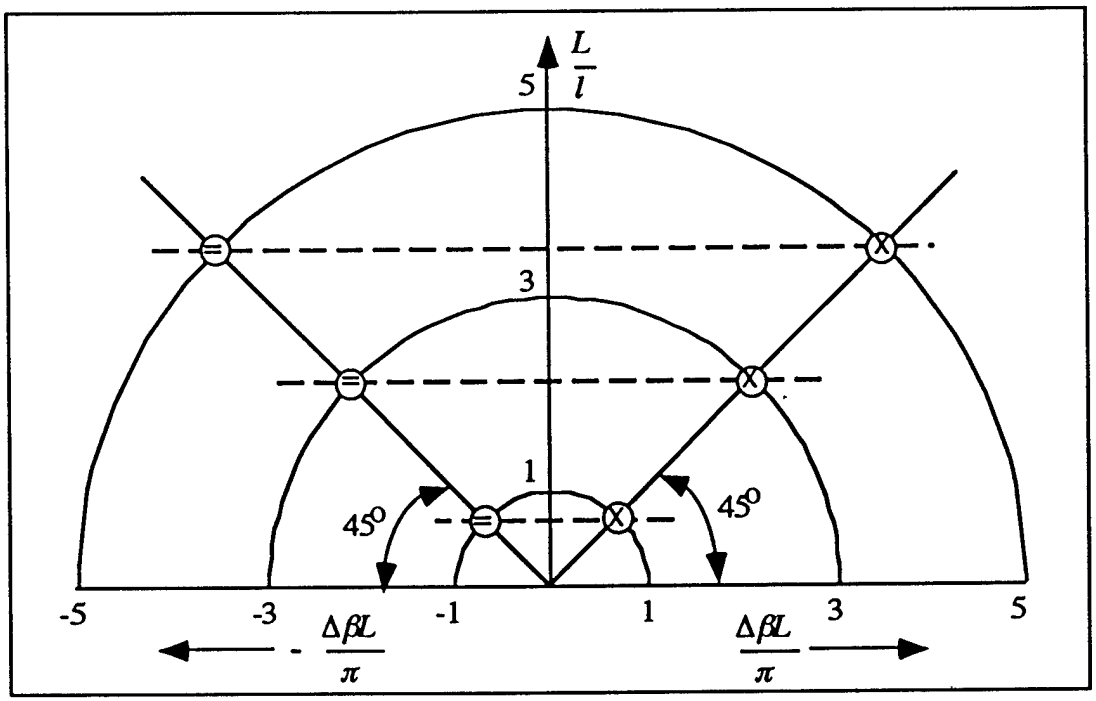

Fig. 9. The switching diagram for a conventional Y-branch waveguide coupler.

The conditions for the cross and bar states can be graphically represented in a switching diagram where we use the values of L/l and $\Delta\beta L/\pi$ as coordinates. According to Fig. 9, the cross states are represented by isolated points on the 45° line through the origin, and the bar states are represented by isolated points on the 135° line through the origin. While in this device configuration the L/l value is essentially independent of the applied voltage, the $\Delta\beta$ values can be controlled electrically. An increase in the voltage moves the point representing the state of the coupler parallel to the $\Delta\beta L/\pi$ axis from left to right. We note that, only for exact odd-integer values of $(\sqrt{2}/2)L/l$, there is always a $\Delta\beta L/\pi$ (voltage) value that will drive a modulator from the bar state to a cross state, i.e., 100% modulation depth can be obtained. However, not all of these solutions can be used as modulators because a modulator requires not only a high modulation depth but also a linearized modulation transfer curve. After checking all the available solutions with L/l up to 15, we have found that only the first point, $L/l = \sqrt{2}/2$ provides a decent linear transfer curve which is similar to that of a conventional directional coupler or Mach-Zehnder interferometer. The modulation efficiency is limited for a linearized modulation for this structure. Fig. 10(a) is the plot of modulation transfer curve for these possible solutions, where $n_{LD-3} = 1.55$, $n_{clad} = 1.53$, w = t = 2.5 μm, s = 7 μm, $\lambda = 1.32$ μm, and $\gamma_{33} = 14$ pm/V. The calculated IMD is plotted in Fig. 9(b) as a function of modulation depth.

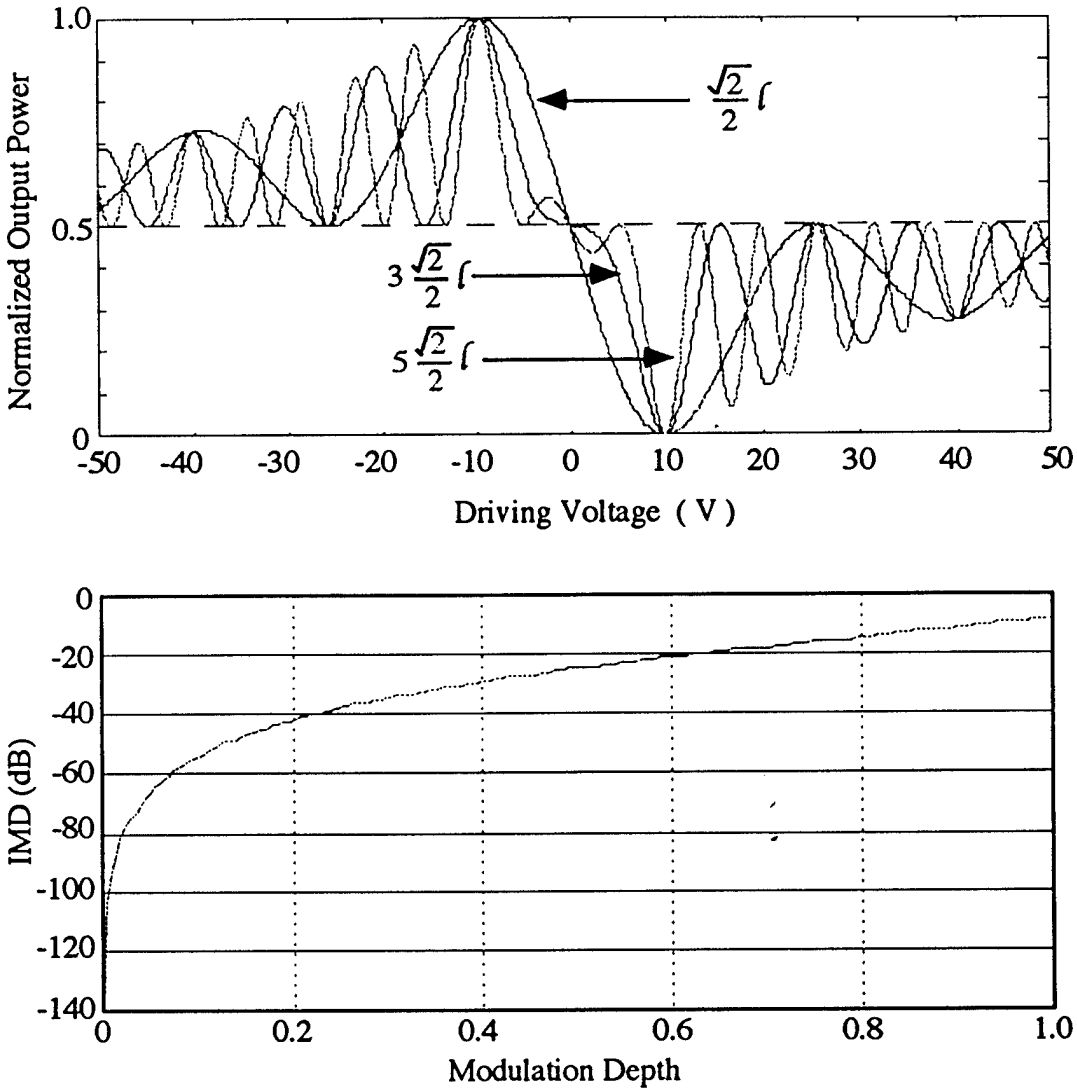

Fig. 10. (a) Plot of modulation transfer curves for conventional Y-branch modulators. (b) The calculated spurious signal as a function of modulation depth.

3.3.3. Domain-inverted Y-branch waveguide modulators

Fig. 11 shows an example of the proposed domain-inverted Y-branch modulator, where the EO polymer-based waveguide coupling region consists of a poled and reverse-poled (domain inverted) section to provide the required $\Delta\beta$ reversal. This $\Delta\beta$ reversal enhances both the modulation linearity and modulation efficiency. In contrast to any existing analog EO modulators[9,29,30], uniform traveling-wave electrodes can be employed for this proposed $\Delta\beta$ reversal structure to ensure the high speed modulation at a simplified device configuration and a relaxed fabrication tolerance. Note that the domain inversion has never before been applied to polymer-based electro-optic modulators. The application of domain-inverted polymers has the

potential to substantially improve the modulation performance with considerable simplification of device configuration. It is important to note that the uniform electrode is much less difficult to fabricate when compared with the conventional phase-reversal electrodes[23,24]. It also makes the impedance matching to a microwave source much easier.

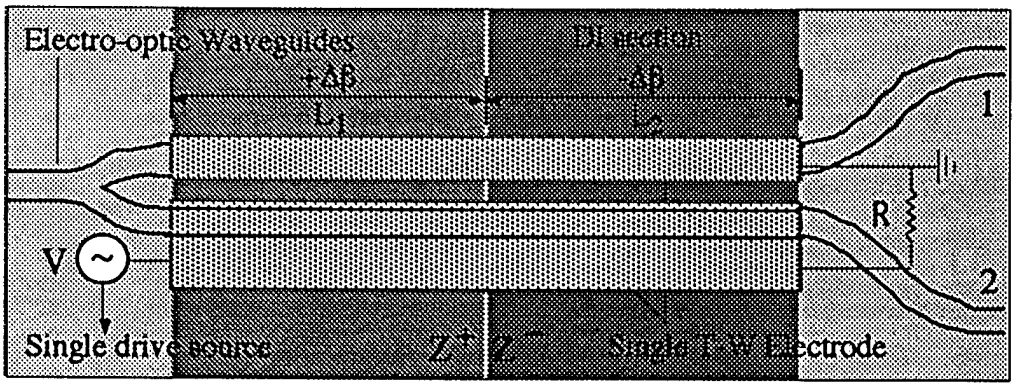

Fig. 11. Schematic diagram of the proposed Y-branch modulator using a uniform electrode in conjunction with two domain-inverted sections.

In this proposed Y-branch modulator configuration, the interaction length L is divided into two equivalent sections. The asynchronism introduced in the two sections is equal in magnitude but reversed in sign, i.e., we have $+\Delta\beta$ in the left section and $-\Delta\beta$ in the right section. The figure indicates the proposed innovative technique to achieve the $\Delta\beta$ reversal based on domain inversion.

For input amplitudes $R_o = S_o$, the solution of the coupled-wave equations can be written in the matrix form

$$\begin{bmatrix} R \\ S \end{bmatrix} = \begin{bmatrix} A^* & -jB \\ -jB^* & A \end{bmatrix} \begin{bmatrix} A & -jB \\ -jB^* & A^* \end{bmatrix} \begin{bmatrix} \frac{1}{\sqrt{2}} \\ \frac{1}{\sqrt{2}} \end{bmatrix} \tag{31}$$

The device is at a cross state when

$$\left(|A|^2 - |B|^2\right) - j\left(2A^*B\right) = 0. \tag{32}$$

Substituting Eqs. (24) in (32), we get

$$\cos^2 \frac{L}{2}\sqrt{\kappa^2+\delta^2} + \frac{\kappa^2-\delta^2-2\kappa\delta}{\kappa^2+\delta^2}\sin^2 \frac{L}{2}\sqrt{\kappa^2+\delta^2} - j\frac{\kappa}{\kappa^2+\delta^2}\sin L\sqrt{\kappa^2+\delta^2} = 0 \tag{33}$$

which corresponds to

$$\left(\frac{\pi}{l}\right)^2 + \left(\frac{\Delta L}{\pi}\right)^2 = 4(2n+1)^2 \qquad (34)$$

and

$$\frac{L}{l} = \pm(\sqrt{2}-1)\frac{\Delta\beta L}{\pi} \qquad (35)$$

These conditions result in some isolated points as marked ⊗ in the switching diagram of Fig. 12.

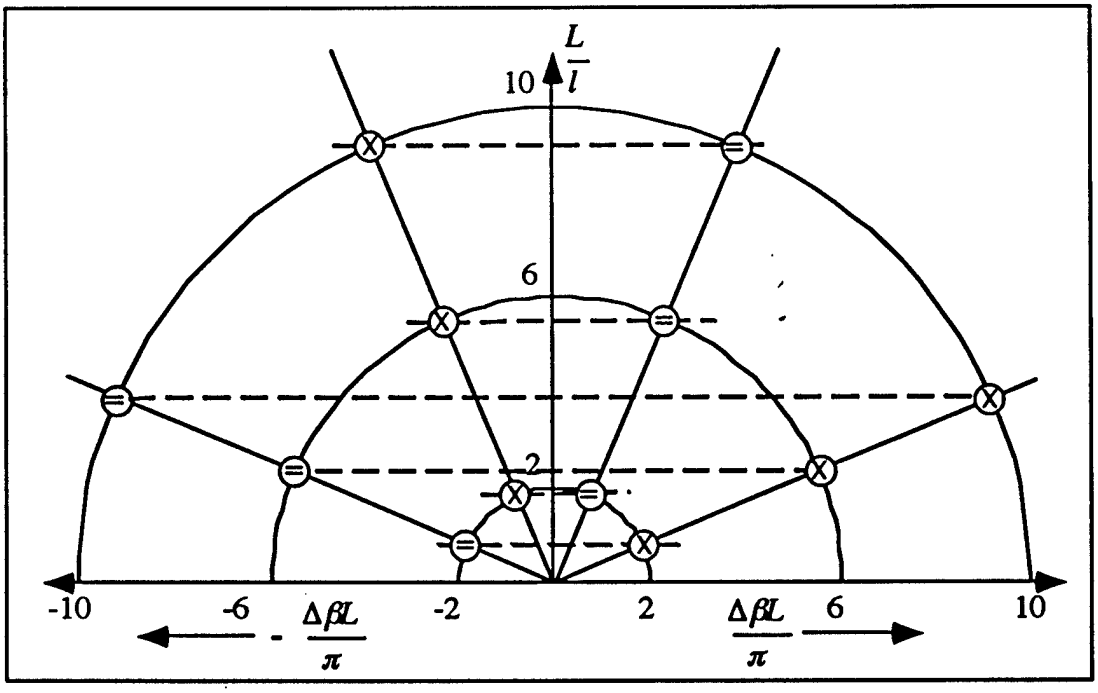

Fig. 12. Switching diagram for a domain-inverted Y-branch waveguide modulator.

The device is at a bar state when

$$\left(|A|^2 - |B|^2\right) - j(2AB) = 0 \ . \qquad (36)$$

Substituting Eqs. (24) in (36), we have

$$\cos^2\frac{L}{2}\sqrt{\kappa^2+\delta^2} + \frac{\kappa^2-\delta^2+2\kappa\delta}{\kappa^2+\delta^2}\sin^2\frac{L}{2}\sqrt{\kappa^2+\delta^2} - j\frac{\kappa}{\kappa^2+\delta^2}\sin L\sqrt{\kappa^2+\delta^2} = 0 \quad (37)$$

The solution of this condition is

$$\left(\frac{\pi}{l}\right)^2 + \left(\frac{\Delta L}{\pi}\right)^2 = 4(2n+1)^2 \qquad (38)$$

and

$$\frac{L}{l} = \pm(\sqrt{2}+1)\frac{\Delta\beta L}{\pi} \quad , \qquad (39)$$

which leads to some isolated points marked ⊖ in the switching diagram of Fig. 12.

According to Fig. 12, the cross states are represented by isolated points on the 22.5° line and 112.5° line through the origin, and the bar states are represented by isolated points on the 67.5° line and 157.5° line. For the suitable L/l values, increasing driving voltage moves the point representing the state of the coupler parallel to the $\Delta\beta L/\pi$ axis from left to right. Only for exact integer values 2, 6, 10 of $\sin(22.5°)L/l$, is there always a $\Delta\beta L/\pi$ (voltage) value that will drive a modulator from the bar state to a cross state, i.e., 100% modulation depth can be obtained. This switching diagram also indicates that the driving voltage is independent of the device interaction length since the ratio of $(L/l)/(\Delta\beta L/\pi)$ has to be a constant, either tan(67.5°) or tan(22.5°) for achieving 100% modulation depth. Not all of these solutions can be used as modulators because a modulator requires not only a high modulation depth but also a linearized modulation transfer curve. After checking all the available solutions with L/l up to 10, we have found that $L/l = 6\sin(67.5°)$ provides an excellent linear transfer curve. The modulation efficiency is nearly 100% for a linearized modulation for this domain-inverted structure.

Fig. 13(a) is a plot of the modulation transfer curve. The calculated spurious signal is plotted in Fig. 13(b) as a function of modulation depth. Unlike conventional Y-branch modulators that have a poor optical modulation depth and nonlinear modulation transfer curve (sine-squared behavior), the proposed domain-inverted modulators can provide a highly linearized modulation transfer curve while ensuring a near-lossless conversion (100% modulation depth) of analog electronic signals to the optical signals. Such a high modulating performance (-30 dB nonlinear distortion and ~100% modulation depth) is based on the innovative approach of domain inversion (See Fig. 13). Conventional modulators can only provide -20 dB nonlinear distortion with modulation depth less than 70% for a linearized operation. Note that modulating efficiency is defined by modulation depth: 10% optical modulation depth equals 10% efficiency, 100% modulation depth equals 100% efficiency. Highly efficient and linearized conversion of RF

carrier-based signals to optical carrier-based signals is of paramount importance for the BMDO and Air Force applications.

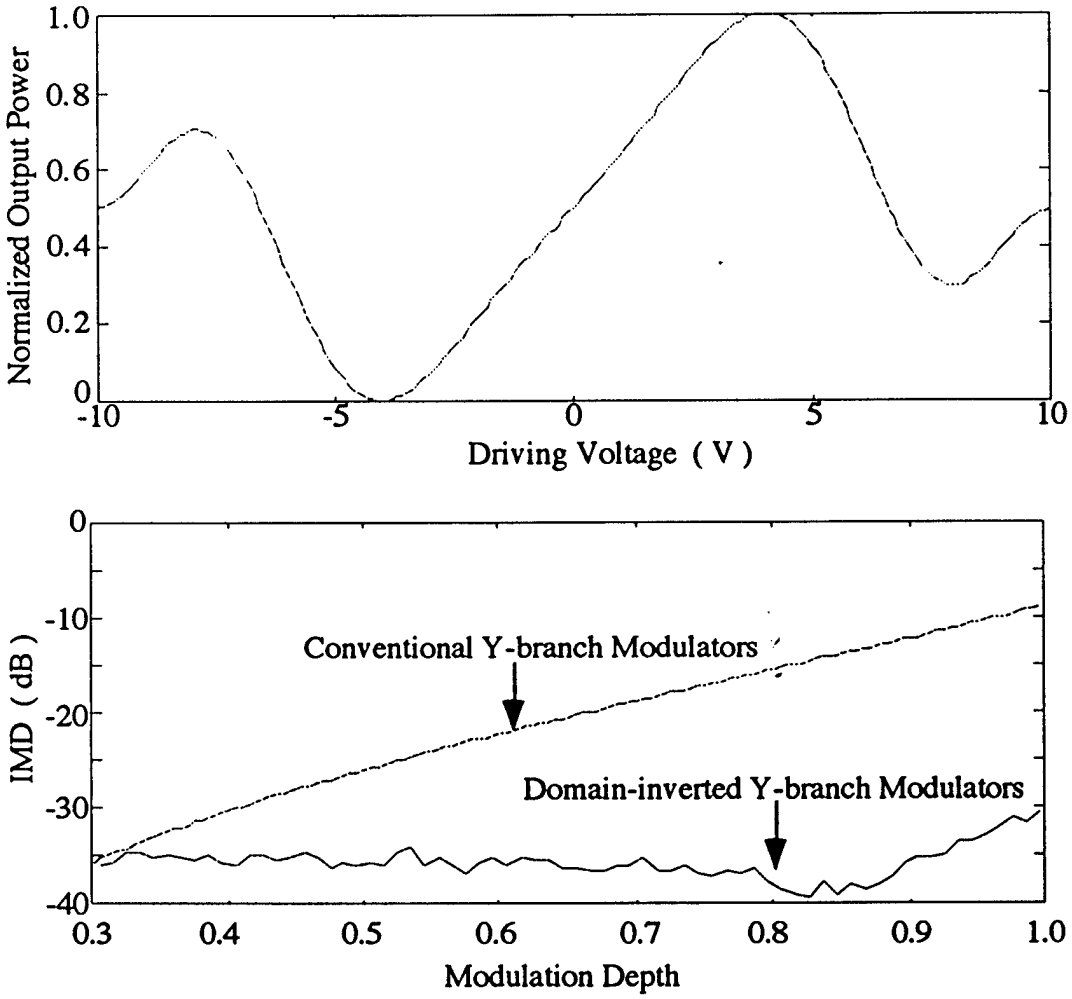

Fig. 13. (a) Modulation transfer curve of the proposed domain inverted Y-branch waveguide modulator for selecting $L = 6\sin(67.5°)\ell$. (b) Spurious signal for the proposed modulator.

To compare the switch diagrams (Fig. 9 and Fig. 12) for both a conventional Y-branch modulator and a domain-inverted Y-branch modulator, there are always more choices for finding a device interaction length L that will drive the device between bar state and cross state. The driving voltage for domain-inverted Y-branch can be 2.4 times lower than that for the conventional one when the solutions of bar and cross states are chosen from the two 67.5° and 112.5° lines. As shown in Fig. 9 the solutions of bar and cross states can only be chosen from the two 45° and

135° lines. The improvement of driving voltage can be seen by comparing the Fig. 10(a) and Fig. 13(a), where the same modulator parameters are used for the simulation.

3.3.4. Improvement of linearity and suppression of nonlinear distortions.

When sinusoidal modulation signals are applied to an electro-optic modulator, the spectrum of output light is known to contain, in general, both terms oscillating at the input signal frequencies (fundamental output) and those with frequencies represented by a set of combinatorial products (nonlinear distortions). Depending on a specific practical analog system, it is customary to distinguish between harmonic and intermodulation nonlinear distortions (IMD) that limit the linear performance in systems with multiple input signals such as CATV links.

The presence of nonlinear terms with frequencies within the detection bandwidth can severely degrade the dynamic range. It is well known that even-order distortions can be effectively suppressed by biasing the modulator to the inflection point of the modulation curve[37]. As pointed out above, the Y-fed coupler is automatically biased to this 3 dB point due to its symmetry. In this case, the dynamic range is determined by the third-order nonlinear products that include, in general, harmonic and intermodulation spectral components both resulting from the cubic nonlinearity of the transfer curve. The harmonics can be filtered out by using a finite bandwidth of photodetection. IMD, on the other hand, can fall into the detection bandwidth.

In order to determine the level of 3rd-order intermodulation products, Fourier analysis of the device response was performed. To characterize the level of IMD, the ratio P_{fund}/P_{IMD} of the fundamental output to 3rd-order IMD is used on account of its invariance to the noise level in a particular analog optical system. Compared to the dynamic range[37], it, therefore, represents a more universal criterion for characterizing device nonlinearity in the frequency domain. The level of IMD suppression can be determined at a specific level of optical modulation depth. Fig. 14 shows (a) the modulation transfer curve, (b) optical output signals, (c) output spectrum in the frequency domain and (d) the nonlinear intermodulation distortion for a conventional Y-branch waveguide modulator. In plotting Fig. 14, two RF signals with two tone frequencies of f_1 = 1 GHz, f_2 = 1.4 GHz were used and spurious signals present the third-order IMD at 1.8 GHz ($2f_2$-f_1) and second harmonic at 2.0 GHz ($2f_1$).

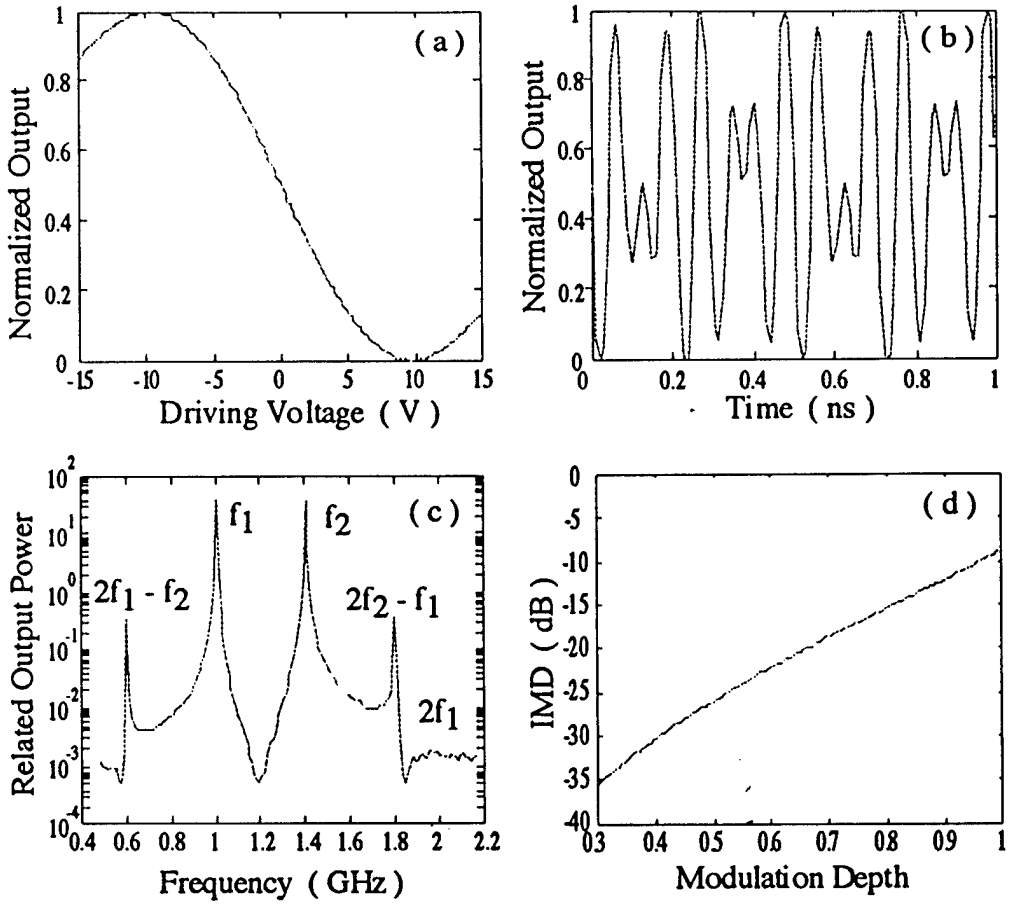

Fig. 14. (a) The modulation transfer curve, (b) optical output signals, (c) output spectrum in the frequency domain and (d) the nonlinear intermodulation distortion for a conventional Y-branch waveguide modulator.

Fig. 15 shows the calculated figures for the proposed domain-inverted Y-branch waveguide modulators. As shown in both Fig. 14(c) and 15(c), the second harmonic distortion is suppressed by the Y-branch structure that automatically biases the modulator to the 3 dB inflection point of the modulation curve. The third-order IMD sets the device limit on linearity. Because the domain inversion, the conventional modulation transfer curve is adjusted to a linearized transfer curve. By comparing Fig. 14(d) and 15(d), it can be seen that the proposed domain-inverted modulator has more than 20 dB (100 times) improvement in modulation linearity for ~100% modulation efficiency. The nonlinear intermodulation distortion is less than 30 dB for the proposed domain-inverted modulators.

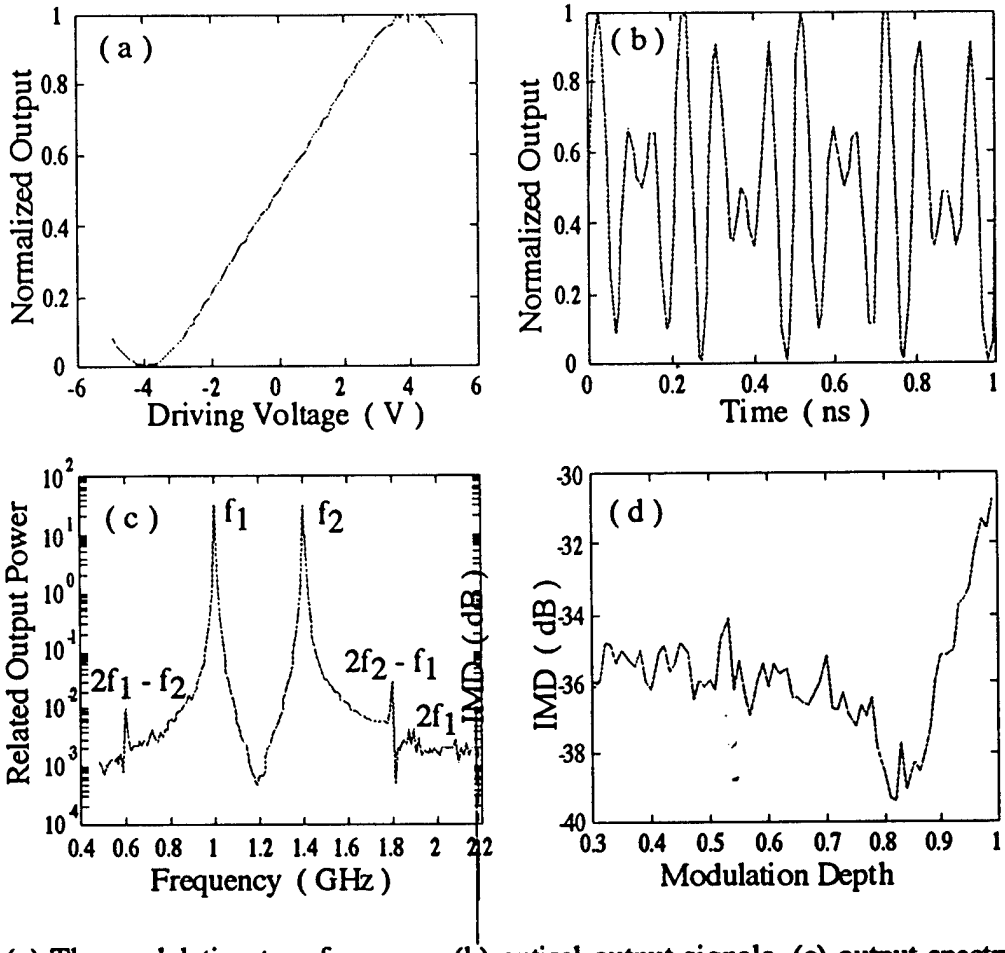

Fig. 15. (a) The modulation transfer curve, (b) optical output signals, (c) output spectrum in the frequency domain and (d) the nonlinear intermodulation distortion for the proposed domain-inverted Y-branch waveguide modulator. More than 20 dB improvement in IMD level occurs for ~100% modulation efficiency.

In order to estimate device tolerance to fabrication deviations, we calculated IMD level over a broad range of values of the interaction-length-to-coupling length ratios L/ℓ. Apparently, the two-section domain -inverted Y-branch coupler is superior to the conventional one in that it provides a linearized modulation transfer curve, ~100% modulation efficiency, and low driving voltage using a single uniform electrode.

In Phase II, our task will be to characterize the level of IMD and to optimize the structural parameters of the modulator in order to achieve the maximum suppression. Two-tone measurements of the IMD level are to be performed using a setup that comprises two sweepers with a frequency range in the 40 GHz region and an electrical signal spectrum analyzer as shown in Fig. 16. A low-noise optical source should be used to ensure a broad usable range of

measurements. The frequencies of the sweepers should be offset and their outputs are applied to the same electrodes. The modulated optical output is detected with a low-noise photodetector whose output is fed to the spectrum analyzer. The IMD level is detected at the frequency of one of the intermodulation products as a function of the amplitude of the modulating signals. Narrowband highly-selective electrical filters may be required after the sweepers to avoid the influence of nonlinear distortion in the spectrum of the modulating signals on the measured values of the IMD level.

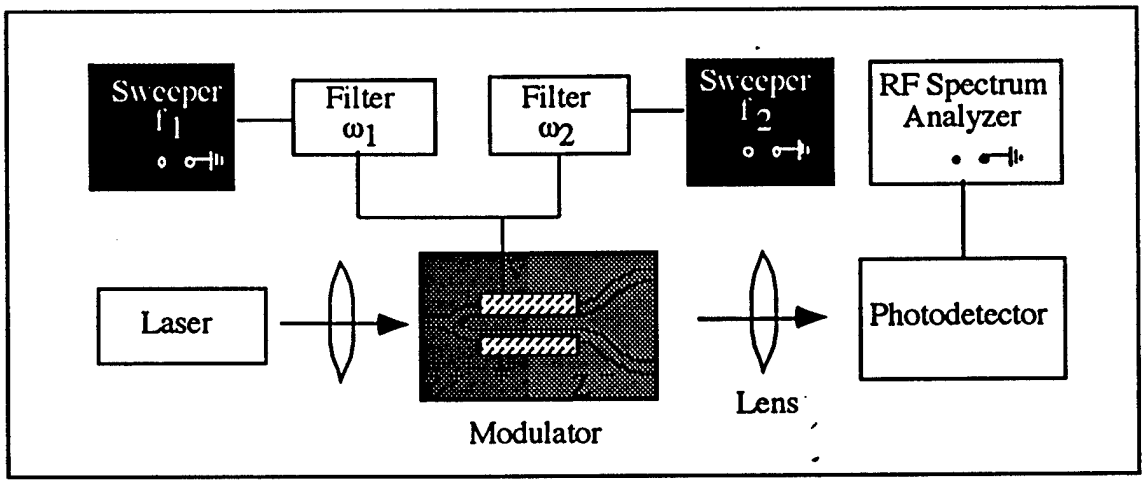

Fig. 16. Experimental setup for two-tone measurement of intermodulation distortion.

3.3.5. Completely polarization-independent modulator based on four domain-inverted sections

We have shown that Y-branch waveguide modulators can be fabricated with improved linearity over 100% modulation depth at a reduced driving voltage by employing domain-inverted polymers. We will show that simultaneous modulation for both TE and TM states of polarization can be further obtained with four domain-inverted sections. Because the electro-optic coefficients are different for TE and TM modes, the electrically induced phase mismatches ($\Delta\beta$) are different for TE and TM modes in an EO waveguide, as calculated in Eq. (22). This results in a polarization-sensitive device that is difficult to use in a fiber optic transmission link, where the input state of polarization is random. In other wards, TE and TM modes cannot be modulated simultaneously from a cross state to a bar state at the same time by a single driving voltage.

To achieve the desired polarization-independent operation with a large dynamic range, Fig. 17 is presented to show the sketch of the proposed modulator in which the interaction length is divided into four equivalent sections with four consecutive 90° domain rotations. The figure

indicates the proposed innovative technique for achieving the $\Delta\beta$ reversals for both TE and TM modes based on two two-section domain inversions, one in the waveguide plane and another in the waveguide transverse plane as indicated in Figure 17. The directions of the four domains are clearly indicated at the bottom of the figure

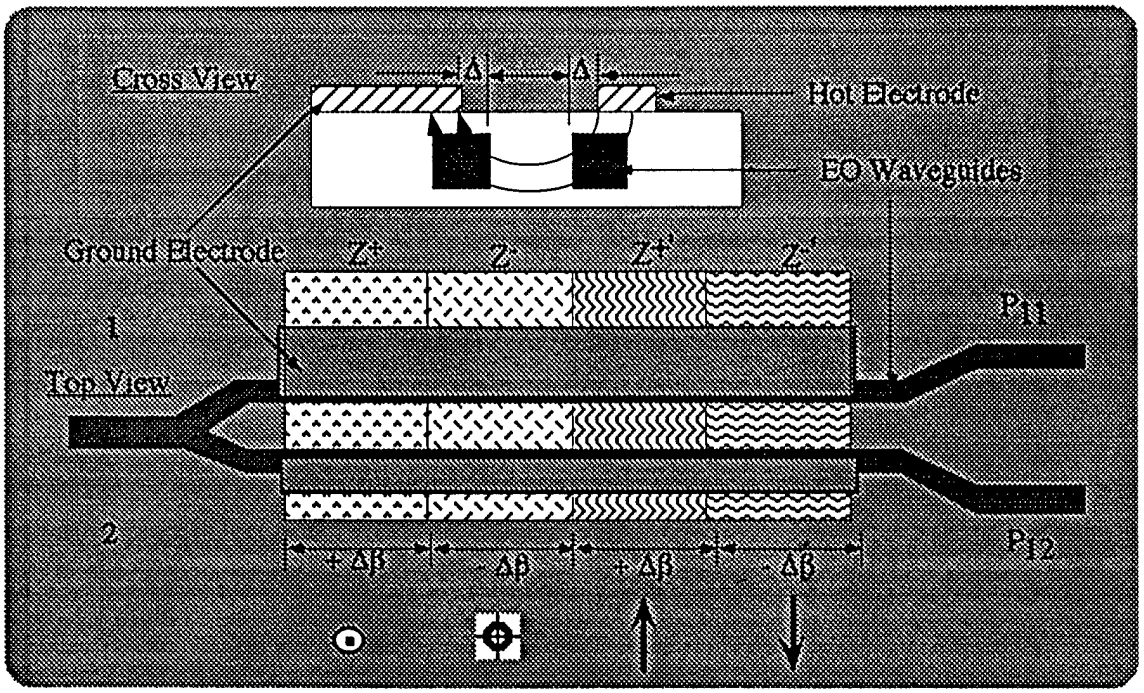

Fig. 17. A polarization-independent Y-branch waveguide modulator using domain-inverted polymers and uniform electrodes. Note that the ground electrode and hot electrode are shifted by a small distance Δ, with respect to the waveguide directional coupler, in order to provide electric field for both TE and TM modes. Double two-section domain inversions, one in the waveguide plane and another in the waveguide transverse plane, are employed.

The coupling matrices M^+ and M^- for a section with conventional domain and inverted domain are given by[19],

$$M^+ = \begin{bmatrix} A & -jB \\ -jB^* & A^* \end{bmatrix} \qquad (40a)$$

$$M^- = \begin{bmatrix} A^* & -jB \\ -jB^* & A \end{bmatrix} \qquad (40b)$$

For the effective coupling matrix of the four sections in this configuration, we obtain

$$M = M^- \cdot M^+ \cdot M^- \cdot M^+ \qquad (41)$$

where M_1^+ and $M_1^{+'}$ are given by Eq. (40a), and M_1^- and $M_1^{-'}$ are given by Eq. (40b) by putting $z = L/4$.

For the TE mode,

$$\Delta\beta^{TE} = \frac{3}{4} k_o n_2^3 \gamma_{33} \frac{v}{d} \qquad (42)$$

when calculating M_1^+ and M_1^-, and

$$\Delta\beta^{TE} = \frac{3}{4} k_o n_2^3 \gamma_{13} \frac{v}{d} \qquad (43)$$

when evaluating $M_1^{-'}$ and $M_1^{+'}$.

For the TM mode

$$\Delta\beta^{TM} = \frac{3}{4} k_o n_2^3 \gamma_{13} \frac{v}{d} \qquad (44)$$

when considering M_1^+ and M_1^-, and

$$\Delta\beta^{TE} = \frac{3}{4} k_o n_2^3 \gamma_{33} \frac{v}{d} \qquad (45)$$

when evaluating $M_1^{-'}$ and $M_1^{+'}$. It is easy to demonstrate that the transfer matrices are identical for both the TE and TM mode. As a result, the device shown in Fig. 17 is completely polarization-independent without requiring any electrical adjustment.

We have developed a simulation model for the proposed high performance EO modulators based on domain-inverted polymer waveguides. Based on the simulation, we concluded that the two-section domain-inverted waveguide Y-branch is the preferred choice for practical implementation. In this device, a high optical modulation efficiency, linearized modulation transfer curve, very low driving voltage, and relaxed sensitivity to fabrication tolerances can be achieved if domain-inverted polymer is employed. Yet another advantage is that the designed structure can be fully compatible to a single drive microwave source to ensure high speed operation.

3.4 Fabrication of Y-branch Waveguide Using EO Polymers

Unlike inorganic crystal-based systems where each fabrication process is substrate-dependent, an EO polymer-based modulator is transferable to any substrate of interest. From the system implementation point of view, such a flexibility greatly enhances the integrability of discrete devices into an optoelectronic system. A universal guided wave modulating module can be built on any substrate of interest. Furthermore, electro-optic polymers exhibit a low and nondispersive dielectric constant. Very high-speed traveling-wave modulators can be made from these materials with simple planar-circuit structures because of the close velocity match between the light wave and the microwave. On the other hand, both $LiNbO_3$ and III-V compound semiconductors have a dielectric constant much larger than that of EO polymeric materials. Better performance with cost-effectiveness with EO polymer-based modulators is expected. The most reliable EO polymer LD-3 crosslinkable polymer that is commercially available from Adtech will be used for this program. It has a proven reliability to over 1000 hours at 180°C.

Among all the feasible methods of synthesizing EO polymer films, crosslinked polymers offer the promise of the best long term temporal stability and chemical resistance. A crosslinkable nonlinear optical (NLO) polymer matrix is needed for processing into high optical quality thin films. The crosslinking process imposes more stringent requirements on the solvents. The process of searching for a better solvent for a crosslinkable NLO polymer is described below. Two phenomena that can occur during the fabrication of electro-optic waveguides from crosslinkable polymers are reported. One is the crystallization of the crosslinker. By anchoring the small crosslinker molecules to the long-chain NLO polymer and precuring the optical adhesive, excellent optical quality LD-3 EO polymer waveguides are prepared.

3.4.1 The uniqueness of the LD-3 EO polymer

Although today's dominant electro-optic devices are still made from inorganic materials such as lithium niobate, it is difficult to integrate these devices with electronic circuits that are usually fabricated on semiconductor wafers. This difficulty prevents reduction of the fabrication cost and hence the wide-spread use of these devices. Compared with their inorganic counterparts, nonlinear optical (NLO) polymeric materials have several well recognized advantages such as compatibility with different substrates, ease of fabrication, and possibly low cost. As a result, many NLO polymers have been synthesized in recent years[39-43]. However, progress in fabricating practical devices has been impeded by the lack of processability of these polymeric materials. A low-loss waveguide with a high and stable NLO coefficient is needed for any

practical device. NLO polyimide materials offer the best stability; however, the polyimide materials that possess optical nonlinearities have relatively high optical losses (>3 dB/cm). Often the losses and processability remain unreported[40]. Other materials do not possess the thermal stability for satisfying commercial or military requirements[44]. Much higher stability can be achieved by crosslinking two ends of an NLO chromophore into the polymer network. Although much effort has been made, only a few NLO materials have achieved long term stability near or up to 100 °C[39-41,43] and LD-3 EO polymer turns out to have a long-term thermal stability satisfying the military requirement of -55 °C to +125 °C[44]. LD-3 is a thermally crosslinkable NLO polymer consisting of a poly (methyl methacrylate) (PMMA) backbone and an azobenzene-sulfone chromophore (Fig. 18(a)). It can be crosslinked by using diisocyanate as the small crosslinker. Using dianisidine diisocyanate (Pfaltz &Bauer, Inc.) as the crosslinker (Fig. 18(b)), an r_{33} value of 13 pm/V at 633 nm was achieved, and a long-term stability at 125 °C was proven through annealing a sample at this temperature for over 1250 hours[45].

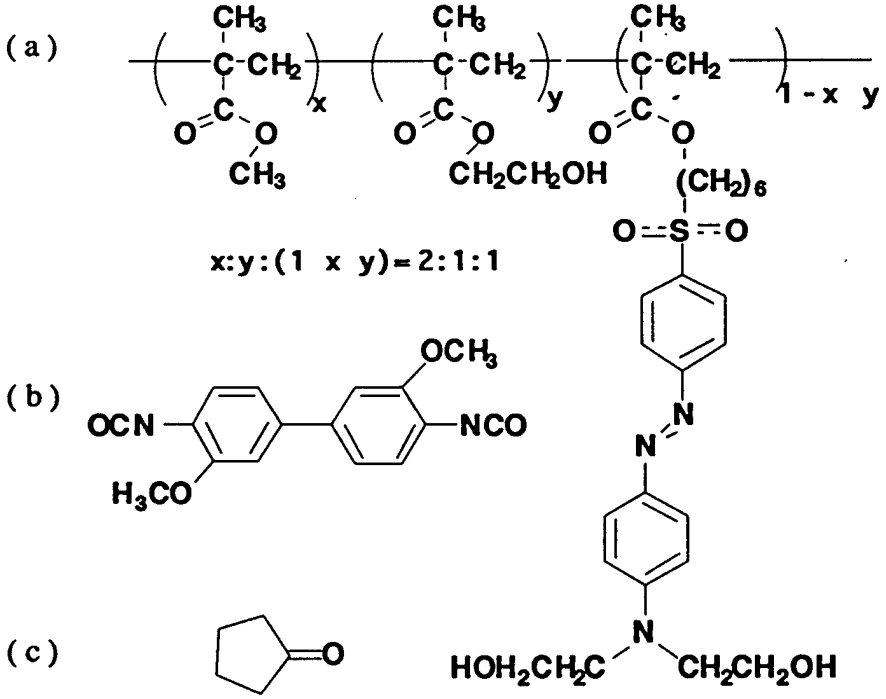

Fig. 18. (a) Structure of an LD-3 polymer, (b) a diisocyanate crosslinker, and (c) a cyclopentanone.

It is both technically and commercially interesting to use crosslinkable NLO polymers to fabricate guided wave EO devices. However, only very few materials have been used in making

useful devices[41,43,46,47]. The excellent stability and the good EO coefficient of the LD-3 polymer make it an ideal candidate for fabricating EO polymer devices. The key part of fabricating LD-3 based NLO polymer-based waveguide modulators is the preparation of thin films from this polymer. For a crosslinkable polymer using a crosslinker, we need to first dissolve the polymer and the crosslinker together to make a spin-coatable solution. Then the chromophores need to be aligned into a noncentrosymmetric order through a poling process to obtain a second-order optical nonlinearity. The alignment of the chromophores is accomplished by applying a high electric field across the film, while heating the film to above the glass transition temperature T_g of the polymer. The alignment is fixed by crosslinking both of the ends of a chromophore into the polymer network at an elevated temperature.

For any NLO polymer, a compatible cladding material is also important for fabrication of low-loss waveguides. Optically, it should have a lower refractive index than the NLO polymer and low absorption at the working wavelength; electrically, it should be more conductive than the NLO polymer at the poling temperature to ensure a poling voltage can be effectively applied across the NLO polymer layer; chemically, it should be resistant to the acid and solvents used in the photolithography process for patterning the waveguide channels and the modulation electrodes. A good choice to use is optical adhesive because the data on the refractive indices, solvent resistance, and thermal stability are available. However, such adhesives are mostly in a liquid state and the films obtained by direct curing usually show wavy surfaces. Therefore, it is significant to understand the cause of the waviness and to find a solution.

3.4.2 Selection of A Better Solvent

A solvent for a crosslinkable NLO polymer must be compatible with all the fabrication processes. It should have good solubility of both the NLO polymer and the crosslinker, react neither with the polymer nor the crosslinker, and should not cause any other side effects. To avoid unwanted crosslinking before poling, the solvent should also be able to be removed by vacuum drying. The lack of an appropriate solvent for LD-3 caused the failure in the first attempt at fabricating a low-loss planar waveguide out of the LD-3 polymer[45]. The only solvent previously reported is tetrahydrofuran (THF), which was also suggested to us by the material supplier. However, due to the high volatility of THF, it is not easy to make smooth films thicker than 0.5 μm[45]. Such a thin film is not useful in making devices because the insertion loss is very large. Even if other kinds of losses are neglected, the coupling loss would make a device unacceptable as simply realized by considering the mismatch of the mode profiles between a 0.5 μm waveguide and a single-mode optical fiber, which typically has a mode diameter from 5 to 10 μm. It is

important to understand the dominating interactions in the polymer in order to find a good solvent since the interaction among the molecules in a solution determines the solubility of a solute in a solvent. High solubility is possible when the interactions among the molecules in the solute are similar to those in the solvent. For polymers with known solubility parameters, a compatible solvent can be found among the solvents that have solubility parameters close to those of the polymers. The LD-3 polymer is a long chain polymer (Fig. 18(a)). The many OH groups in the polymer produce strong hydrogen bonding and the push-pull structure of the NLO chromophore results in a very strong dipole-dipole interaction in the polymer. It is well known that some long chain polymers with many OH groups such as polyvinyl alcohol and polyacrylic acid can only be dissolved in water or alcohol. Therefore the difficulty of dissolving LD-3 polymer into some commonly used NLO polymer solvents such as cyclohexanone, dioxane, and chloroform is understandable. Our results show that the solubility of LD-3 polymer at room temperature is less than 10% (weight percentage) in cyclohexanone, very poor in dioxane, and actually zero in chloroform. The solubility in THF is better, but no more than 20%. The crosslinking process prohibits the use of any solvent that reacts with the crosslinker. Thus water or any alcohol has to be excluded. Considering the strong hydrogen-bonding interaction and dipole-dipole interaction in the polymer, we chose other solvents with vapor pressures lower than that of THF, but with stronger hydrogen bonding and a dipole-dipole interaction. More than 10 solvents have been tested and several solvents do have good solubility for LD-3 polymer. However, most are not compatible with the film fabrication. For example, pyridine offers good solubility (>20%) to LD-3, but it catalyzes the crosslinking reaction between the polymer and the crosslinker and therefore makes the solution turn quickly into a useless gel before spin-coating can be carried out. After ruling out these solvents, which are either chemically reactive or difficult to remove, only one solvent, cyclopentanone, remains. The structure of cyclopentanone is shown in Fig. 18(c). The solubility of LD-3 polymer in cyclopentanone is measured to be higher than 50%. The dissolving speed of the LD-3 polymer in cyclopentanone is very slow. To prepare a high concentration solution, we let the solution sit overnight to allow the polymer to be totally dissolved. This might explain why other researchers have not found cyclopentanone to be a compatible solvent for the LD-3 polymer, although it is not an uncommon solvent.

Thicker films are fabricated using cyclopentanone as the solvent than with the previously used solvents. The films are prepared by dissolving both the polymer and crosslinker in the solvent. The solution is then filtered and spin coated onto silicon wafers, or onto indium-tin-oxide (ITO) coated glass slides for measuring the EO coefficients. The ratio of the crosslinker to the polymer is 60:100 in weight. This ratio ensures the chromophores are fully crosslinked and hence ensures a high thermal stability. The resulting films have thickness from 1.2 μm to 2.4 μm, which

is determined by an Alpha Step 200 surface profiler. Such a thickness provides us with a single-mode waveguide with the lowest waveguide loss due to the well-above cut-off condition.

3.4.3 Elimination of Recrystallization

The crystallization of the crosslinker on the film surface is another obstacle. This phenomenon also bothers other researchers working on the same material. Fig. 19(a) shows a microscope picture of the grains of crystallized crosslinker formed on an LD-3 film surface. The crystals form tree-branch patterns on the polymer surface. Usually there are more crystals formed along the edge of the silicon wafer than at the center. In extreme cases, the tree-shape pattern can cover areas of several square centimeters in total along the edge. We have tried other substrates, including glass slides, metals, and polymers, but the crystallization always occurs. Therefore, it is not a problem of substrates. To solve this problem we carefully investigated when the crystallization occurred. The grains are formed during drying of the film in vacuum. This indicates that the crystallization occurs when the solvent is being removed from the film and there is a phase segregation between the polymer and the crosslinker during this process. The role of the solvent in the crosslinker crystallization is not clear, but the phase segregation is dictated by the free energy of the system of the crosslinker and the polymer. If the crystallization of the crosslinker lowers the free energy of the system, it will occur no matter what solvent is used. This means the solid solubility of the crosslinker in the LD-3 polymer is low. One way to solve this problem is to reduce the crosslinker to polymer ratio. However, the ratio is determined by the stoichiometry of the crosslinking reaction and does not allow change. Another way is to use other crosslinkers that might have higher solid solubility in the LD-3 polymer. Since this will change the composition of the resulting films, the stability of the NLO properties may also change. Some other crosslinkers tested do result in inferior stability[45].

The slow reaction between the polymer and crosslinker in the solution gives a clue for solution of this problem. Clearly there are three competing processes: the polymer-crosslinker reaction, the solvent evaporation, and the crosslinker diffusion and crystallization. If the polymer-crosslinker reaction rate could consume enough crosslinkers so that the concentration of the free crosslinkers can be maintained lower than the solubility of the crosslinker in the polymer-crosslinker-solvent system during the solvent evaporation process, then the crosslinker would not be crystallized. The simplest way to do this is by slowing down the solvent evaporation speed during vacuum drying. However, there might be another problem. Once the crosslinker has had enough time to react with the polymer, most of the chromophores might be crosslinked before poling. There might be a possibility that only one of the two ends of a crosslinker reacts with the

LD-3 polymer within a certain period of time, so that the segregation of the crosslinker is not possible. One end reaction with the chromophore can still be aligned by electric-field poling, because a crosslinking bridge forms only when both of the ends of a crosslinker react. Statistically, it is not possible to have all the crosslinker at a single end. However, if the crosslinking density is very low (for e.g., <1%), there will be no appreciable decrease in the EO coefficient. Different levels of vacuum, from 10^{-2} torr to 1 torr, are used to control the evaporation rate. When a vacuum of 1 torr is used, good films free from crystal dots of the crosslinker are consistently obtained (Fig. 19), when observed under a microscope. For higher vacuum, some crystal dots always appear on the film surface. Of course, a longer drying time is needed when the vacuum is lower. About 48 hours are needed to totally dry the films with 1 torr vacuum.

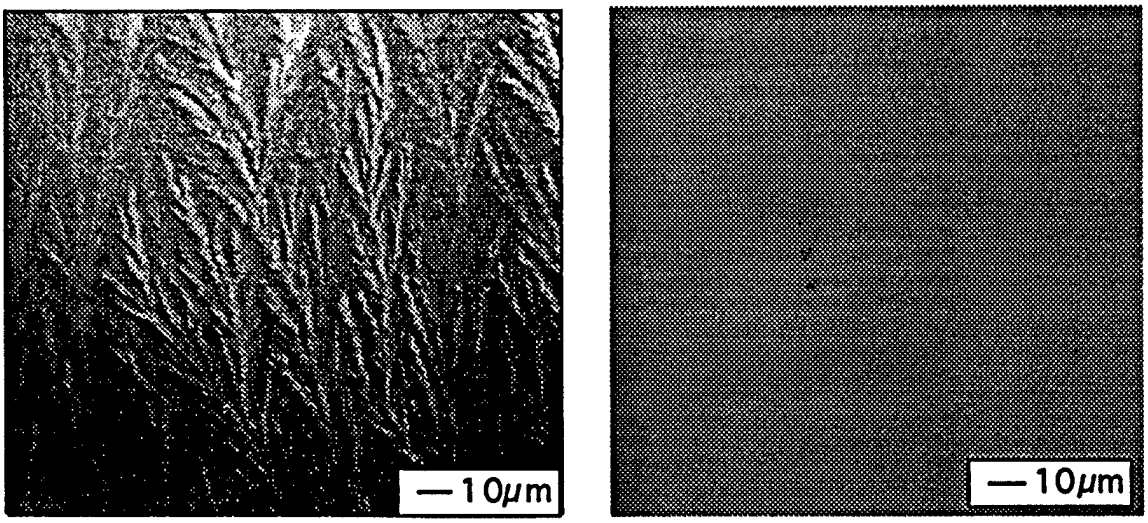

Fig. 19. (a) Tree-branch pattern of crosslinker-crystal grains formed on an LD-3 film due to fast removal of the solvent. (b) A waveguide film showing no crystallization after the improvement made with the new process.

The measurement of the EO coefficients show that this method causes no observable decrease in the r_{33} value. We obtain r_{33} values around 16 pm/V in corona poled films at the wavelength of 633 nm which is at least as good as the previously reported value at the same wavelength (13 pm/V).

Polymer films prepared in this way show no observable crystallization, regardless of what substrates are used. The films prepared on a silicon wafer are very smooth and featureless under microscope observation.

3.4.4 Cladding Layer Formation

We observed that directly curing the NOA61 films with appropriate post-coating processes provides us with a smooth cladding. A layer of NOA61 is directly coated on a 1" x 1" microscope glass slide. The newly fresh NOA61 is dissolved in dry cyclopentanone and vigorously stirred by a magnetic stirrer. UV light with an intensity of 10 mW/cm^2 is used. Controlling the precuring time is critical. If the precuring is too short and the resulting molecular size is still small, a substantial volume change can still occur. On the other hand, if the precuring is too long, the solution will turn into a gel. Even if the solution does not turn into a gel, sometimes it may still not go through a 0.2 μm-syringe filter. The curing time determined from the experiments ranges from 10 seconds to 5 minutes depending on the concentration of the solution. The properly prepared solutions can easily go through the syringe filters and good films are always obtainable.

Two cladding layers are needed to facilitate the electrode deposition. The three-layer structure of an LD-3 waveguide is illustrated in Fig. 20, where the thickness of the buffer layers is designed to produce a low-loss waveguide while maintaining a high electric field within the active layer. Note that such a guided wave device can be implemented on any surface of interest which significantly eases system integration issues.

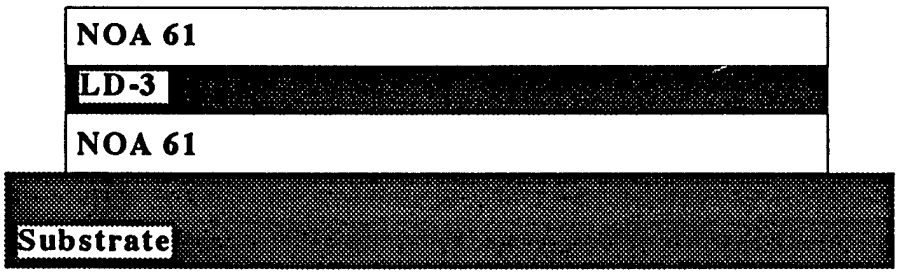

Fig. 20. A planarized three-layer polymer waveguide structure.

3.4.5 Formation of High Quality LD-3 EO Channel Waveguides.

The ultimate check of the effectiveness of the film preparation method is the extent of waveguide loss. Our test sample consists of a multilayer planar waveguide on a 4-inch silicon wafer. First an aluminum layer is deposited as the ground electrode. Then a 3-μm thick layer of NOA61 optical adhesive is coated as the lower cladding, then a 1.2-μm thick layer of LD-3 polymer, and finally a 1-μm thick layer of NOA61 as the upper cladding. A planar waveguide is thus formed. Waveguiding is first confirmed experimentally by prism coupling and observing a guided mode at a wavelength of 1.3 μm. The result is shown in Fig. 21. The propagation of the

light from the center of the wafer to the edge is clearly observed using a CCD camera. It propagates nearly 5 cm and then emerges from the wafer edge. By employing reactive ion etching (RIE), a linear channel waveguide array having a channel width of 6 μm and a channel-to-channel separation of 30 μm has been fabricated.

Fig. 22(a) is a section of the LD-3 polymer-based channel waveguide array and Fig. 22(b) is the near field mode profile of an edge-coupled channel waveguide. Note that the waveguide is single-mode. The loss of such a waveguide is determined by measuring the scattered light intensity along the light streak[48]. Fig. 22(c) shows the loss measurement result. A loss figure of 1.3 dB/cm is achieved. An even lower loss (less than 1 dB/cm) can be expected if the core and the lower cladding thickness are further optimized. There are no reported loss data for LD-3 polymer. Compared with other reported results for NLO polymers[41,48], this loss is acceptable and further improvement will be investigated in Phase II to further reduce the system insertion loss.

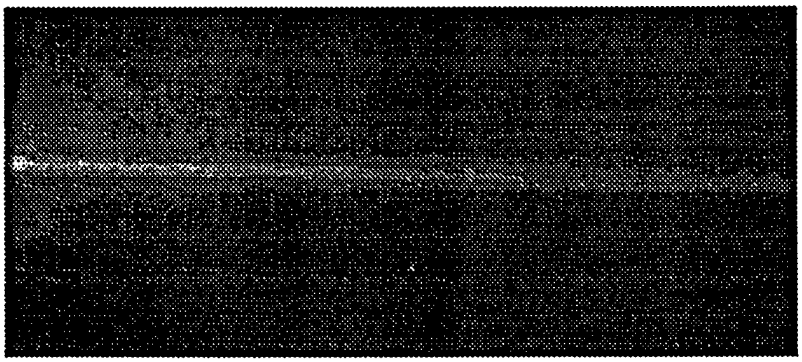

Fig. 21. Observation of LD-3 planar waveguide at 1.32 μm.

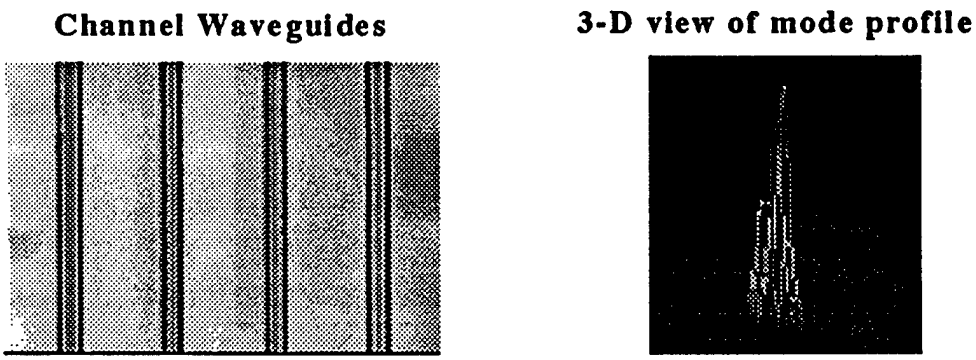

Fig. 22. Formation of channel waveguides using LD-3 thin film: (a) channel waveguide array, (b) edge-coupled near field profile of the guided mode at 1.32 μm.

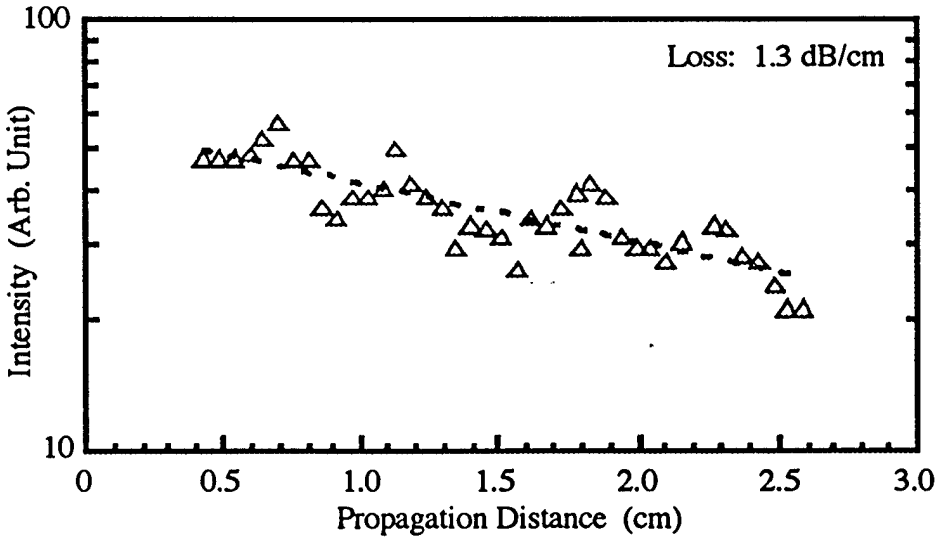

Fig. 22(c). Optical loss measurement of a planar LD-3 polymer waveguide.

3.4.6 Fabrication of Y-branch Waveguide Couplers Using LD-3 Polymers.

Processing steps have been developed for fabricating the LD-3 Y-branch waveguide couplers. First, a bottom cladding polymer layer of NOA-61 is spun onto a silicon wafer to form a 3-μm layer. The NOA-61 layer is then cured with UV light. Next, LD-3 electro-optic polymer is spin coated onto the NOA-61 layer. This results in an LD-3 layer with a thickness of ~2.0 μm. The LD-3 layer can be electrically poled using the liquid contact poling technique or the corona poling technique. After the polymer is cured, AZ5209 photoresist is then spun onto the LD-3 layer and patterned using standard microlithography for fabricating the directional coupler. The sample is then developed with AZ425 developer and reactive ion etched to define the channel waveguide regions. A top NOA-61 cladding is further applied to the sample and cured. The silicon wafer is then scribed and cut, so that the ends of the device are at the edges of the wafer. The input and output ends are then polished using a Beuhler polisher with diamond abrasive films of various grits. First, a 9 μm diamond abrasive film is used for fifteen minutes at 50 rpm. Then abrasive films of 6 μm, 3 μm, and 1 μm grits are used for the same amount of time and angular rotation speed. The polishing resulted in a smooth interface for coupling. A schematic of the cross section of the interaction region is shown in Fig. 23. For this design, the interaction length is about 8.1 mm, equal to the determined coupling length.

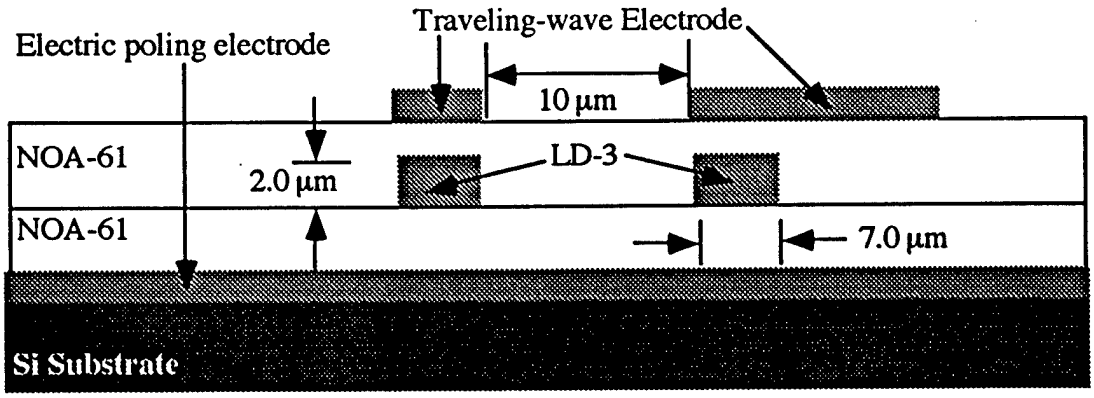

Fig. 23. Schematic of the cross section of an LD-3 Y-branch waveguide coupler.

The Y-branch coupler sample is mounted between two microscope objective lenses in a butt-coupling arrangement as shown in Fig. 24(c), where a top-view photo of the LD-3 Y-branch waveguide coupler and waveguide coupling section are shown in Fig. 24(a) and 24(b). Output from a 1.3 μm Santa Fe Laser is coupled into the waveguide using a 40x objective and the light is coupled out using a 40x objective. The near field pattern is imaged on a screen about a foot away from the output coupler and viewed with an infrared camera. For our test sample, the input and output taper regions have been removed. Therefore, straight channels 10 μm apart remain. The laser beam can be coupled into either channel waveguide individually or both channels at the same time, due to the narrow separation of the channels. Fig. 25(a) shows the near field pattern observed with a laser beam profiler when light is coupled out from both channel waveguides. By applying different voltages through the electrode, light can be modulated from one channel to another. The switching voltage for this device is about 26 V. The EO waveguide propagation loss was measured at ~1 dB/cm at a wavelength of 1.3 μm.

We have successfully fabricated Y-branch waveguide modulator using LD-3 electro-optical polymer. Suitable optical cladding polymer, i.e. NOA-61, has been found. The EO coefficient r_{33} is measured up to 14 pm/V at 1320 nm. Suitable optical cladding polymer, i.e. the NOA-61, has been found. The propagation loss of the electro-optic waveguide is less than 1 dB/cm. In Phase II, domain-inverted polymer will be applied to this Y-branch waveguide coupler to fully demonstrate the advantages of the proposed high performance EO modulators, such as linearized modulation transfer curve and nearly 100% modulation efficiency. The driving voltage can be reduced below 8 volts for the proposed domain-inverted modulators in an optimized design using domain-inverted polymers.

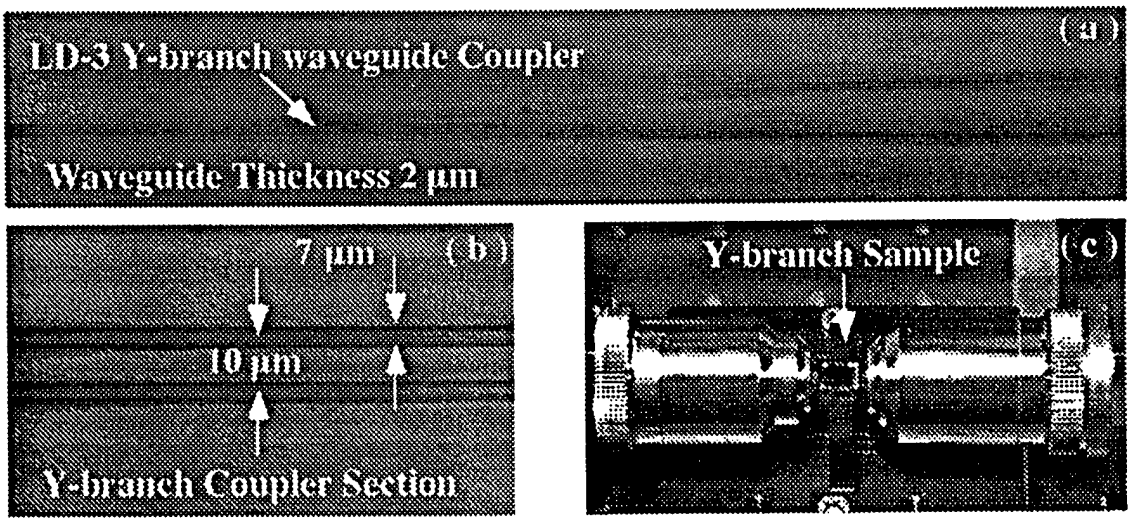

Fig. 24. (a) Top-view photo of a fabricated LD-3 Y-branch waveguide coupler, (b) photo of a Y-branch waveguide coupling section, and (c) butt-coupling setup using micro objective lenses.

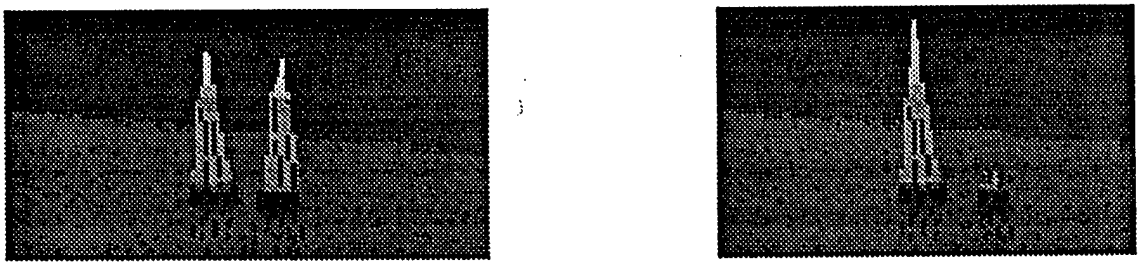

(a) (b)

Fig. 25. (a) 3-D output near-field patterns of a Y-branch waveguide modulator at a biasing voltage of V = 15 V, and (b) V = 0 V, respectively.

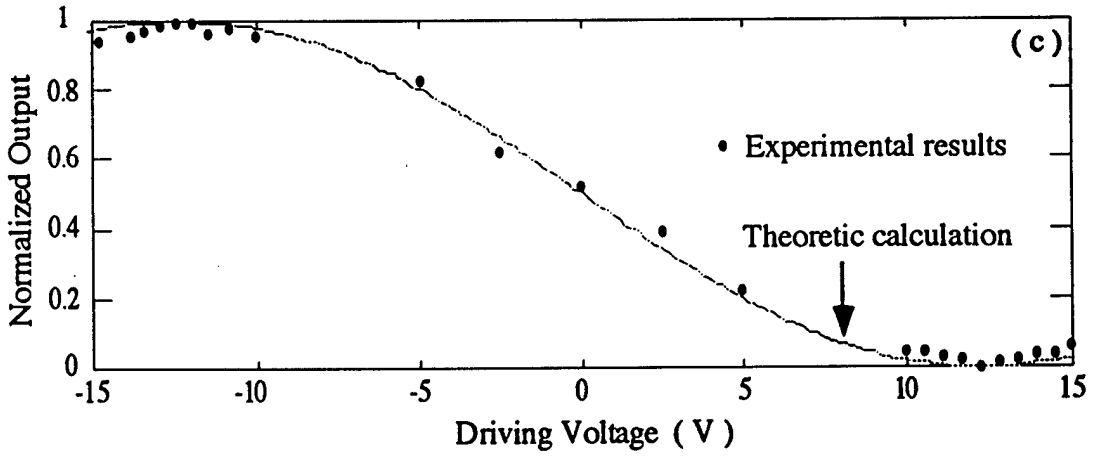

Fig. 25. (c) Measured modulation transfer curves.

3.5 Advanced Liquid Contact Electric Poling Technique

An advanced liquid electric poling technique has been developed through the Phase I research in order to produce high performance EO polymers and domain-inverted polymers. There are two conventional methods for doing the external electric field poling process of the polymers: metal contact poling and corona poling[42,45,52,53]. The contact poling frequently generates a localized destructive current at pinhole defects. One single defect created during the film processing may introduce a catastrophic short circuit and finally destroy the fabricated device. As a result, contact poling in most cases can only be performed at a field much lower than the dielectric breakdown permitted by the polymer film[53]. This prevents us from obtaining high performance polymers with large EO coefficient, γ_{33}. In corona poling the high electric field is produced by the charge deposited on the film surface through the corona discharge process, where a poling electric field close to the dielectric breakdown can be obtained[54]. Larger poling fields activate larger nonlinearities compared with metal contact poling, however, surface damage, resulting in large optical loss, is a major concern for corona poling[53]. Due to the nature of the corona poling process, EO polymers with well defined domain-inverted sections are very difficult to obtain, if not impossible.

The liquid contact electric poling setup is shown in Fig. 26. The upper electrode is made of chromium that is evaporated onto glass microslides and patterned by wet etching. A gap of ~10 μm between the upper electrode and the film is maintained by epoxy spacers. The contact liquid, hexatriacontane, doped with conjugated molecules such as azobenzene or porphyrine, is a solid at room temperature and melts at 75 ^{o}C. The hexatriacontane becomes more conductive when it melts, and is automatically sucked into the gap by capillary force with no bubble formed. As a result, an electrically conductive path between the upper electrode and the polymer film is formed through the melted liquid layer, so most of the voltage applied to the electrodes will drop within the polymer films.

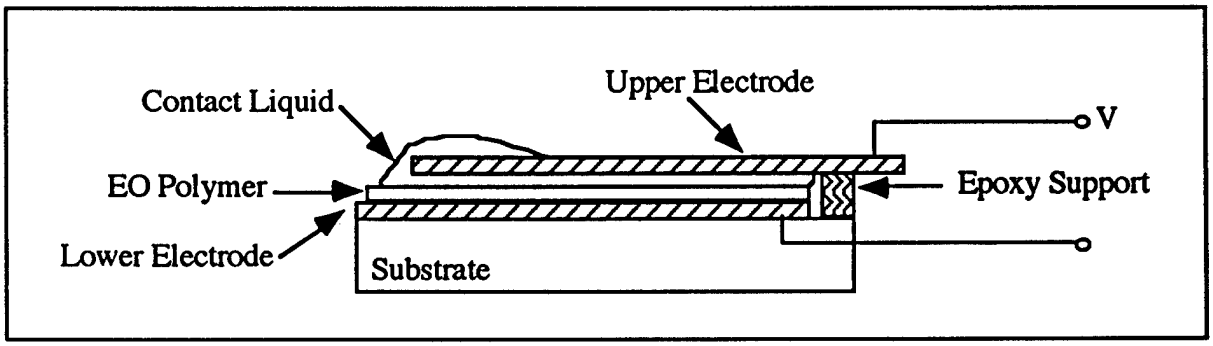

Fig. 26. Schematic of the liquid contact electric poling setup.

It is necessary to have a contact liquid with high breakdown voltage to insure that high poling field can be applied during the poling. Fig. 27 shows the measured I-V curve at 160 °C for the contact liquid doped with 0.1% azobenzene dye. The cell used in this measurement is similar to that shown in Fig. 26 but without the polymer film. The breakdown voltage is above 300 volts for the 10μm cell. For such a high voltage, the field applied across the 1.2 μm LD-3 film should be 250V/μm, which is comparable to the corona poling field strength reported[52,53]. This contact liquid also avoids short circuits in case of any local breakdown in the polymer film.

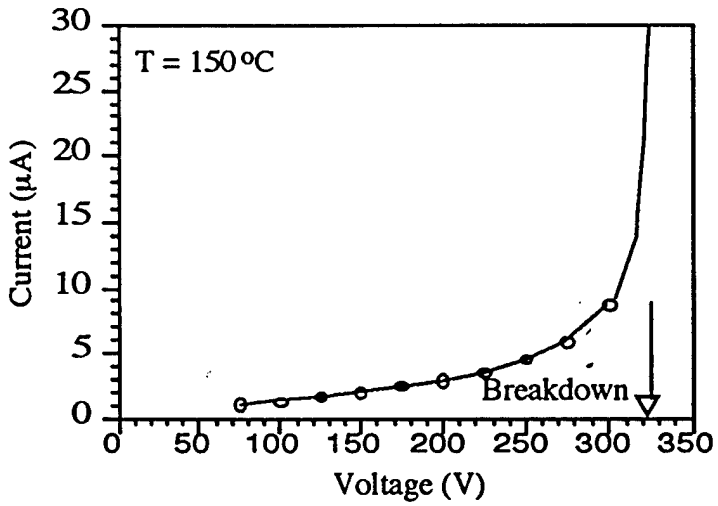

Fig. 27. Measurement of the breakdown voltage of the contact liquid.

The experiment is carried out in an ambient environment. Fig. 28 shows the poling process that can be divided into three stages. In the first stage the sample is heated to above the melting point of the contact material, which has been applied to the opening of the gap of the cell before heating. The second stage is to provide electrical poling while continuously heating the sample. After the liquid contact is formed, a poling voltage of 300 volts is applied at 114 °C. During this period, most of the chromophores have not been crosslinked and are able to rotate to align their dipoles with the applied field once they have acquired enough thermal energy during the heating process. The current associated with dipole orientation is small, so the increase of the current is mainly due to the change of conductivity of the materials with temperature. During the third stage, the temperature is maintained at 160 °C while keeping the poling voltage on. At first the current decreases quickly, then the decrease slows down. This trend is commonly observed in the poling process of crosslinkable polymers. We also observe such a phenomenon in the corona poling experiments with the same material. The decrease of the poling current is due to the

crosslinking process, because the more the polymer is crosslinked, the higher the electrical resistance is. After the LD-3 polymer is fully cured, the heater is turned off and the sample is cooled to 100 °C within 10 minutes. Then the poling voltage is turned off and the upper electrode is separated while the contact material is still in a liquid state. The fully crosslinked LD-3 polymer has very strong solvent resistance and abrasive resistance, so that the contact material can be removed by solvents such as xylene or alcohol, dependent on the doping. After the removal of the contact material, the polymer surface looked shiny.

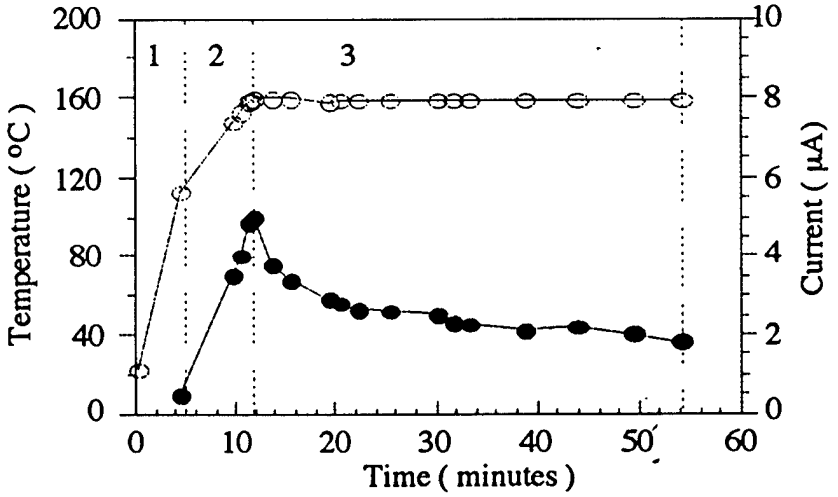

Fig. 28. Time diagram of electric poling process.

3.5.1 40% enhancement of electro-optic (EO) coefficient

The developed liquid contact poling method can not only alleviate the surface damage problems, but also allows a higher poling field to be applied. It provides an electric poling field as high as 250V/μm in LD-3 EO polymer film with little surface damage. The superior r_{33} value obtained was 18 pm/V at 633 nm, which is ~40% larger than the previously reported value of 13 pm/V. Little surface damage has been found compared with the conventional poling techniques. More importantly, this technique allows us to produce the poled and reverse-poled micro structure in EO polymers. As a result, domain inverted sections can be formed for fabricating the proposed novel electro-optical devices.

The crosslinkable LD-3 polymer used in the experiment is supplied by AdTech System Corporation. 100 mg of the polymer and 60 mg of the crosslinker is dissolved in 1 ml cyclopentanone and filtered by a syringe filter of 0.2 μm. Then the solution is spin-coated on indium tin oxide (ITO) films and is dried in a house vacuum.

A chromium electrode is deposited on the polymer by electron beam evaporation and the r_{33} value was measured using a reflection technique[54,55]. r_{33} as high as 18 pm/V are obtained at a wavelength of 633 nm. On the other hand, we have only obtained r_{33} = 14 pm/V under the optimized poling conditions of 5 kV using the corona poling technique. The previously reported r_{33} of LD-3 is 13 pm/V at the same wavelength[42]. Although the impressive liquid poling results are obtained using the crosslinkable LD-3 polymer, we do believe that the poling technique developed here can be further extended to other EO polymers with improved electro-optical properties.

3.6 Two-Section Domain Inverted Poling and Characterization

The availability of a new technology for domain inversion in electro-optic polymer is a cornerstone for the proposed high performance EO modulators. RRI has developed a reliable technology for fabricating domain-inverted polymers. Based on this new technology, RRI has demonstrated the first domain-inverted EO polymer during the course of the Phase I research[56]. An effective measurement technique has also been investigated for characterizing this new type of fabricated polymer.

Domain inversion in an EO polymer is the reversal of the orientation of the ferroelectric domains so that the polymer has two domains in two opposite orientations. Because the ferroelectric domain is a result of a noncentrosymmetric polymeric structure, created artificially by aligning chromophores into a noncentrosymmetric order through the application of an external electric field, the effective way for inverting the polymeric domain is to electrically pole the polymer film simultaneously in two opposite directions. As a result, all corresponding physical parameters, such as electro-optic coefficient, are inverted with respect to each other.

RRI has demonstrated the first domain-inverted EO polymer during the Phase I research[56]. **(Note that so far the domain-inverted EO polymer has not yet been demonstrated by others.)** The conventional corona poling technique, widely used by other researchers, is not suitable for fabrication of domain inverted polymers[47,53]. In corona poling, high electric field is produced by the charge dropped on the film surface through the corona discharge process. Therefore, the electric field can only point in one direction, not two opposite directions as desired. Besides, it is also difficult to precisely control the poling area under the electric corona. Realization of the proposed new class of electro-optic modulators, with an improved modulation performance and simplified design, necessitates the development of a method for achieving domain inversion in the EO polymers.

3.6.1 Fabrication of domain-inverted polymers.

In order to obtain the proposed domain inverted polymers, we have developed a new high-temperature liquid-contact electric poling technique[57]. Fig. 29 illustrates the poling scheme developed to obtain domain inverted polymers based on the liquid-contact electric poling technique. The polymer-based planar waveguide consists of a 3 μm NOA-61 upper cladding layer, an 1.2 μm LD-3 electro-optic polymer layer and a 3 μm NOA-61 bottom cladding layer. The length of the poling sample is over 2.0 cm. The two top transparent electrodes are made of indium-tin-oxide (ITO) patterned on one side of a glass plate (Corning No. 1). A 150 μm wide by 25 μm tall insulating wall, made out of photo polyimide using laser writing, is employed to separate the two top electrodes, which can survive at temperature up to 400 °C. In the experiment, the thickness of the contact liquid is controlled by the epoxy spacers as shown in Fig. 29, having a thickness of 10 μm. The contact liquid, hexatriacontane, is carefully selected to satisfy the requirements imposed by the poling requirements. It is a solid at room temperature and becomes a liquid at 75 °C. When is melts, its resistivity becomes much lower compared to that of LD-3 polymers and it gets sucked into the gap between ITO and the planar polymer waveguide due to capillary action. As a result, an electrically conductive path between the ITO and the polymer film is formed through this liquid layer. No bubble is formed during the whole process. The bottom electrode is made of chromium evaporated on a glass substrate.

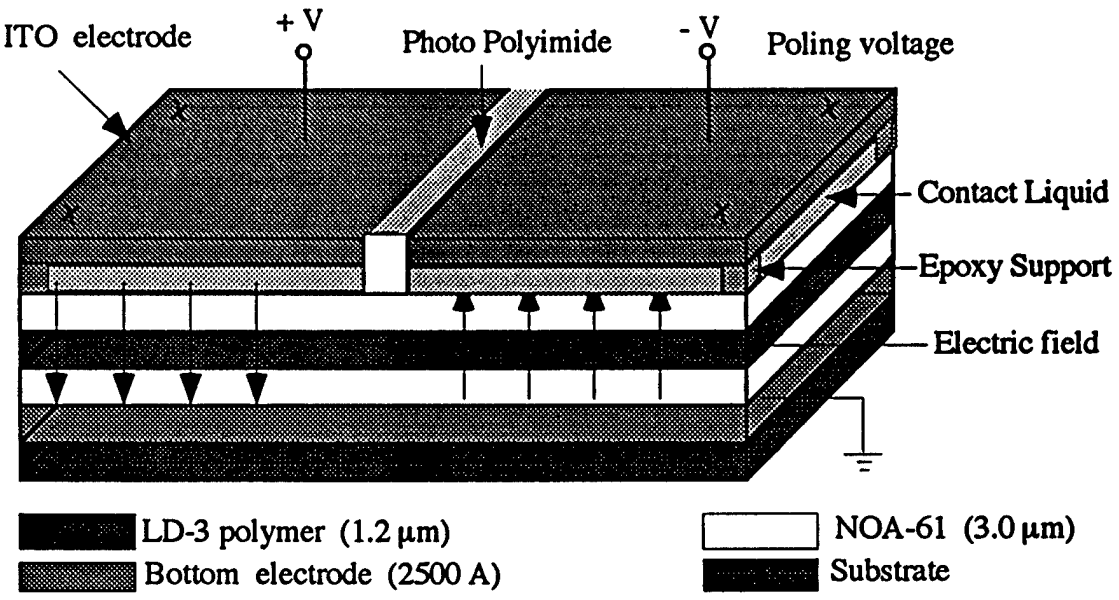

Fig. 29. Schematic diagram for obtaining domain inverted polymers using a novel liquid-contact electric poling technique.

Two electrical voltage supplies are employed for poling the domain inverted polymer, having a common ground (bottom electrode) as shown in Fig. 29. The same voltage is applied to the two top electrodes with reversed polarities during the poling. Note that the gap between the two top electrodes is much larger than the distance between the top electrodes and the bottom electrode, so the electric field is perpendicular to the polymer film, except for small areas near the center edges. The length of this area should also be small enough to ensure the designed device performance. A voltage of 550 V has been successfully applied during the poling at a temperature of 165 °C for 55 minutes. The breakdown voltage is determined above to be above 600 V in our experiments. No short circuit was found during the breakdown,.but we reduced the poling voltage to 550 V to avoid breakdown.

It has been found that the self-curing property of the contact liquid plays a useful role in saving the cell from being permanently destroyed by an occurrence of breakdown. This is very useful for producing polymers with higher electro-optic coefficient due to the fact that higher electric poling field can be applied. The EO polymer poled by this liquid contact technique has an electro-optic coefficient of γ_{33} = 18 pm/V that is 40% higher than that poled by any other techniques, including corona poling[53] and metal contact poling[58]. To compare with direct contact poling, we have made several cells similar to that in Fig. 29 using the metal contact poling technique. The metal contact electrode is placed directly on top of the NOA-61 cladding layer. At a poling voltage of 460 V, all samples using metal contacts experience an electrical breakdown. Some cells break down at the beginning of the poling process, some in the middle of the poling, some near the end.

3.6.2 Fabrication of two-section domain-rotated polymers.

In order to obtain the two-section domain rotation, which is crucial for polarization insensitive operation, the liquid-contact electric poling technique is further modified. Fig. 30 illustrates the poling scheme developed. A thin film poling electrode is first deposited on the silicon substrate. A 3 μm NOA-61 polymer is spin-coated on top of the substrate as a waveguide cladding layer. Then a 2-μm LD-3 electro-optic polymer is formed on top of the cladding layer. The insulating wall for separating the liquid-contact-poling electrodes is made out of a thick photopolyimide film (25 μm), which is spin-coated and photolithographically patterned on top of the LD-3, as shown in Fig. 30(a). Fig. 30(b) is the photo of the T-type insulating wall made of photopolyimide fabricated on the top of LD-3 waveguides for the in-plane liquid-contact poling. The length of the poling sample is 2.0 cm. The photopolyimide walls are designed to be 30-60 μm wide and 25 μm tall, and fabricated by using a laser beam direct-writing technique. It is employed

to separate the two top electrodes, which can survive at temperatures up to 400 °C. In the experiment, the thickness of the contact liquid can be controlled in the range of 10 μm. Four DC power supplies are employed to carry out the desired four-section poling. It has been found that the width of the wall has to be much larger than the polymer thickness under poling for best poling results. Both in-plane and surface-normal domain inversions have been demonstrated during the course of this Phase I research.

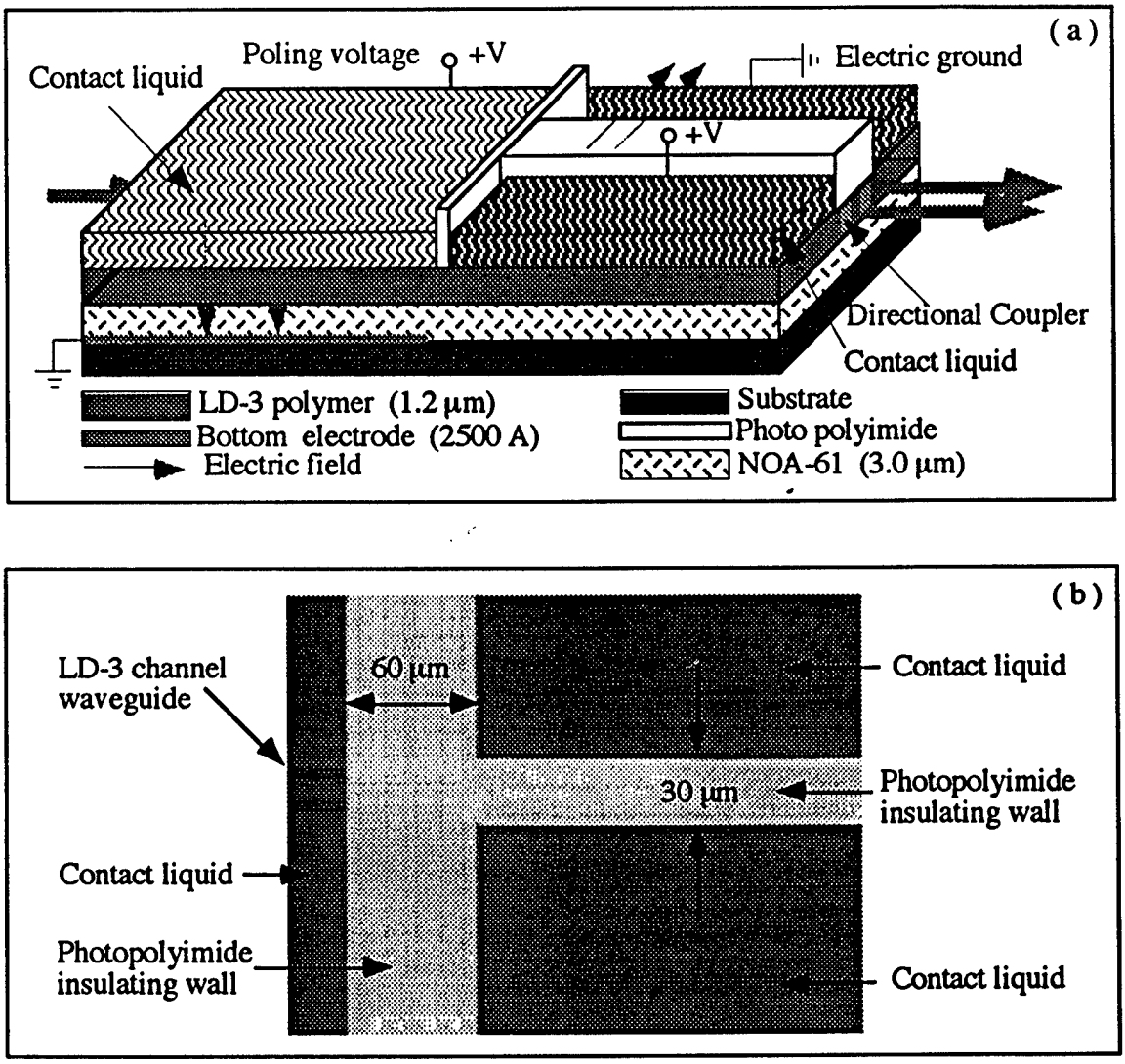

Fig. 30. (a) Fabrication of a two-section domain-rotated electro-optic polymer using photo polyimide patterned liquid contact poling. Both in-plane and surface-normal electro-optic domains are created in a single polymer film. (b) Photo of the polyimide-based insulating wall photolithographically defined on LD-3 polymer channel waveguides.

3.6.3 Characterization of domain-inverted polymers

Successful inverted poling of two domains in LD-3 polymer is demonstrated by measuring the electro-optic response of each domain using a reflection technique[58,59]. A schematic diagram of the experimental setup for this reflection technique is given in Fig. 31. This technique is capable of addressing both the magnitude and the sign of the electro-optic response of polymers.

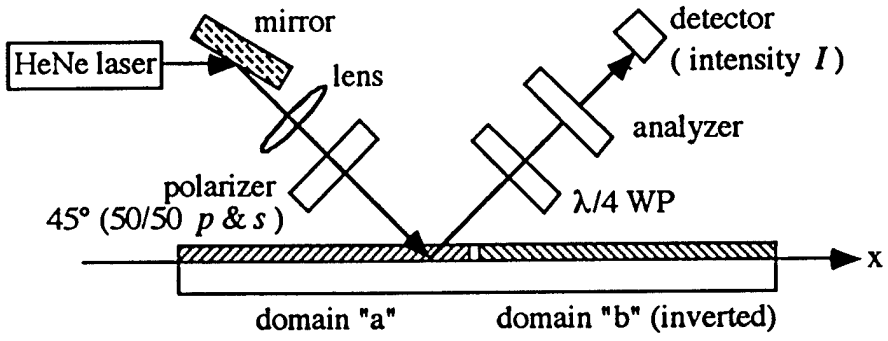

Fig. 31. Schematic of the experimental setup used to measure the electro-optic response.

The theoretical description of the measurement scheme is developed by analyzing the modification of the polarization state of the reflected light by the electro-optic effect. The intensity throughput of a entire optical system depicted in Fig. 31 is[59]

$$I = 2I_c \sin^2(\psi_{ps}/2) \ , \qquad (46)$$

where ψ_{ps} is the phase difference between the p and s waves. The $\lambda/4$ waveplate provides approximately a retardation between the p and s waves such that

$$\psi_{ps} \approx 90° + \delta\psi_{ps} \ . \qquad (47)$$

The quantity $\delta\psi_{ps}$ is the phase difference between the p and s waves as introduced by the electro-optic effect. For no applied driving voltage, this phase difference is zero. A Babinet-Soleil compensator could be used to make the relation in Eq. (47) exact, since it can be set to any retardation as required to correct for the small amount of phase difference between the p and s waves as introduced by propagation through and reflection off of the multiple layers of the actual sample. The intensity given by Eq. (46), with ψ_{ps} given by Eq. (47), reduces to

$$I \approx I_c + I_c \delta\psi_{ps} \ . \qquad (48)$$

The phase retardation $\delta\psi_p$ and $\delta\psi_s$ for the p and s waves, respectively, caused by the electro-optic effect are not equal. For a modulated voltage

$$V = V_m \sin(\omega_m t) \qquad (49)$$

driving the electro-optic effect, the phase difference is

$$\delta\psi_{ps} = \delta\psi_p - \delta\psi_s = \Gamma_m \sin(\omega_m t) \ , \qquad (50)$$

where Γ_m is the magnitude of the modulation in the phase difference. For the remainder of our analysis here, we need only know that [48,49]

$$\Gamma_m \propto r_{33} V_m \ . \qquad (51)$$

The strength of the electro-optic effect is given by the tensor component r_{33}, where we have made use of the relation $r_{33} = 3r_{31}$ among the tensor components. The indices 3 and 1 indicate directions perpendicular and parallel to the film, respectively.

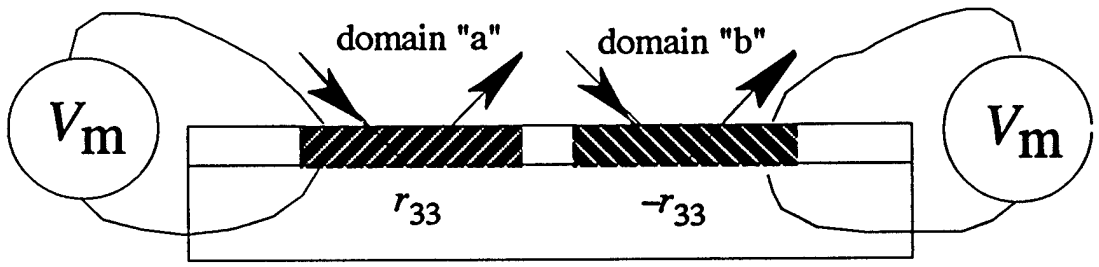

Fig. 32. Polymer waveguide containing two domains poled 180° with respect to each other. The lines with arrow heads depict a laser beam probing either of the two domains.

A modulated voltage driving the electro-optic effect would thus introduce a ripple on the observed intensity I. Measurement of this ripple in the intensity in turn can be used to deduce the magnitude and sign of the electro-optic tensor component r_{33}. To demonstrate that two different domains in the polymer sample are poled in opposite directions, all we need to do is show that the sign of r_{33} changes between the two

domains. By using the same driving voltage, as given by Eq. (49), for each of the two domains, any change in the response will be due to changes in r_{33}. For poling equal in magnitude, but opposite in sign, the situation will be as depicted in Fig. 32. The intensity as a function of the position x across the two domains (see Fig. 29 and Fig. 30) will follow the equations

$$I(x) \approx I_c + I_c \left| \delta\psi_{ps} \right| \text{ , for } x \text{ in domain "a",} \qquad (52)$$

$$I(x) \approx I_c - I_c \left| \delta\psi_{ps} \right| \text{ , for } x \text{ in domain "b",} \qquad (53)$$

which differ only by a sign change.

The most straightforward way to conceptually demonstrate the actual measurement would be to simultaneously record the intensity of two laser beams, where each is reflected by one of the two domains. Under ideal conditions, an oscilloscope would display the signal voltages of the photodetectors as depicted in Fig. 33(a). However, the modulation voltage is typically very small compared to the DC portion of the signal voltage and is obscured by noise. Thus we use a lock-in amplifier to examine the signal voltages. The lock-in amplifier can be configured to operate as shown in Fig. 33. The quadrature-voltage Q1 would be positive for domain "a" and negative for domain "b" where the magnitudes would be equal. The opposite would occur for quadrature Q3.

We make our actual measurement by translating the sample in the direction x through a single laser beam as depicted in Fig. 31. The measured quadrature-voltage (like Q1 in Fig. 33) for our sample is given in Fig. 34. The electro-optic response is positive for positions x less than 0 mm and negative for positions x greater than 0 mm. Hence, domain inversion is demonstrated. The finite transition from one domain to the other is probed by the laser beam and is what causes the slope in the measured response for positions x crossing through 0 mm. For the present test sample, the extent of the finite transition from one domain to the other is about 200 μm. The electro-optic coefficient is measured up to 18 pm/V.

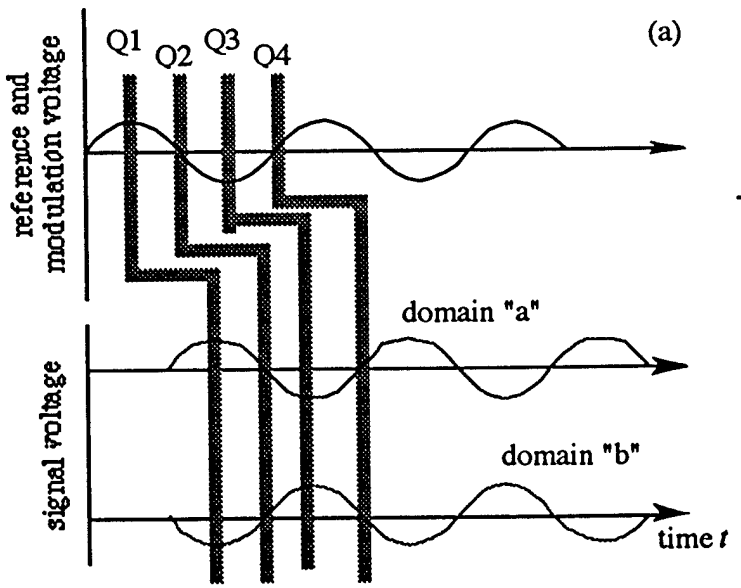

(b)

quadrature	signal voltage "a"	signal voltage "b"
Q1	V_s	$-V_s$
Q2	zero	zero
Q3	$-V_s$	V_s
Q4	zero	zero

Fig. 33. Domain-inversion measurement scheme using a lock-in amplifier. (a) Relation between the quadratures of the lock-in amplifier (i.e., the reference voltage) and of the electro-optic response (i.e., the signal voltage). (b) Quantitative nature of the quadrature measurements.

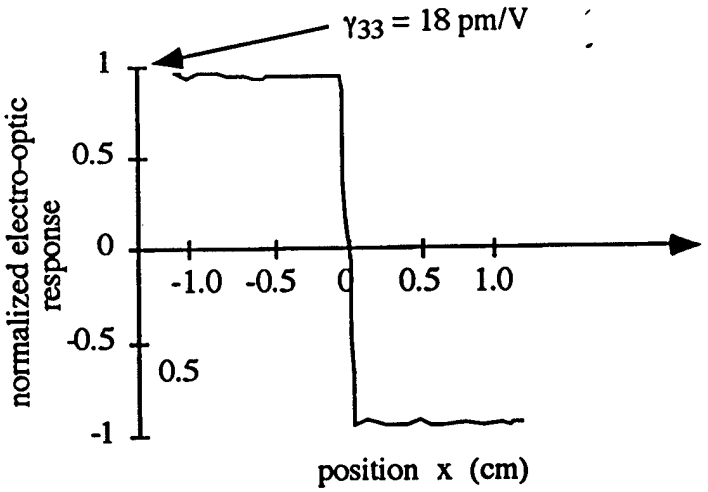

Fig. 34. Electro-optic response as a function of the position of a probing laser beam.

We have demonstrated a new technology for fabricating domain inversion in electro-optic polymers, which is considered as a cornerstone for the proposed high performance EO modulators. This new type of polymer with two opposite ferroelectric domains has been characterized by an effective measuring technique developed during the course of our research. It is shown that a state-of-the-art electro-optic coefficient has been obtained. The dimension of the domains can be well-controlled to satisfy the device design and fabrication needs.

3.7 Design and Fabrication of Thick Traveling-Wave Electrodes

Through the Phase I research, we have established a standard process for fabricating low-loss traveling-wave electrodes, and developed a preliminary simulation model for determining the electrode transmission characteristics. To ensure the high-speed operation of an integrated electro-optic modulator, it is mandatory to employ traveling-wave electrodes[1,5,47]. The bandwidth of the electro-optic modulator employing a traveling-wave electrode is limited by the velocity mismatch between the microwave and optical mode as well as the RF transmission loss of the electrode. Thick traveling-wave electrodes are required to reduce the microwave transmission loss and to provide the required velocity match.

3.7.1 Fabrication of traveling-wave electrodes

There are two types of traveling-wave electrodes that can be implemented in the proposed devices. They are coplanar strip line electrodes (CPS)[60] and coplanar waveguide electrodes (CPW)[61,62]. In general, a CPS electrode has a lower transmission loss and lower driving voltage for a directional coupler modulator compared to a CPW electrode. For CPS electrodes, the transmission loss is largely determined by the transverse resonance in the substrate, while the coupling between the fundamental coplanar waveguide mode and a substrate mode affects the loss of CPW electrodes[63]. In the course of this effort, we are pursuing an innovative approach that employs domain inverted waveguide sections, which allows the use of a uniform electrode structure to simplify device design and leads to a relaxed fabrication tolerance. A coplanar strip line electrode, as shown in Fig. 35, will be employed for the proposed high-speed polymer-based electro-optic modulators.

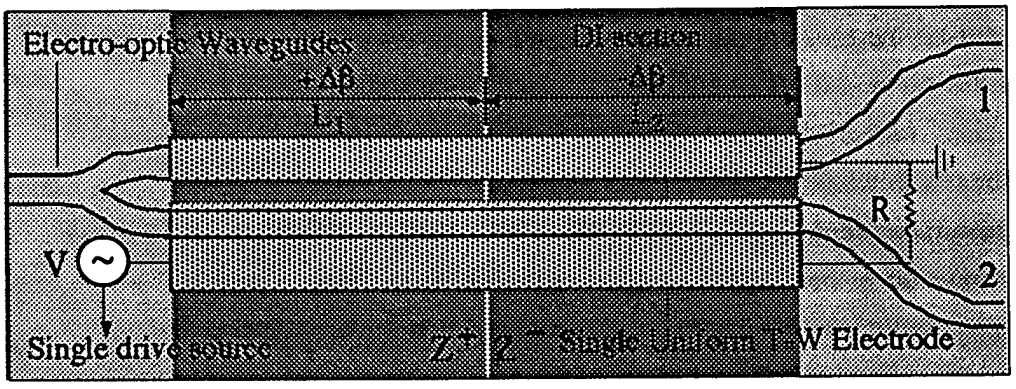

Fig. 35. Uniform traveling-wave CPS electrode for high-speed electro-optic modulators with a domain-inverted section.

In fabricating a thick traveling-wave electrode, various device parameters should be considered, such as the electrode dimension, thickness, inter-electrode gap, and cladding layer thickness. There are four important rules to follow:

(1) bring the characteristic impedance to 50 Ω,

(2) match the phase velocities of microwave and optical mode,

(3) minimize the microwave transmission loss, and

(4) reduce the driving voltage.

The design rules given above necessitate using multiple processing steps in order to fabricate thick electrodes, including:

(a) metal film deposition,

(b) micro photolithography,

(c) metal electroplating, and

(d) chemical etching.

(a) Metal thin film deposition

A thin Cr film (500 Å) will be first deposited on the buffer layer by an e-beam evaporator. This step is important to ensure adequate adhesion of the electrode to the polymer cladding layer. Then, a thin Au film, with a thickness of 2000~3000 Å, will be further deposited on top of the Cr by an e-beam evaporator, which will serve as the seed layer for electroplating thick Au electrodes.

(b) Microphotolithography

Because the photoresist pattern is used as the guide for the electroplated Au layer, the photoresist thickness is required to be equal to the desired electrode thickness. As such a photoresist with a thickness ranging from $T_l = 1.5$ μm to $T_u = 8$ μm is necessary. Here $T_l = 2d$ is determined by the electrode skin depth d, and T_u is determined based on tradeoff among the fabrication tolerance, drive power, bandwidth, and microwave impedance match. Special photolithography techniques are required to spin-coat a thick photoresist film. An appropriate fabrication procedure will be established to spin-coat a thick photoresist layer. The electrode pattern will be defined by an optical mask through the patterned thick photoresist layer.

(c) Au electroplating

Electroplating will be used to fabricate a thick gold electrode. The required electrode thickness ranges from 1.5 μm to 8 μm to reduce microwave loss and to obtain a 50 Ω characteristic impedance. The technological parameters for the electroplating process, including solution formula, electroplating current, and temperature, will be determined in order to achieve a low loss Au traveling-wave electrode.

(d) Ion-milling or chemical etching

Ion-milling (reactive ion etching) will be employed to remove the Cr-Au film from inter electrode gaps. The proper etching condition will be determined for fully removing the thin Cr-Au film while not damaging the electroplated electrode.

The fabrication procedure we plan to implement is shown in Fig. 36. A polymer-based waveguide directional coupler with domain inverted sections is first fabricated. A Cr-Au film is then deposited on the cladding layer. The thick photoresist is further spin-coated on top of the thin metal film. By using standard photolithography, an electrode pattern is defined through a photomask. This pattern is then utilized as the electroplating guide, and a thick gold electrode is grown from the deposited Cr-Au film, being defined by the photoresist walls. The photoresist pattern is dissolved after electroplating. Finally, the Cr-Au film is removed from the area between the electrodes by using ion-milling. Referring to Fig. 36, it should be noted that some of the required technological steps have been established by the RRI research group. They include

* Cr-Au thin film deposition,
* micro photolithography,
* photoresist processing, and
* ion-milling and chemical etching.

We are in the stage of establishing the other two necessary techniques: thick photoresist coating and gold electroplating.

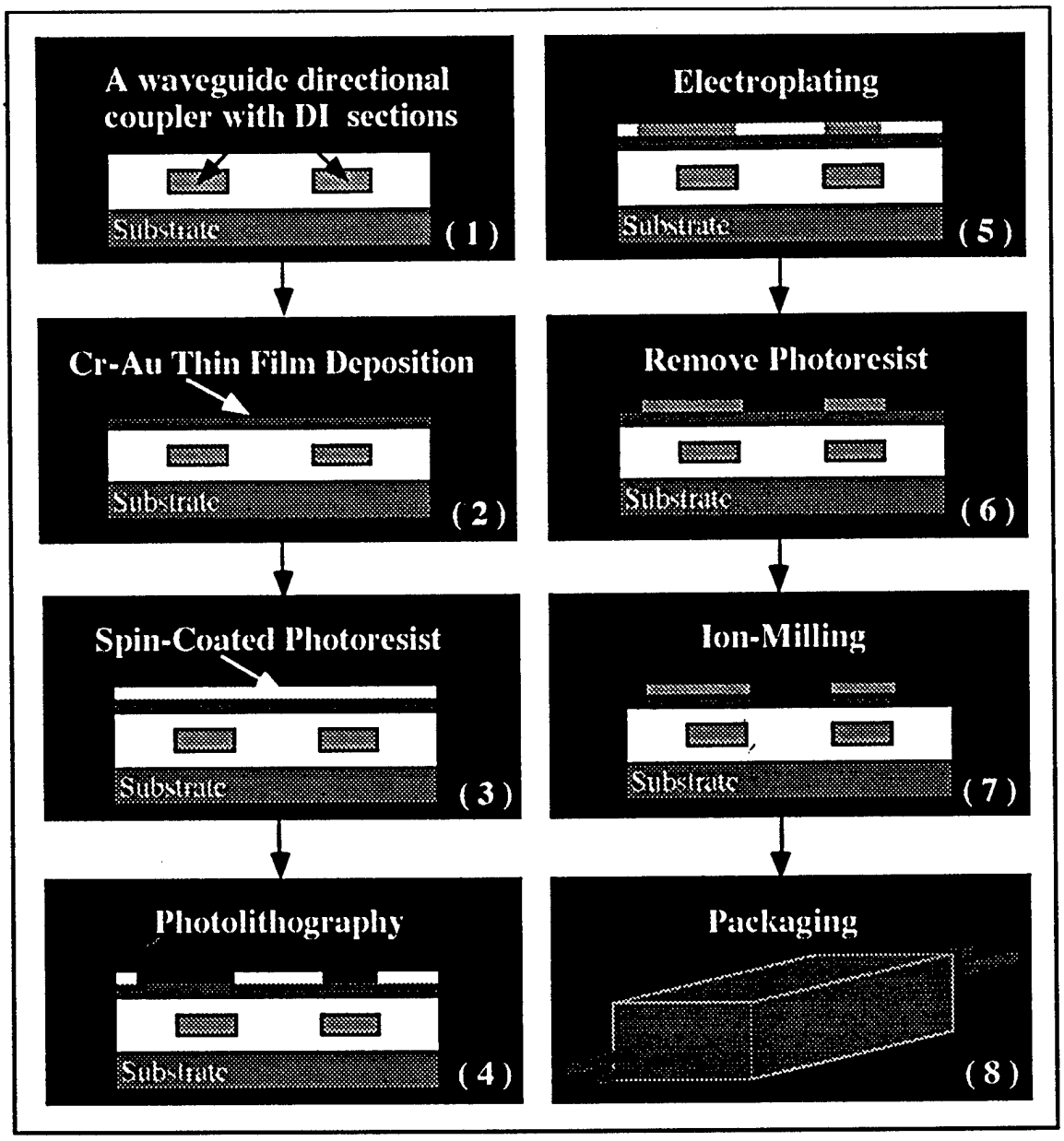

Fig. 36. Processing steps in fabricating thick electrodes.

Two techniques will be tried for forming a thick photoresist pattern. One uses a conventional photoresist, and hence requires several cycles of spin-coating. The other technique employs a special thick photoresist with one step of spin-coating. For both techniques, the photoresist thickness can be controlled by the spin speed. To ensure high-quality photoresist film, the polymer cladding should be free of contamination and excessive physically absorbed moisture.

Table 3 lists the steps required in processing the thick photoresist. The optimum spin speed (step 6) is determined by the desired photoresist film thickness.

Table 3. Processing steps for deposition of thick photoresist layer.

Step	Operation	Time (sec)	Speed (rpm)
1	Substrate Cleaning	--------	--------
2	Softbake	1800	--------
3	Hold	10	--------
4	Spread	20	100
5	Spin	2	2000
6	Spin	250	Optimum Speed
7	End		

Fig. 37(a) shows the relation between the photoresist thickness and spin speed. As an example, for a photoresist thickness of 8 μm, the required spin speed is 6000 rpm based on Fig. 37. Deep trenches that can be used to guide the thick electrode fabrication are successfully fabricated using this type of thick photoresist. Fig. 37(b) shows the measurement result for a 5 μm deep trench formed by using thick photoresist..

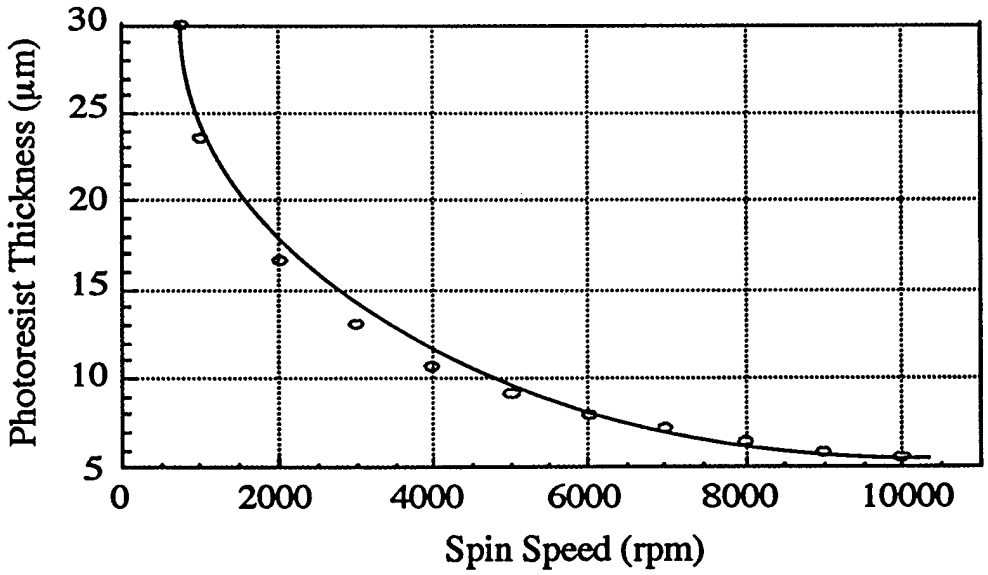

Fig. 37(a). Photoresist thickness versus the speed of spin-coating.

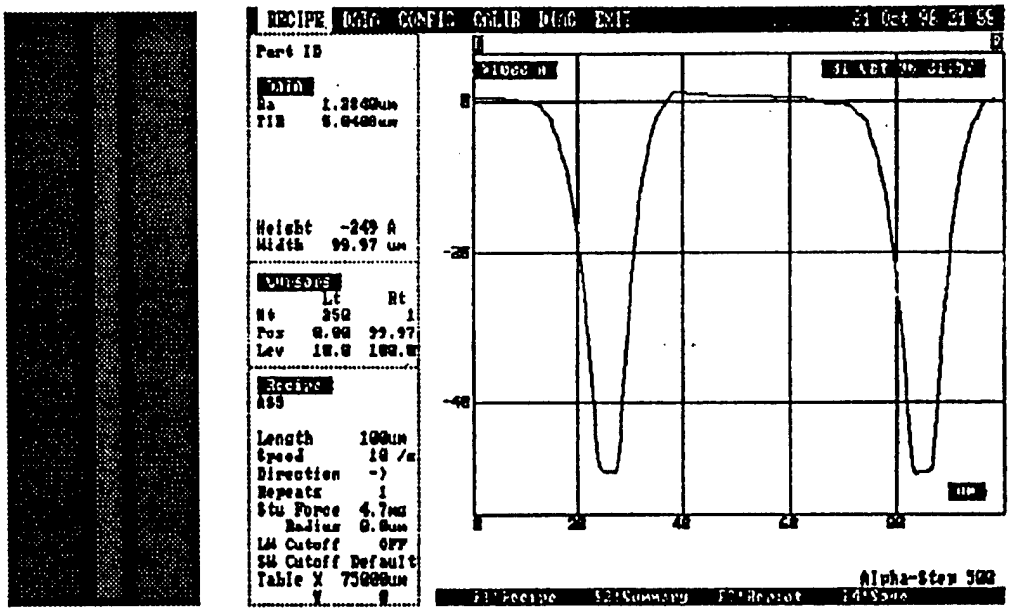

(b) (c)

Fig. 37. (b) Photo of a 5 μm deep trench formed by using thick photoresist, (c) Measurement result for a 5 μm deep trench.

Neutral pure 24 kt gold is chosen to produce ultra pure satin bright deposition. The deposited layer can be stress free, extremely ductile and tight grained with exceptional heat and electrical conductivity. The selected electroplating solution contains no brighteners, either organic or inorganic, as well as no free cyanide or harsh alkalis and acids. Therefore, it is relatively safe and inexpensive to use. Table 4 details the electroplating equipment and formula of the plating solution.

To obtain a high quality electroplated thick layer, careful preparation is essential. The required preparation steps are

1) Fill glass container two-thirds full with deionized water.
2) Heat the water to 140 °F.
3) Add the Orotemp 24 Gold Salts. Stir until completely dissolved.
4) Add deionized water to bring up to operating level. Mix thoroughly.
5) Adjust pH to 5.0-7.0 with Technic Acid C Salts or Potassium Hydroxide.

Table 4. Electroplating equipment and plating solution formula.

Equipment	Description
Containers	Glass
Anodes	Platinum plated niobium
Heater	Temperature controlling electrical heater
Contact Probe	Micropositioner with electrical probing pin

Formula	1 Gallon
Orotemp Additive	1-1/2 lbs.
Orotemp 24 Gold Salt	1 troy oz.
Potassium Hydroxide	0.2 oz.
Technic Acid C Salt	1 lb.

The operating conditions are listed in Table 5. During the electroplating, the pH of Orotemp 24 slowly rises. The pH should be checked periodically with a glass electrode pH meter (Beckman Portable), or equivalent. If the pH drops below 5.0 the current efficiency will drop rapidly, reaching a value of 50 percent at a pH of 4.5. To speed up the plating, high current density can be applied at an increased bath temperature while a good quality electrode can still be obtained.

Table 5. Operatiing conditions for gold electroplating.

pH (Electrometric)	5.0 - 7.0
pH (Paper)	5.3 - 7.3
Specific Gravity	1.08 - 1.15; 11^{o} - 16^{o} Baume
Agitation	Preferred
Temperature	130 - 160 ^{o}F
Current Density	1 - 10 ASF
Time to plate 3 μm	80 min. at 0.5 ASF at pH of 6.2

Electroplating a thick gold electrode without uneven thickness, cracking, and lift-off is known to be difficult. This is due to the fact that there are many variables in the fabrication process [63], which include (1) spin-coating of EO polymers, (2) metal film deposition, (3) spin-coating thick photoresist and the photolithography of thick photoresist, (4) gold electroplating, and (5) chemical/plasma etching.

A schematic of the electroplating setup is shown in Fig. 38. The gold electroplating solution is prepared by using Orotemp 24 gold salts. The anode is made from platinum plated niobium. The plating temperature is controlled by a hot plate. The plating current is provided by a DC current source. To obtain a stable plating current, it is necessary to include a 1-20 kW resistor in the plating circuit.

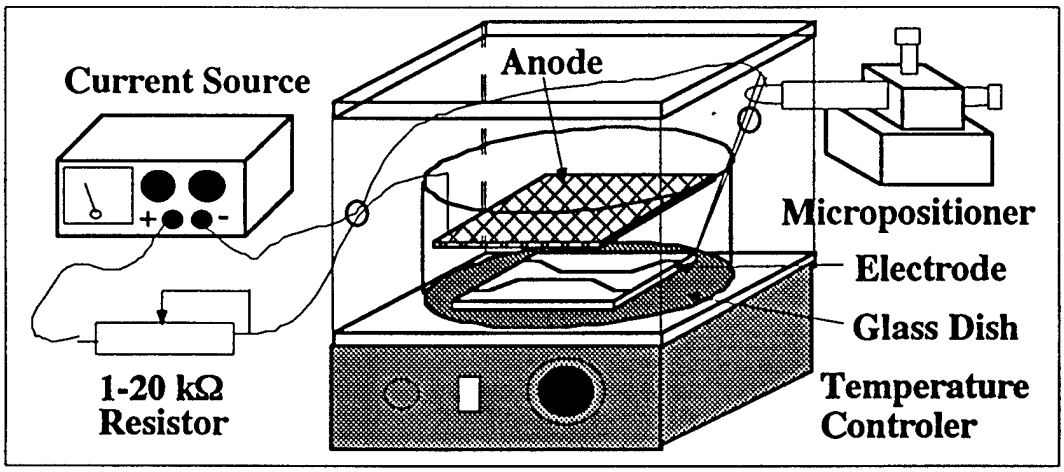

Fig. 38. Schematic of the electroplating setup.

A Cr film is chosen to form the base metal for electroplating a thick gold electrode. Cr has excellent adhesion to both a polymer cladding layer and a gold film. In our experiments, a 200 Å Cr film was deposited first by an e-beam evaporator, using 100% chromium as the evaporating metal source. It has been found that thicker deposition may cause film cracking and surface roughness. In order to increase the adhesion of the gold plate and the Cr film, a thin gold film deposition was made on the top of the Cr thin film. This step was found to be necessary to avoid surface passivation of the Cr film, which prevents even plating and proper adhesion of the gold plate, resulting in an uneven thickness distribution and/or peeling.

Careful surface cleaning is required to have the exposed photoresist fully removed by the photoresist developer. It has been found that the un-removed photoresist causes severe blistering, chipping, and peeling of the plated gold electrode. Substrate dehydration is also preferred before it gets into the plating solution. It should be noted that contaminated plating solution also results in poor adhesion, poor distribution of the plate, rough plate, and cracked plates.

It has been discovered that plating conditions have significant impact on the quality of plated thick gold electrodes. Three major plating parameters have been studied in APT. They are (1) pH value of the plating solution, (2) plating temperature, and (3) plating current density. In

general, the pH decreases slowly during the electroplating process. The operating pH range of the gold solution employed is found between 5.0 and 7.0. A higher pH (>7.0) can cause a loss of surface smoothness and can also affect plating thickness. A lower pH (<5.0) causes precipitation of gold. In our experiments, it has been discovered that the plating temperature should be in the range of 40 °C to 80 °C. Lower temperatures (<40 °C) appear to lead to poor adhesion, poor gold coverage, and brittleness. Higher temperature (>80 °C) can result in loss of surface smoothness. Besides, the plating speed is strongly affected by the plating temperature. To minimize photoresist lift-off and solution contamination, a high plating speed (i.e., high temperature) is preferred.

The current density is the most important factor in the plating process. It has been discovered that when the current density is too high, the plating solution tends to attach to the base metal (NiCr/Au) too strongly. The gold in the solution is pulled to the NiCr/Au so forcefully that it tends to undercut the photoresist and lift it off the wafer from the bottom. On the other hand, if the wafer is in the plating solution too long, the solution degrades the photoresist and lifts it off from the top. Since the current density is a function of the applied current and the area to be plated, the area must be carefully computed so that the correct current is applied. This is essential in determining the time for plating the desired thickness over a given part.

It has been discovered that the plating speed is about 2 μm per minute at a current density of 5 mA/cm^2 and a plating temperature of 60 °C. A lower current density is applied preferably at the beginning of the plating process, until the deposited gold has built up sufficiently to prevent the undercutting. A higher current density is applied later in the plating process, to accelerate the plating process. Fig. 39 shows the appearance of the fabricated electrodes under a current density of 5 mA/cm^2. The plating temperature is 30 °C and pH value of the solution is 6.5. The thickness and width of the plated electrode is measured at 4.2 μm and 10 μm as shown in Fig. 39. Thicker electrodes can be fabricated with a longer plating time and a thicker photoresist.

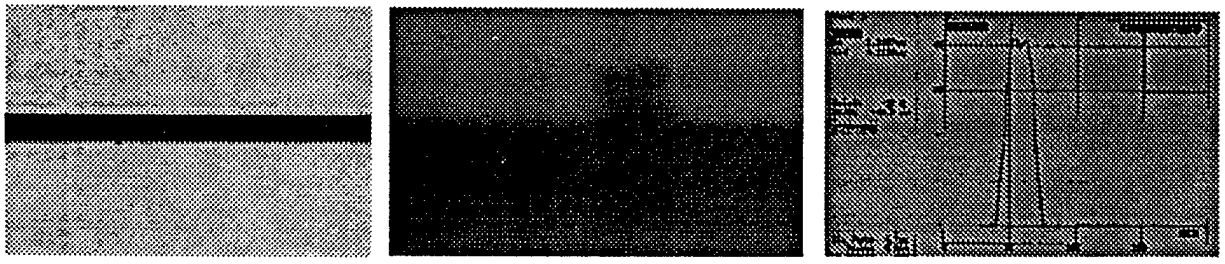

(a) (b) (c)

Fig. 39. Photographs of electroplated electrodes under a current density of 5 mA/cm^2, (a) a top view, (b) an end view, and (c) a measured structure profile.

3.7.2 Preliminary Design of Traveling-Wave Electrodes

For modeling and optimization of the traveling-wave electrodes, the electrode effective microwave index and drive voltage need to be calculated versus the electrode parameters and waveguide parameters. The design of the high-speed traveling-wave electrodes is aimed at obtaining:

(a) near 50 Ω characteristic impedance,
(b) a low microwave electrode loss,
(c) a desired microwave effective index that matches the optical waveguide effective index, and
(d) low drive voltage.

(a) Microwave impedance

The electrode characteristic impedance affects both the flatness of the frequency response and the driving power. In order to reduce the reflections of microwaves at each end of an electrode, it is essential to have impedance matching among the electrode, drive circuit, and terminating load. It is the underlying principle of the traveling-wave electrode concept to make the electrode appear as an extension of the driving transmission line. The electrode should, therefore, have the same characteristic impedance as the driving source. A 50-Ω characteristic impedance of the electrode is required since most commercial microwave components are designed to have a 50-Ω output impedance. The characteristic impedance depends on the electrode capacitance C and electrode length L, given by

$$Z = \frac{\sqrt{\varepsilon_{eff}}}{c} \frac{L}{C} \qquad (54)$$

where ε_{eff} is the effective microwave dielectric constant, and c is the speed of light in free space. ε_{eff} is a function, in general rather complex, of the microwave dielectric constants of the substrate and buffer layer as well as of the dimensions. In order to design an impedance-matched structure, the optimum ratio of the electrode gap G to the strip width W should be calculated.

(b) Microwave transmission loss

The electrode transmission loss also affects the modulation bandwidth, especially at high frequencies. Two factors contribute to the loss of traveling-wave electrodes: ohmic loss and dielectric loss. The ohmic loss α_c depends on the geometry of the electrode. For an electrode thickness of $t > 2d$, the electrode ohmic loss is independent of the electrode thickness being

determined by the modulation frequency and the inter-electrode gap. Here d is the electrode skin depth, given by

$$d = \left(\frac{1}{\pi\mu f\sigma}\right)^{1/2} \qquad (55)$$

where f is the operating frequency, μ and σ are the susceptibility and conductivity of the electrode metal, respectively. On the other hand, if $t < 2d$, the electrode ohmic loss is a function of electrode thickness, and increases as the electrode thickness decreases. To reduce the electrode ohmic loss, a minimum electrode thickness ($t > 2d$) of ~ 1.5 μm is needed (f = 10 GHz assumed). Besides, the electrode should be made of a metal with large electrical conductivity, such as Au, Ag or Al. The dielectric loss is mainly related to the frequency-dependent permitivities of materials composing the EO modulator and is a complex function of modulation frequency[64]. We have chosen pure gold (Au) over silver (Ag) and aluminum (Al), as the electrode material, although silver has better electrical conductivity than gold. The decision is backed by the superior chemical stability of gold and the existing technology of electrical gold contacts developed by the Si VLSI industry. Thick electrodes can be formed by electroplating, which will be established in the course of this effort.

(c) Microwave and optical guided mode phase matching

Microwave and optical mode phase matching is crucial to reduce the drive power while maintaining high-speed operation. We propose to achieve this goal by employing uniform thick traveling-wave electrodes. The bandwidth can be found by setting the position dependent phase term of the effective modulating microwave, as seen by the co-propagating light wave, equal to π [13]. This condition yields

$$f_d = \frac{c}{2N_m L}(1-N_o/N_m)^{-1} \qquad (56)$$

where L is the interaction length of the waveguide directional coupler, and N_o and N_m are the effective indices of the guided optical wave and the modulating microwave, respectively. The effective index N_m is a complicated function of the electrode thickness, electrode gap, cladding layer thickness and the dielectric constant of polymers employed. If the effective index N_m is much larger than N_o, short device length L has to be employed in order to obtain a required modulating speed, resulting in a large driving voltage.

(d) Driving voltage

The driving voltage V_s depends on the electro-optic coefficient γ, operating wavelength λ and electrode geometry including electrode gap d, length L, and the overlap between the electrical and optical fields Γ, given by [3]

$$V_s = \frac{\lambda d}{\gamma n^3 L \Gamma} \qquad (57)$$

where n is the refractive index. The overlap between the microwave and optical guided wave is an important factor affecting the drive power. If coplanar strip line electrodes are employed, the hot electrode should be positioned right above the center of the waveguide, and the width of the hot electrode should be close to the width of the optical waveguide for efficient interaction between the microwave and optical wave. To avoid excessive attenuation due to the presence of the metal electrode, a cladding layer with lower refractive index is required to isolate the optical guided mode from the metal electrode. As indicated by Eq. (56) and (57), there is a tradeoff between the modulating speed and driving voltage. To increase the modulating speed, shorter interaction length L is preferred, resulting in a higher driving voltage.

Simultaneous optimization of these performance characteristics is rather complicated on account of the trade-offs existing among them. For device modeling and optimization, the electrode effective microwave index and drive voltage need to be calculated versus the electrode parameters and waveguide parameters. In the following, a computational model for simulating thick traveling-wave electrodes in conjunction with polymer-based EO modulators will be reported together with some simulation results.

For traveling-wave (TW) electrodes, it has been found that the quasi-TEM approximation holds over a wide frequency range (up to 100 GHz)[65,66], hence, a quasi-TEM wave transmission is assumed and employed. For the coplanar strip transmission line shown in Fig. 40, the characteristic impedance can be expressed as

$$Z = \frac{\sqrt{\varepsilon_{eff}}}{c}\frac{1}{C} = \frac{1}{c\sqrt{C C_o}} \qquad (58)$$

$$n_{eff} = \sqrt{\varepsilon_{eff}} = \sqrt{\frac{C}{C_o}} \qquad (59)$$

where C is the capacitance per unit length, and C_o the capacitance per unit length of the structure when the substrate is replaced by air (see Fig. 40); ε_{eff} is the effective relative permittivity, c is the speed of light in free space.

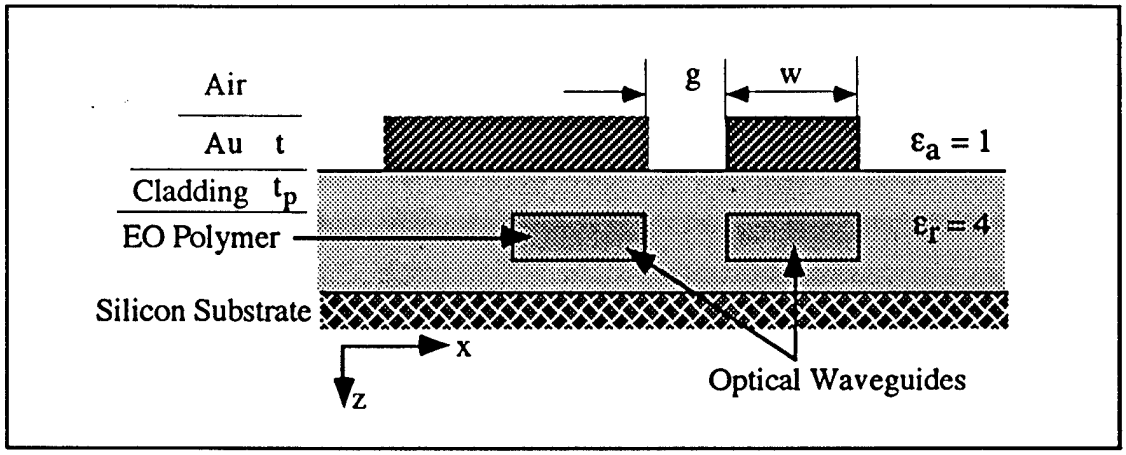

Fig. 40. Cross section of a coplanar strip electrode for the proposed electro-optic modulator.

For the case of thin CPW electrodes, the capacitance C and C_o obtained by using the conformal mapping method are given by [66]:

$$C = \varepsilon_o(1 + \varepsilon_r)K(k')/K(k) \quad (60)$$

$$C_o = 2\varepsilon_o K(k')/K(k) \quad (61)$$

$$k = (1 + w/g)^{-1/2} \quad (62)$$

$$k' = (1 - k^2)^{1/2} \quad (63)$$

where K is the complete elliptic integral of the first kind; g and w are the electrode gap and width, respectively; ε_o is the permittivity of free space, and ε_r is the relative permittivity of the optical polymer.

Commonly, a thick electrode structure is employed to reduce the microwave propagation loss, the excess capacitance C_t due to the increased thickness is treated as the capacitance of the parallel plate capacitors formed by the side walls of the thick electrode. This excess capacitance should be added to the right sides of Eqs. (60) and (61). It has been shown that C_t can be approximated by [66,67]:

$$C_t = \pi\varepsilon_o \frac{a_1 - a_2 \ln(w/g) + a_3 \ln(a_4 + t/g)}{\ln(4g/t) + 1/8\,(t/g)^2} \quad (64)$$

where $a_1 = 0.56677$, $a_2 = 0.03834$, $a_3 = 0.22411$, $a_4 = 0.08893$, and t is the electrode thickness.

Because of the presence of the polymer cladding layer, the total capacitance depends on the thickness of the cladding layer, which may also have a different dielectric constant ($\varepsilon_p = 4.0$). An approximate expression for this additional capacitance C_b is given by [66,67]:

$$C_b = b_1 \varepsilon_o \varepsilon_{SiO_2} \ln (1 + b_2 k) \ln (b_3 + b_4 t_b/g) \qquad (65)$$

where t_p is the cladding layer thickness, and $b_1 = 0.1341$, $b_2 = 10.477$, $b_3 = 1.0658$, and $b_4 = 34.9426$ are the empirical fitting parameters obtained using the Green's function method [66].

The effective capacitance C and C_o for a finite electrode thickness with a polymer-based cladding buffer layer can thus be written as:

$$C = \varepsilon_o(1 + \varepsilon_r)K(k')/K(k) - C_p + C_t \qquad (66)$$

$$C_o = 2\varepsilon_o K(k')/K(k) + C_t \qquad (67)$$

The accuracy of Eqs. (66) and (67) has been tested against the results obtained with the Green's function method [65-67]. The discrepancy was determined to be less than 10% . In order to build an accurate simulation model, the simulated result will be tested against the experimental results in our future research.

The microwave effective index, computed with the use of Eqs. (59), (66), and (67), versus hot electrode width is plotted in Figs. 2(a) and 2(b), with the electrode thickness and cladding layer thickness as parameters, respectively. To obtain a desired microwave effective index that matches to the optical waveguide effective index, a wide hot electrode is preferred. A thin electrode structure is useful to increase the microwave effective index, perhaps at the expense of a higher electrode propagation loss. As an example, for w = 15 μm, g = 15 μm, t = 5 μm, and t_b = 0.5 μm, we have $n_{eff} = 1.28$ based on Fig. 41(a). Fig. 41(a) indicates that n_{eff} decreases from $n_{eff} = 1.28$ to $n_{eff} = 1.25$ if the electrode thickness increases from 5 μm to 10 μm. As demonstrated by Fig. 41(b), a thick buffer layer may also be used to reduce the microwave effective index. As a result, a longer electrode length can be employed to lower the device voltage for a required modulation bandwidth.

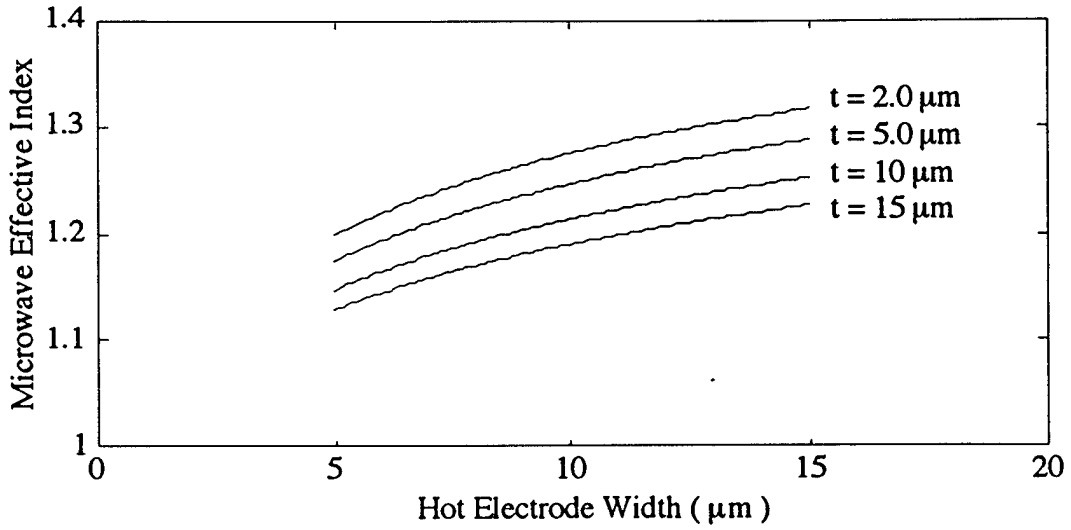

Fig. 41(a). Effective index calculated vs. electrode width for g = 15 μm, and t_b = 1.0 μm.

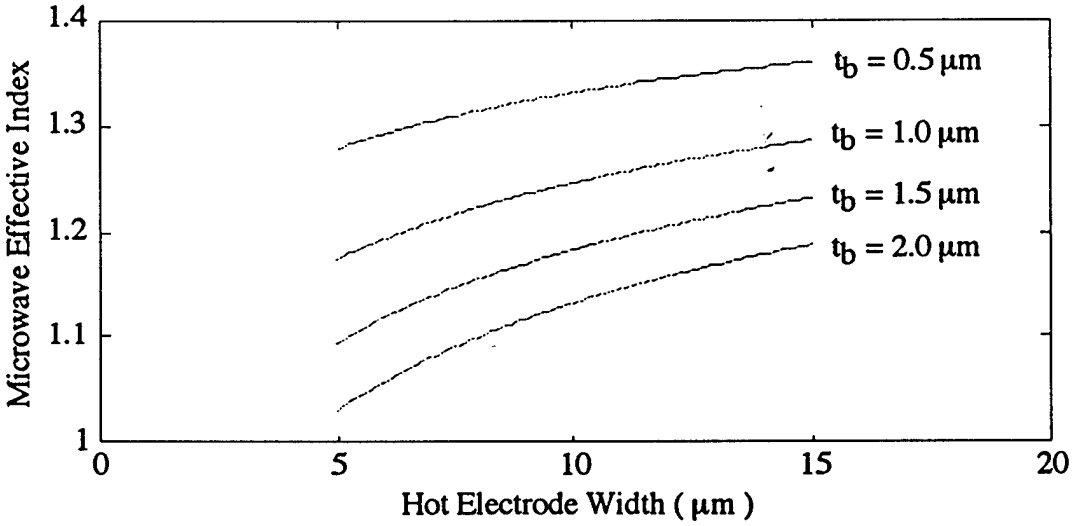

Fig. 41(b). Effective index calculated versus electrode width for g = 15 μm and t = 5.0 μm.

The characteristic impedance, calculated with the use of Eqs. (59), (66), and (67), versus hot electrode width is plotted in Figs. 47(a) and 47(b), with the cladding layer thickness and electrode thickness as parameters, respectively. The impedance decreases as the electrode thickness increases and/or the buffer layer thickness decreases. As an example, for g = 10 μm, w = 15 μm, t = 10 μm, and t_b = 0.5 μm, we have Z = 67 Ω. To reduce the microwave impedance to 50 Ω, a thin polymer cladding layer is desired at the top of the electro-optic waveguides.

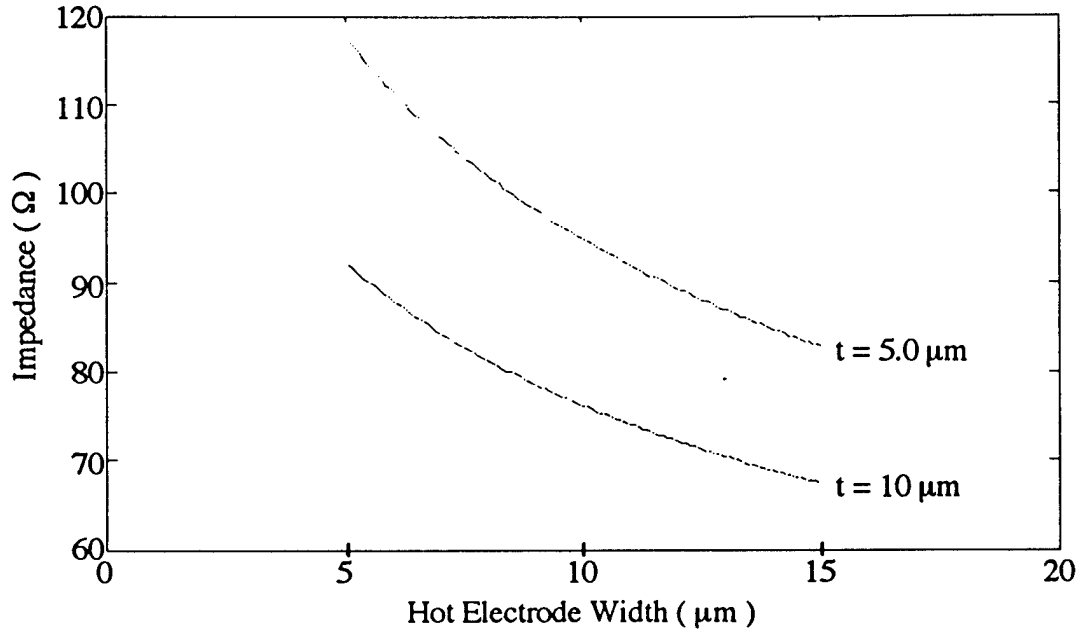

Fig. 42(a). Calculated impedance versus electrode width for g = 10 μm and t_b = 0.5 μm.

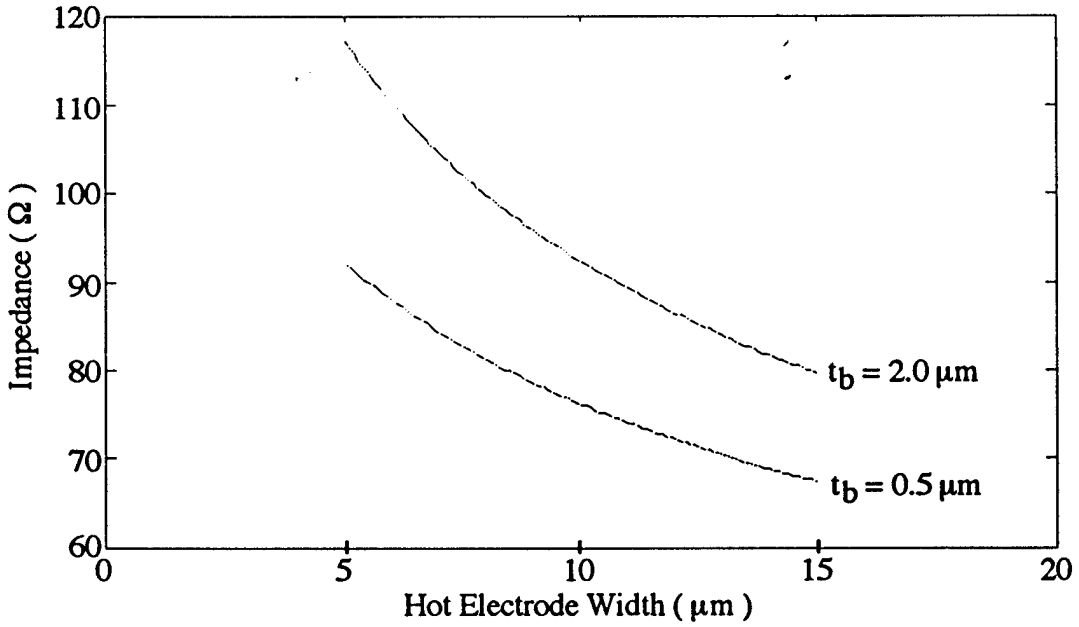

Fig. 42(b). Calculated impedance versus electrode width for g = 15 μm and t = 10 μm.

A preliminary model has been developed for design of the high-speed traveling-wave electrodes. Based on this model, the impedance and microwave effective index for a coplanar stripe line traveling-wave electrode are analyzed as a function of the microwave electrode parameters and buffer layer thickness. The technique outlined here is valid for the proposed electro-optic modulator using domain inverted sections. It should be noted that several parameters

of the individual cross-points are important in characterizing an electro-optic modulator. The primary parameters are driving voltage, modulating speed, and crosstalk. Simultaneous optimization of these performance characteristics is rather complicated on account of the trade-offs existing between the design of the waveguide directional couplers and the design of the high-speed traveling-wave electrodes. Based on the two calculation models (the simulation model traveling-wave electrode and the simulation model for electro-optic directional coupler), we will try to find an optimization procedure to determine all the design parameters, including the dimensions of single-mode polymer-based waveguides, waveguide directional couplers, and the coplanar stripe line traveling-wave electrodes. An optimization procedure, involving all the relevant design parameters (Z, n_{eff}, w, g, t, t_b, V_π) together with waveguide parameters, is under development.

3.8 CAD Tool for High-speed Linear Modulator Simulation

A CAD tool is under construction for simulation of the domain-inverted high performance waveguide modulators. To design and fabricate the Y-branch waveguide modulators, the first step is to calculate the modes of the channel waveguides to ensure a single-mode operation. Then, the coupling coefficient can be further determined and can be used to calculate the coupling length. The waveguide separation should be optimized to obtain a low driving voltage. The interaction length can be determined by the switching diagram to ensure not only the required modulation linearity but also a high modulation efficiency. Due to the employment of domain inversion, linearity of the modulation curve is significantly enhanced. The BPM-CAD under construction will be capable of determining all the required design parameters.

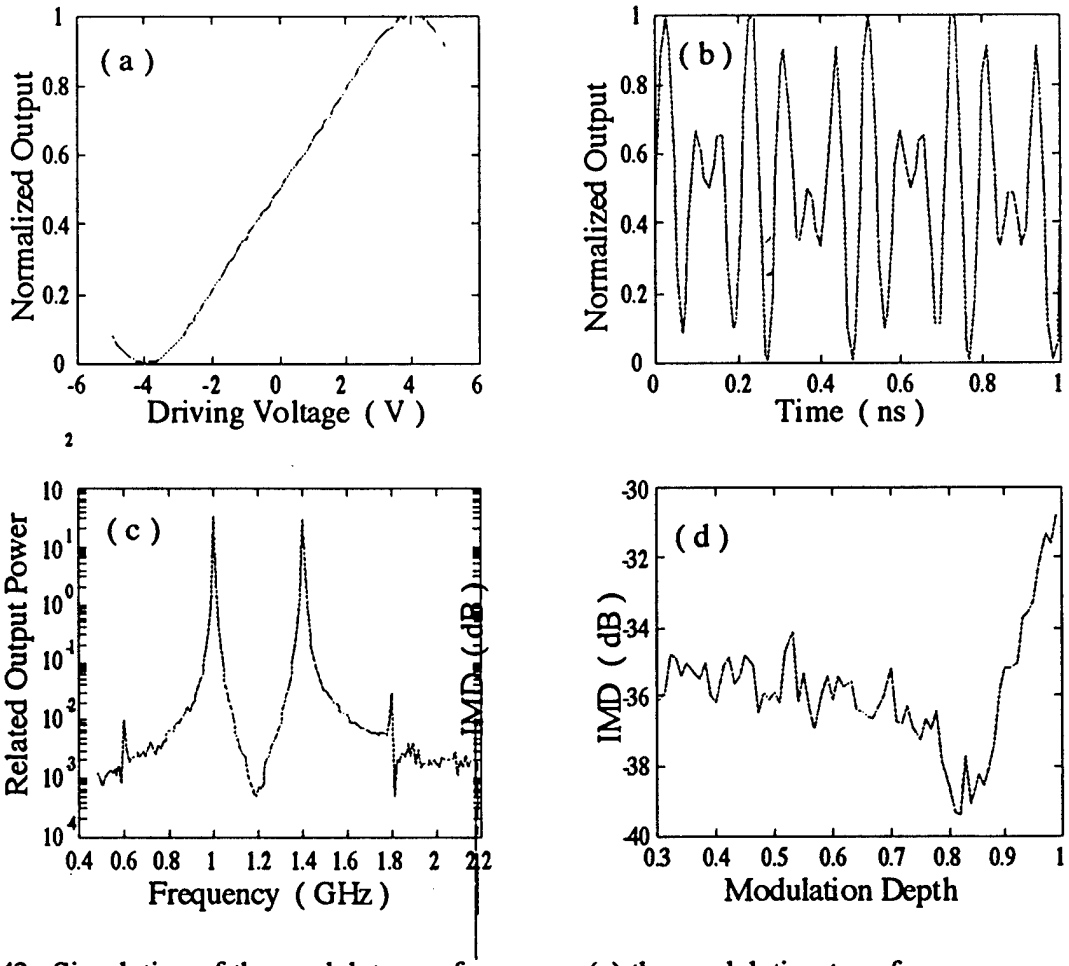

Fig. 43. Simulation of the modulator performance, (a) the modulation transfer curve, (b) optical output signals, (c) output spectrum in the frequency domain, and (d) the nonlinear intermodulation distortion for the proposed domain-inverted Y-branch waveguide modulator.

Based on the CAD tool developed, we have estimated the modulator performance shown in Fig. 43. In the simulation, a typical single-mode LD-3 channel waveguide is selected with the waveguide width of 2.5 μm and depth of 2.5 μm, and with EO waveguide index of 1.55. Optical cladding polymer NOA-61 is selected as the top and bottom cladding layer with an index of 1.53 at an operating wavelength of 1.3 μm. A directional coupler is simulated using two 2.5 μm x 2.5 μm channel waveguides separated by 7 μm. A complete CAD tool is under construction, which will be fully developed in Phase II for design and simulation of the proposed domain-inverted optoelectronic modulators based on a waveguide directional coupler.

4.0 SUMMARY OF PHASE I RESEARCH

The primary objectives of the Phase I work were to explore the feasibility and advantages of using domain inverted polymers, to improve the performance of electro-optic modulators, and to establish the technical foundation for the design and fabrication of a new class of electro-optical modulators with improved performance, simplified structure, and relaxed fabrication tolerance. The improved performance includes high modulation efficiency, a highly linearized modulation transfer curve, high-speed operation, low driving voltage, and polarization-insensitive operation.

By accomplishing the tasks of the Phase I effort, we have established the theoretical and technical foundation for the realization of high performance Y-branch waveguide modulators based on domain-inverted polymers and a uniform traveling-wave electrode. At present, all the building blocks essential for the fabrication and modeling of the proposed innovative devices are available. The achievements strongly encourage us to pursue further R&D efforts in Phase II, aimed at the fabrication of high performance EO modulators as required by BMDO and Air Force for their advanced RF photonic systems[1,15]. High-speed optical analog modulators also play an important role in a wide variety of practical applications, including CATV fiber-optic links[16,17], optoelectronic interconnects[11,12], and microwave instruments[2].

Through the Phase I research, we have accomplished six technical goals, which are outlined in the following:

(1) ***Analysis and design of the novel domain-inverted Y-branch modulators that have a significantly improved performance, relaxed fabrication tolerance and simplified device scheme.***

Both the conventional Y-branch waveguide modulator and the proposed domain-inverted Δß-type waveguide modulator have been analyzed and compared in terms of modulation depth, linearity of modulation transfer curves, driving voltage, polarization sensitivity, and fabrication tolerance. We have shown that our proposed domain-inverted structure exhibits superior performance over conventional approaches. Only a single uniform traveling-wave electrode is required to achieve 100% modulation depth and linearized modulation, ensuring high speed operation with a relaxed fabrication tolerance. The uniform electrode required in this design is much less difficult to fabricate and makes matching to a microwave source much easier compared with the conventional phase-reversal electrodes.

In the past, the Δß-type operation has been realized by using multiple electrode sections with applied voltages of reversed polarities. This straightforward approach has, however, a major drawback with its inherent incompatibility to a single drive source. This requirement makes high-speed applications of the device impossible. Recognizing this fact, we have proposed a novel approach based on the application of domain-inverted polymers to electro-optical waveguides, which results in a simple, compact modulating device. This waveguide structure with domain-inverted sections is capable

of providing the required reversed Δß modulation and polarization-independent operation using a single electrode.

(2) ***Establishment of a powerful liquid-contact electric-poling technique providing 40% enhancement of the electro-optic coefficient.***

In the course of the Phase I effort, an advanced liquid electric-poling technique has been developed to produce high performance EO polymers. A poling field as high as 250V/μm in an LD-3 EO polymer film was obtained with little surface damage. The r_{33} value was measured to be 18 pm/V at 633 nm and 14 pm/V at 1310 nm which are 40% higher than the previously reported results. Such a high poling field and therefore larger r_{33} value are not achieved through neither the conventional metal contact poling nor corona poling. EO polymer with higher electro-optic coefficient can be realized with further improvement of the liquid-contact poling technique.

(3) ***Establishment of a reliable domain-inversion technology.***

The availability of a new technology for domain inversion in electro-optic polymer is the cornerstone for the proposed high performance EO modulators. Based on the Phase I proposal, we have concentrated on the development of a technological foundation for the fabrication of the two-section Y-branch with reversed Δß-type modulation. A reliable new technology for fabricating domain-inverted polymers has been developed based on a modified high-temperature liquid-contact poling technique. The dimensions of the poling and reverse-poling sections are precisely defined through microlithography. Using these techniques developed through the Phase I research, we are now able to fabricate polymer-based domain-inverted electro-optic waveguides. ***Domain-inverted polymers have been demonstrated for the first time through this Phase I effort.***

An effective reflection measurement technique has also been investigated as a means to characterize this new type of polymer. Successful inverted poling of two domains in LD-3 polymer is demonstrated by measuring the electro-optic response of each domain using this reflection technique. This measurement technique is capable of addressing both the magnitude and the sign of the electro-optic response of polymers. Furthermore, the measurement technique is non-destructive and therefore it can be repeatedly conducted without damaging the sample under test.

(4) ***Demonstration of domain-rotated polymers.***

The availability of a new technology for fabricating 90° domain-rotated polymers is another cornerstone for the proposed new class of EO modulators. We have successfully demonstrated a two section 90° domain-rotated polymer using a metal contact poling technique. Such a 90° domain rotation is crucial for polarization insensitive operation because the effective electro-optic modulation can be equalized for both TE and TM mode. It should be noted that domain-rotated EO waveguides cannot be obtained in any inorganic materials such as $LiNbO_3$, GaAs, and InP. In Phase II research, the liquid-contact poling technique will be further investigated for electric poling of 45° domain-rotated polymers. Other applications of domain-rotated polymers will be further investigated.

(5) Fabrication of EO channel waveguides and Y-branch waveguide couplers using LD-3 polymers.

An LD-3 EO polymer-based waveguide fabrication process has been established. Based on this process, polymer-based EO channel waveguides and Y-branch waveguide directional couplers have been realized using LD-3 polymer, which is one of the most reliable EO polymers, demonstrated as suitable for military applications. The waveguide thickness is fabricated up to 2.5 μm, which is state of the art. The propagation loss is determined to be about 1 dB/cm at a wavelength of 1.3 μm.

(6) Design and Fabrication of high-speed traveling-wave electrodes.

A preliminary simulation model has been developed in order to design the high-speed traveling-wave electrodes. Based on this model, the microwave transmission characteristics, including the impedance and microwave effective index for a coplanar stripe line traveling-wave electrode were analyzed as a function of electrode parameters and buffer layer thickness.

To ensure high-speed operation, it is mandatory to employ thick traveling-wave electrodes for reducing the microwave transmission loss and velocity mismatch. We have established a gold electroplating technique for fabricating thick traveling wave electrodes. Thick traveling-wave electrodes have been fabricated with thickness greater than 10 μm.

5.0. REFERENCES

1. Rod. C. Alferness, "Integrated Optics: Beyond the field of dreams," in Integrated Photonics Research, vol. 7, paper L2-1, Dana Point, CA, 1995;
2. R. L. Jungerman et al, "High-speed optical modulator for application in instrumentation," IEEE J. Lightwave Technol., vol. LT-8, pp. 1363-1369, 1990.
3. R. C. Alferness, "Waveguide electrooptic modulators," IEEE Trans.Microwave Theory Tech., vol. MTT-30, pp. 1121-1137, 1982.
4. G. E. Bodeep and T. E. Darcie, "Semiconductor lasers versus external modulators: A comparison of nonlinear distortion for lightwave subcarrier CATV applications," IEEE Photon.Technol.Lett., vol. 1, pp. 401-403, 1989.
5. Kazuto Noguchi, Osamu Mitomi, Hiroshi Miyazawa, and Shunji Seki, "A broadband Ti: $LiNbO_3$ optical modulator with a ridge structure," J. of Lightwave Technol., vol. 13, pp. 1164-1166, 1995.
6. H. Nagata and J. Nayyer, "Stability and reliability of Lithium Niobate Optical Modulators," OSA/IEEE Integrated Photon. Research, Technical Digest Series, vol. 7, pp. 290-292, 1995.
7. J. Nayyer and H. Nagata, "Suppression of thermal drifts of high speed Ti: $LiNbO_3$ optical modulators," IEEE Photon. Technol. Lett., vol. 6, no. 8, pp. 952-955, 1994.
8. C. H. Bulmer and W. K. Burns, "Polarization characteristics of $LiNbO_3$ channel waveguide directional coupler," J. Lightwave Technol., LT-1, pp.227-236, 1993.
9. (a) Mark L. Farwell, Zong-Qi Lin, Ed Wooten, and William S. C. Chang, "An electrooptic intensity modulator with improved linearity," IEEE Photon. Technol. Lett., vol. 3, pp. 792-794, 1991. (b) J. H. Schaffner,W. B. Bridges, "A study of broadband microwave fiber optic links with linearized integrated optic modulators," SPIE, vol. 2155, pp. 218-228, 1995.
10. Lawrence A. Hornak, "Polymers for lightwave and integrated optics: technology and applications," Marcel Dekker, 1992.
11. **Ray T. Chen**, "Polymer-based Photonic Integrated Circuits," (Invited Review Paper), Optics and Laser Technology, vol. 25, pp. 347-365, 1993.
12. **Ray T. Chen**, H. Lu, D. Robinson, Z. Sun, T. Jannson, D. V. Plant and H. R. Fetterman, "60 GHz Board-to-board Optical Interconnection using Polymer Optical Buses in Conjunction with Microprism Couplers," Appl. Phys. Lett., vol. 60, pp. 536-538, 1992.
13. Wenshen Wang, Datong Chen, Harold R. Fetterman, Yongqiang Shi, William H. Steier and Larry R. Dalton, "40-GHz polymer electrooptic phase modulators," IEEE Photon. Technol. Lett., vol. 7, no. 6, pp. 638-640, 1995.
14. W. Wang, D. Chen, H.R. Fetterman, Y. Shi, W. H. Steier, and L. Dalton, "Traveling wave electro-optic phase modulator using cross-linked nonlinear optical polymer," Appl. Phys. Lett., vol. 65, no. 8, pp. 929-931, 1994.
15. Henry Zmuda, "Photonics Aspects of Modern Radar", 1996, Artech House, and Henry Zmuda, and Edward N. Toughlian, Photonic Aspects of Modern Radar, (Artect House, Inc., Norwood MA 1994), Chap. 13, 17.
16. F. J. Leonberger, S. W. Merritt and P. G. Suchoski, "Optical modulators find wider use in CATV and telecommunications," Laser Focus World, pp. 135-137, July 1995.
17. Gray E. Betts, L. M. Walpita, W . S. C. Walpita, W. S. C. Chang, and R. F. Mathis, "On the linear dynamic range of integrated electrooptic modulators," J. of Quantum Electron., vol. QE-22, pp. 1009-1011, 1996..
18. S. Thaniyavarn, "Modified 1x2 directional coupler waveguide modulator," Electron. Lett., vol. 22, pp. 941-942, 1986.
19. Herwig Kogelnik and Ronald V. Schmidt, "Switches directional couplers with alternating Δß," IEEE J. of Quantum Electron., vol. QE-12, pp. 396-401,1986.
20. P. Granestrand, "Four-sectioned polarization-independent directional coupler with extremely relaxed fabrication tolerance," IEEE Photonics Technol. Lett., vol. 4, pp. 594-596, 1992.
21. Edmond J. Murphy, "Recent progress on guide-wave switch arrays," OSA/IEEE Integrated Photonics Research, Technical Digest Series, vol. 7, pp. 182-183, 1994.

22. J. J. Veselka, D. A. Herr, T. O. Murphy, L. L. Buhl, and S. K. Korotky, "Crosstalk measurements of integrated high-speed Ti: LiNbO3 Δß-reversal switching circuits," IEEE J. of Lightwave Technol., vol. 7, pp. 908-910, 1989.
23. Moshe Nazarathy, David W. Dolfi, and Roger J. Jungerman, "Spread Spectrum frequency response of coded phase reversal traveling wave modulators," IEEE J. of Lightwave Technol., vol. 5, pp. 1433-1443,1987.
24. Yi Zhou, Masayuki Izutsu and Tadasi Sueta, "Low-drive-power asymmetric Mach-Zehnder modulator with band-limited operation," IEEE J. of Lightwave Technol., vol. 9, pp. 750-753, 1991.
25. D. W. Dolfi, M. Nazarathy, and R. L. Jungerman, "40 GHz electro-optic modulator with 7.5V drive voltage," Electron. Lett., vol. 24, pp. 528-529, 1988
26. M. Yamada, K. Kishima, "Fabrication of preiodically reversed domain structure for SHG in LiNbO3 by direct electron beam lithography at room temperature," Electron. Lett., vol. 27, pp. 828-810, 1991.
27. M. Yamada, N. Nada, M. Saito, and K. Watanabe, "First order quasi phase matched LiNbO3 waveguide periodically poled by applying an external field for efficient blue light second harmonic generation," Appl. Phys. Lett., vol. 62, pp. 435-437, 1993.
28. Kiminori Mizuuchi and Kazuhisa Yamamoto, "Harmonic blue light generation in bulk periodically poled $LiTaO_3$," Appl. Phys. Lett., vol. 66, no. 22, pp. 2943-2945, 1995.
29. Juan F. Lam and Gregory L. Tanggonan, "A novel modulator system with enhanced linearization properties," IEEE Photon. Technol. Lett., vol. 3, pp. 1102-1104, 1991.
30. E. M. Zolotov and R. F. Tavlykaeo, "Integrated optical Mach-Zehnder modulator with a linearized modulation characteristic," Sov. J. Quantum Electron, vol. 18, pp. 401-402, 1988.
31. A. Yariv, "Coupled mode theory for guided wave optics", IEEE J. Quantum Electron., vol. QE-9, pp. 919-933, 1973.
32. E.A.J. Marcatili, "Dielectric rectangular waveguide and directional coupler for integrated optics," Bell System Technical Journal, vol. 53, no. 4, pp. 2071-2102, 1974.
33. K. S. Chiang, "Dual effective index method for the analysis of rectangular dielectric waveguides," Appl. Optics, 1986, vol. 25, no. 13, pp. 2169-2174, 1986.
34. **Suning Tang**, Ray. T. Chen and Dave Gerold, "Channel cross-coupling in a polymer-based bus array," IEEE J. of Light. Technol., vol. 13, no. 1, pp. 37-41, 1995.
35. C. Bulmer and W. Burns, "Linear interometric modulators in Ti:$LiNbO_3$," J. of Lightwave Technol., vol. 2, pp. 512-521, 1994.
36. P. R. Ashley and W. S. C. Chang, "Improved linearity of mode extinction modulator using Ti:$LiNbO_3$ channel waveguide," Appl. Phys. Lett., vol. 45, pp. 840-842, 1994.
37. B. H. Kolner and D. W. Dolfi, "Intermodulation distortion and compression in an integrated electro-optic modulator," Appl. Opt., vol. 26, pp. 3676-3680, 1989.
38. Halvor Skeie, Richard V Johnson, " Linearization of electro-optic modulators by a cascade coupling of phase-modulating electrode," SPIE, vol. 1583, pp. 153-164, 1991.
39. (a) R. A. Norwood, T. Findakly, H. A. Goldberg, G. Khanarian, J. B. Stamatoff, and H. N. Yoon, "Optical polymers and multifunctional materials," in *Polymers for lightwave and integrated optics*, edited by L. A. Hornak, 287-320 (Marcel Dekker, New York, 1992).
40. T. C. Kowalczyk, T.Z. Kosc, K.D. Singer, A.J. Beuhler, D.A. Wargoski, P.A. Cahill, C.H. Seager, and M.B. Meihardt, "Crosslinked polyimide electro-optic materials," J. Appl. Phys., vol. 78, p. 5876, 1995.
41. E.M. Cross, K.M. White, R.S. Moshrefzadeh, C.V. Francis, "Azobenzeimidazole compounds and polymers for nonlinear optics", Macromolecules, vol. **28**, p. 2526, 1995.
42. C. Xu, B. Wu, O. Todorava, L. Dalton, Y. Shi, P. M. Ranon, and W.H. Steier, "Stabilization of dipole alignment of poled nonlinear optical polymers by ultrastructure synthesis", Macromolecules, vol. 26, p. 5303, 1993.
43. R. Levenson, J. Liang, C. Rossier, R. Hierle, E. Taussaere, N. Bouadma and J. Zyss, Advances in organic polymer-based optoelectronics", in *Polymer for second-order nonlinear optics*, (American Chemical Society, Washington, DC, 1995), p. 436.

44. G.F. Lipscomb, R. S. Lytel, A.J. Tickmnor, T. E. Van Eck, S.L. Kwinatwowski, and D.G. Girton, "Developments in organic electro-optic devices at Lockheed", *Proc. SPIE*, vol. 1337, p. 23, 1990.
45. Peter M. Ranon, "Second order optical properties study and the poling induced dipole alignment stabilization of second order nonlinear optical polymers," Ph.D. dissertation, University of Southern California, 1993. (Note: LD-3 is SC-XL12B)
46. J.H. Bechtel, Y. Shi, and W. Wang, "Electro-optic polymer modulators for externally modulated fiber-optic transmitters", Proc. SPIE, vol. 2690, p. 202, 1996.
47. W. Wang, D. Chen, H.R. Feterman, Y. Shi, W.H. Steier, L. Dalton, R.-M.D. Chow, "Optical heterodyne detection of 60 GHz electro-optic modulation from polymer waveguide modulators", Appl. Phys. Lett., vol. 67, p. 1806, 1995.
48. H. Nishihana, Optical Integrated Circuits, (McGraw-Hill Book Co., New York ,1987).
49. **Ray. T. Chen, Suning Tang**, T. Jannson and J. Jannson, "A 45-cm long compression-molded polymer-based optical bus," Appl. Phys. Lett., vol. 1032-1034, 1993.
50. K. Mizuuchi, K. Yamamoto and T. Taniuchi, "High-efficiency coupling of laser diodes in tapered proton-exchanged waveguides," Electron. Lett., vol. 26, pp. 1992-1994, 1992.
51. **Ray T. Chen**, "Graded index linear and curved polymer channel waveguides for massively parallel optical interconnects," Appl. Phys. Lett. vol. 61, pp. 2278-2280, 1992.
52. T. Verbiest, D.M. Burland, M.C. Jurich, V.Y. Lee, R.D. Miller, and W. Volksen, "Electrooptic properties of side chain polyimides with exceptional thermal stability," Macromolecules, vol. 28, p. 3005, 1995.
53. R. A. Hill, A. Knoesen, and M. A. Mortazavi, "Corona poling of nonlinear polymer thin films for electro-optic modulators", Appl. Phys. Lett., vol. 65, no. 14, p. 1733, 1994.
54. Jay S. Schildkraut, "Determination of the electrooptic coefficient of a poled polymer film," Appl. Opt., vol. 29, no. 19, p. 2839, 1990.
55. C.C. Teng and H.T. Man, "Simple reflection technique for measuring the electro-optic coefficient of poled polymers," Appl. Phys. Lett., vol. 56, no. 18, p.1734, 1990.
56. Haujun Tang, John Tadoada, **Suning Tang, Ray T. Chen**, "Domain-inversion technique for crosslinked electro-optic polymers," SPIE, vol. 3006, paper 51, 1997.
57. Huajun Tang, John Tadoada, Gaohua Cha, Richard Lee, and Ray T. Chen, "Enhanced electro-optic coefficient of nonlinear optical polymer using liquid contact poling," Appl. Phys. Lett., vol. 70, no. 5, pp. 538-540, 1996.
58. Dave Gerold, **Ray T. Chen**, William A. Farone, and David Pelka, "Poled electro-optic photolime gel polymer doped with chlorophenol red and bromomethyl blue chromophores," Appl. Phys. Lett., vol. 66, no. 20, pp. 2631-2633, 1995.
59. C.C. Teng and H. T. Man, "Simple reflection technique for measuring the electro-optic coefficient of poled polymers," Appl. Phys. Lett. vol. 56, pp. 1734-1736, 1990.
60. C. M. Gee, G. D. Thurmond, and H. W. Yen, "17-GHz bandwidth electro-optic modulator," Appl. Phys. Lett., vol. 43, no. 11, pp. 998-1000, 1993.
61. K. Noguchi, K. Kawano, T. Nozawa, and T. Suzuki, "A Ti:$LiNbO_3$ optical modulator with more than 20 GHz bandwidth and 5.2 V driving voltage," IEEE Photon. Technol. Lett., vol. 5, no. 1, pp. 52-55, 1993.
62. K. Noguchi, O. Mitomi, K. Kawano, and M. Yanagibashi, "High efficient 40-GHz bandwidth Ti:$LiNbO_3$ optical modulator employing ridge structure," IEEE Photon. Technol. Lett., vol. 4, no. 9, pp. 1020-1022, 1992.
63. G. K. Gopalakrishnan, W. K. Burns and C. H. Bulmer, "Electrical loss mechanisms in traveling-wave $LiNbO_3$ optical modulators," Electron. Lett., vol. 28, pp. 207-209, 1992.
64. K. Kawano, T. Kitoh, H. Jumonich and T. Nozawa, "Spectral domain analysis of coplanar waveguide traveling-wave electrodes and their applications to Ti: $LiNbO_3$ Mach-Zehnder optical modulator," IEEE Trans. on Microwave Theory Tech., vol. 39, pp. 1595-1601, 1991.
65. Kazuhiko Atsuki and Eikichi Yamashita, "Transmission line aspects of the design of broad band electrooptic traveling-wave modulators," IEEE J. Lightwave Technol., vol. LT-5, no. 3, pp. 316-319, 1987.

66. Haeyang Chung, William S. C. Chang, and Gray E. Betts, "Microwave properties of traveling-wave $LiNbO_3$ electrooptic modulators," IEEE J. Lightwave Technol., vol. 11, no. 8, pp. 1274-1278, 1994.
67. N. G. Alexopoulas and C. M. Krowne, "Characteristics of single and coupled microstrips on anisotropic substrate, " IEEE Trans. Microwave Theory Tech., vol. 26, pp. 387-393, 1988.
68. N. Keil, H. H. Yao, and C. Zawadzki, "Polymer waveguide optical switch with <-40 dB polarisation independent crosstalk," Electron. Lett., vol. 32, no. 7, pp. 655-656, 1996.
69. Ray T. Chen, Maggie M. Li, **Suning Tang** and Dave Gerold, "Nd^{3+}-Doped graded index single-mode polymer waveguide amplifier working at 1.06 and 1.32 μm," Proc. SPIE, vol. 2042, pp. 462-463, 1993.
70. E. Litchman, A. A. Friesem, R. G. Waarts and **Suning Tang**, "Cross-induced polarization changes in single-mode fibers," Appl. Opt., vol. 28, pp. 4056-4058, 1990.
71. E. Litchman, A. A. Friesem, **Suning Tang** and R. G. Waarts, "Nonlinear Kerr interactions between modulated waves propagating in a single-mode fiber," IEEE J. of Light. Technol., vol. 9, pp. 422-426, 1991.
72. **Suning Tang**, Rob Mayer, Maggie M. Li, Luke Graham, and Ray T. Chen, "A novel wavelength-division-demultiplexer with optical in-plane to surface-normal conversion," IEEE Photon. Technol. Lett., vol. 7, no. 8, pp. 908-910, 1995.